

**A SCINDA-GPS STUDY OF EQUATORIAL PLASMA BUBBLES OVER KISUMU,  
KENYA DURING 2013 -2014 PERIOD**

**Edward Nyongesa Uluma**

A research Thesis Submitted in Partial Fulfillment of the Requirements for the  
Degree of Master of Science in Physics of Masinde Muliro University of Science  
and Technology

**OCTOBER 2020**

**DECLARATION**

I declare that this thesis is my original work prepared from no other than the indicated sources and support and has not been presented anywhere for any degree or any other award in any University.

Signature.....

Date.....

Edward Nyongesa Uluma

SPH/G/25/2015

The undersigned certify that they have read and hereby recommend for acceptance of Masinde Muliro University of Science and Technology a research thesis entitled “A *SCINDA-GPS study of Equatorial plasma bubbles over Kisumu, Kenya during 2013 and 2014 period*”

Signature.....

Date.....

Dr. Boniface Ndinya  
Department of Physics  
Masinde Muliro University of Science and Technology.  
P.O Box 190-50100,  
Kakamega.

Signature.....

Date.....

Dr. George Omondi  
Department of Physics and Materials Science  
Maseno University.  
P.O Box 333-40105,  
Maseno.

## **COPYRIGHT**

This thesis is copyright materials protected under the Berne convention, the copyright Act 1999 and other international and national enactments in that behalf, on intellectual property. It may not be reproduced by any means in full or in part except for short extracts in fair dealing so for research or private study, critical scholarly review or discourse with acknowledgement, with written permission of the Dean School of Graduate Studies on behalf of both the author and Masinde Muliro University of Science and Technology.

## **DEDICATION**

This work is dedicated to my Mum Marctil Liaka Uluma and my late Dad, Lawrence Mwenya Uluma.

## **ACKNOWLEDGEMENT**

I would like to extend my sincere gratitude and deepest appreciation to my supervisors Dr. Boniface Ndinya, Department of Physics, Masinde Muliro University of Science and Technology and Dr. George Omondi, Department of Physics and Materials Science, Maseno University for their invaluable support, advice and great ideas that have been very useful in the undertaking of this research. Many thanks go to the Head of Department of Physics and Materials Science at Maseno University, Professor Andrew Oduor for allowing me access SCINDA-GPS data from the Kisumu GPS station, my lecturers in the Department of Physics, Masinde Muliro University of Science and Technology; Prof. Thomas Sakwa, Dr. Maxwell Mageto, Dr. Henry Baraza and Dr. Benard Rapando for their thorough comments and remarks which were essential in understanding the subject matter. Great thanks to Boston college and Dr. Gopi Krishna Seemala who developed the GPS-TEC software which was very useful in processing the raw data from SCINDA-GPS station. Special thanks goes to Joshua Rombosia of Craft Silicon and all my family members for their moral support and encouragement during the whole study period of my course. I finally wish to thank God for granting me the opportunity to undertake this course and seeing me through up to its completion.

## ABSTRACT

The ionosphere is the ionized portion of the atmosphere that stretches from about 50 km to 1000 km above the ground. It plays a very important role in the solar effects felt on Earth. Despite various studies having been carried out on occurrence of Equatorial plasma bubbles (EPBs) in Africa, more research needs to be done within East Africa since the ionosphere is a highly variable medium resulting from ionizing radiation from the Sun and changes from region to region. The problem in this study was to investigate the occurrence of EPBs over Kisumu, Kenya during selected quiet and storm days between 1<sup>st</sup> January 2013 to 31<sup>st</sup> December 2014, which was a high solar activity period for solar cycle 24 using TEC and amplitude scintillation ( $S_4$ ) data. This study was carried out by analyzing Receiver Independent Exchange (RINEX) Total Electron Content (TEC) data retrieved from the Kisumu high data rate NovAtel GSV4004B SCINDA-GPS receiver situated at Maseno University (Geographic coordinates: 0.02°S, 34.6°E; geomagnetic coordinates, 9.64°S, 108.59°E). The TEC data was unzipped using WinRAR program and processed using Gopi software. The resulting output data was used to plot Vertical Total Electron Content (VTEC) &  $S_4$  plots and ROT & ROTI plots all against universal time (UT) for selected quiet and storm days of the year 2013 and 2014. The results obtained from this study shows notable TEC depletions followed by TEC enhancement which corresponded with enhanced  $S_4$  after local sunset for most of the selected quiet and storm days of 2013 and 2014. An average TEC value of 59 TECU was attained in the equinoctial period (March, April, August and September) while an average TEC value of 55 TECU was attained in the solstice period (June, July, November and December). There was an increased ROT fluctuation which corresponded with high ROTI values after local sunset for most selected quiet and storm days. The percentage EPB occurrence was 6.49% in the year 2013 and 4.32% in the year 2014. The storm days had EPB occurrence of 21.42% in the year 2013 and 21.88% in the year 2014 while the quiet days which had 18.75% in the year 2013 and 7.89% in the year 2014. The storm period had a higher percentage EPB occurrence than the quiet period and was attributed to the effect of prompt penetration electric field (PPEF) which is enhanced during storms, hence increasing the vertical  $\mathbf{E} \times \mathbf{B}$  drift. Seasonal EPB occurrence pattern during quiet and disturbed geomagnetic period was also brought out with March equinox having higher percentage EPB occurrence of 33.33% in the year 2013 and 30.76% in the year 2014 while June solstice had the lowest percentage of EPB occurrence with 6.67% in the year 2013 and 7.69% in the year 2014. In conclusion, this study confirms the presence of EPBs over Kisumu, Kenya in both quiet and storm days of 2013 and 2014. This study was limited to data from a single SCINDA-GPS station in Kenya, hence future work should involve more SCINDA stations in East Africa and an extension of this study should involve correlation between ROTI daily variability of  $\mathbf{E} \times \mathbf{B}$  vertical plasma drift and F2 layer changes.

## TABLE OF CONTENTS

|                                        |          |
|----------------------------------------|----------|
| DECLARATION.....                       | ii       |
| COPYRIGHT .....                        | iii      |
| DEDICATION.....                        | iv       |
| ACKNOWLEDGEMENT.....                   | v        |
| ABSTRACT.....                          | vi       |
| LIST OF TABLES.....                    | x        |
| LIST OF FIGURES.....                   | xi       |
| LIST OF ABBREVIATIONS.....             | xiii     |
| LIST OF SYMBOLS.....                   | xv       |
| <b>CHAPTER ONE.....</b>                | <b>1</b> |
| <b>INTRODUCTION.....</b>               | <b>1</b> |
| 1.0 Background information.....        | 1        |
| 1.1 Statement of the Problem.....      | 6        |
| 1.2 Objectives.....                    | 6        |
| 1.3 Justification of the Study.....    | 7        |
| 1.4 Scope and Limitations .....        | 7        |
| <b>CHAPTER TWO.....</b>                | <b>8</b> |
| <b>LITERATURE REVIEW.....</b>          | <b>8</b> |
| 2.0 Background Information.....        | 8        |
| 2.1 The ionosphere.....                | 8        |
| 2.2 Total Electron Content.....        | 9        |
| 2.3 Amplitude Scintillation Index..... | 12       |
| 2.4 Geomagnetic storms.....            | 14       |
| 2.4.1 Geomagnetic storm indices.....   | 14       |
| 2.4.1.1 Kp index.....                  | 14       |
| 2.4.1.2 Dst index.....                 | 15       |
| 2.5 Equatorial plasma bubbles.....     | 16       |

|                                                                                            |    |
|--------------------------------------------------------------------------------------------|----|
| <b>CHAPTER THREE</b> .....                                                                 | 22 |
| <b>MATERIALS AND METHODS</b> .....                                                         | 22 |
| 3.0 Introduction.....                                                                      | 22 |
| 3.1 Data sources.....                                                                      | 22 |
| 3.2 Methods.....                                                                           | 24 |
| 3.2.1 Establishing TEC depletions.....                                                     | 25 |
| 3.2.2 Investigating ROT and ROTI.....                                                      | 25 |
| 3.2.3 Inferring occurrence of EPBs using TEC depletion, S <sub>4</sub> , ROT and ROTI..... | 26 |
| <b>CHAPTER FOUR</b> .....                                                                  | 27 |
| <b>RESULTS AND DISCUSSION</b> .....                                                        | 27 |
| 4.0 Introduction.....                                                                      | 27 |
| 4.1 Establishing TEC depletions.....                                                       | 27 |
| 4.1.1 TEC depletions for selected quiet days of the year 2013.....                         | 27 |
| 4.1.2 TEC depletions for selected quiet days of the year 2014.....                         | 31 |
| 4.1.3 TEC depletions for selected storm days of the year 2013.....                         | 35 |
| 4.1.4 TEC depletions for selected storm days of the year 2014.....                         | 38 |
| 4.2 Investigating ROT and ROTI.....                                                        | 45 |
| 4.2.1 ROT and ROTI plots for selected quiet days of 2013.....                              | 45 |
| 4.2.2 ROT and ROTI plots for selected quiet days of 2014.....                              | 48 |
| 4.2.3 ROT and ROTI plots for selected storm days of 2013.....                              | 50 |
| 4.3.4 ROT and ROTI plots for selected storm days of 2014.....                              | 52 |
| 4.3 Inferring EPB presence using TEC depletion, S <sub>4</sub> , ROT and ROTI.....         | 55 |
| 4.3.1. Inferring EPBs for selected quiet days of 2013.....                                 | 56 |
| 4.3.2 Inferring EPBs for selected quiet days of 2014.....                                  | 58 |
| 4.3.3 Inferring EPBs for selected storm days of 2013.....                                  | 60 |
| 4.3.4 Inferring EPBs for selected storm days of 2014.....                                  | 61 |
| 4.3.5 Percentage occurrence of EPs in the year 2013 and 2014.....                          | 63 |
| 4.3.6 Seasonal occurrence of EPBs in the year 2013 and 2014.....                           | 65 |

|                                                                                                                   |    |
|-------------------------------------------------------------------------------------------------------------------|----|
| <b>CHAPTER FIVE</b> .....                                                                                         | 68 |
| <b>CONCLUSIONS AND RECOMMENDATIONS</b> .....                                                                      | 68 |
| 5.0 Conclusions.....                                                                                              | 65 |
| 5.2 Recommendation for future work.....                                                                           | 70 |
| <b>REFERENCES</b> .....                                                                                           | 71 |
| <b>APPENDICES:</b> .....                                                                                          | 81 |
| APPENDIX I: Sample of VTEC and S <sub>4</sub> filtering script for all PRNS using SQL server<br>2017 program..... | 81 |
| APPENDIX II: Sample of VTEC and S <sub>4</sub> MATLAB plotting code.....                                          | 82 |
| APPENDIX III: Sample of ROT calculating script using SQL server 2017 program.....                                 | 83 |
| APPENDIX IV: Sample of ROT and ROTI MATLAB plotting code.....                                                     | 84 |
| APPENDIX V: Sample of percentage EPB occurrence MATLAB plotting code.....                                         | 85 |
| APPENDIX VI: Sample of seasonal EPB variation MATLAB plotting code.....                                           | 85 |

## LIST OF TABLES

|                                                                                                           |    |
|-----------------------------------------------------------------------------------------------------------|----|
| <b>Table 2.1:</b> Kp index scale.....                                                                     | 15 |
| <b>Table 3.1:</b> Selected quiet days from Dst and Kp index for 2013.....                                 | 23 |
| <b>Table 3.2:</b> Selected quiet days from Dst and Kp index for 2014.....                                 | 23 |
| <b>Table 3.3:</b> Selected storm days from Dst and Kp index for 2013.....                                 | 24 |
| <b>Table 3.4:</b> Selected storm days from Dst and Kp index for 2014.....                                 | 24 |
| <b>Table 4.1:</b> Summary of TEC depletions for selected quiet days of 2013.....                          | 29 |
| <b>Table 4.2:</b> Summary of TEC depletions for selected quiet days of 2014.....                          | 33 |
| <b>Table 4.3:</b> Summary of TEC depletions for selected storm days of 2013.....                          | 37 |
| <b>Table 4.4:</b> Summary of TEC depletions for selected storm days of 2014.....                          | 40 |
| <b>Table 4.5:</b> Summary of TEC depletion, S <sub>4</sub> , ROT and ROTI for quiet days of 2013.....     | 56 |
| <b>Table 4.6:</b> Summary of TEC depletion, S <sub>4</sub> , ROT and ROTI for quiet days of 2014.....     | 58 |
| <b>Table 4.7:</b> Summary of TEC depletion, S <sub>4</sub> , ROT and ROTI for disturbed days of 2013...60 |    |
| <b>Table 4.8:</b> Summary of TEC depletion, S <sub>4</sub> , ROT and ROTI for disturbed days of 2014...61 |    |
| <b>Table 4.9:</b> Summary of percentage EPB occurrence for the year 2013 and 2014.....                    | 63 |
| <b>Table 4.10:</b> Seasonal Variation of EPBs for 2013-2014 period.....                                   | 66 |

## LIST OF FIGURES

|                                                                                                               |    |
|---------------------------------------------------------------------------------------------------------------|----|
| <b>Figure 1.1:</b> TEC plot from a GPS observing station at Abidjan, Cote d'Ivoire.....                       | 2  |
| <b>Figure 1.2:</b> Depiction of the different layers of Earth's ionosphere.....                               | 3  |
| <b>Figure 2.1:</b> Sample of TEC depletions and $S_4$ .....                                                   | 10 |
| <b>Figure 2.2:</b> Dst index plot for April 2014.....                                                         | 15 |
| <b>Figure 2.3:</b> The temporal development of EPB in equatorial ionosphere.....                              | 17 |
| <b>Figure 2.4:</b> N-S cross-section of F-region equatorial anomaly peaks for two different<br>sunspots ..... | 18 |
| <b>Figure 3.1:</b> GPS-SCINDA system component.....                                                           | 22 |
| <b>Figure 4.1.1:</b> VTEC and $S_4$ plots for selected quiet days between Jan-Dec 2013.....                   | 28 |
| <b>Figure 4.1.1.1:</b> TEC depletion depth & $S_4$ plot for selected quiet days of 2013.....                  | 30 |
| <b>Figure 4.1.2:</b> VTEC and $S_4$ plots for selected quiet days between Jan-Dec. 2014.....                  | 32 |
| <b>Figure 4.1.2.1:</b> TEC depletion depth & $S_4$ plot for selected quiet days of 2014 .....                 | 34 |
| <b>Figure 4.1.3:</b> VTEC and $S_4$ plots for selected storm days between March-Dec. 2013.....                | 36 |
| <b>Figure 4.1.3.1:</b> TEC depletion depth & $S_4$ plot for selected storm days of 2013.....                  | 38 |
| <b>Figure 4.1.4:</b> VTEC and $S_4$ plots for selected disturbed days between Feb-Nov. 2014....               | 39 |
| <b>Figure 4.1.4.2:</b> TEC depletion depth & $S_4$ plot for selected storm days of 2014.....                  | 42 |
| <b>Figure 4.2.1:</b> ROT and ROTI plots for selected quiet days between March-Nov. 2013....                   | 46 |
| <b>Figure 4.2.2:</b> ROT and ROTI plots for selected quiet days between Jan-Dec. 2014.....                    | 49 |
| <b>Figure 4.2.3:</b> ROT and ROTI plots for selected storm days between Jan-Dec. 2013.....                    | 51 |
| <b>Figure 4.2.4.1:</b> ROT and ROTI plots for selected storm days between Feb-Oct. 2014....                   | 54 |
| <b>Figure 4.3.1:</b> TEC depletion depth & ROTI plots for selected quiet days of 2013 .....                   | 57 |
| <b>Figure 4.3.2:</b> TEC depletion depth & ROTI plots for selected quiet days of 2014 .....                   | 59 |

|                                                                                             |    |
|---------------------------------------------------------------------------------------------|----|
| <b>Figure 4.3.3:</b> TEC depletion depth & ROTI plots for selected storm days of 2013 ..... | 61 |
| <b>Figure 4.3.4:</b> TEC depletion depth & ROTI plots for selected storm days of 2014 ..... | 62 |
| <b>Figure 4.3.5:</b> Bar graph of percentage EPB occurrence for 2013 and 2014.....          | 64 |
| <b>Figure 4.3.6:</b> Bar graph showing seasonal variation of EPBs for 2013-2014.....        | 66 |

## LIST OF ABBREVIATIONS

|        |                                               |
|--------|-----------------------------------------------|
| AFRL   | Air Force Research Laboratory                 |
| AR     | Active Regions                                |
| CMEs   | Coronal Mass Ejections                        |
| DDEF   | Disturbance Dynamo Electric Field             |
| Dst    | Disturbance Storm Time                        |
| EIA    | Equatorial Ionization Anomaly                 |
| EM     | Electromagnetic                               |
| EPBs   | Equatorial Plasma Bubbles                     |
| GNSS   | Global Navigation Satellite system            |
| GPS    | Global Positioning System                     |
| HF     | High Frequency                                |
| HSA    | High Solar Activity                           |
| IDD    | Ionospheric Disturbance Dynamo                |
| IMF    | Interplanetary Magnetic Field                 |
| Kp     | Planetary K- index                            |
| LISN   | Low Latitude Ionospheric Network              |
| LSA    | Low Solar Activity                            |
| LT     | Local Time                                    |
| LTE    | Localized TEC Enhancement                     |
| MATLAB | Matrix laboratory                             |
| NASA   | National Aeronautics and Space Administration |
| nT     | nano-Tesla                                    |
| PPEF   | Prompt Penetration Electric Field             |
| Psn    | Position                                      |
| PRE    | Pre-reversal Enhancement                      |
| PRN    | Pseudo Random Number                          |
| RINEX  | Receiver Independent Exchange Format          |
| UoN    | University of Nairobi                         |
| ROT    | Rate of Change of TEC                         |

|        |                                    |
|--------|------------------------------------|
| ROTI   | Rate of Change of TEC Index        |
| RTI    | Rayleigh-Taylor Instability        |
| Scn    | Scintillation                      |
| SCINDA | Scintillation Network Decision Aid |
| SEUV   | Solar Extreme Ultra Violet         |
| Sfu    | Solar Flux Units                   |
| SSN    | Smoothed Sunspot Number            |
| TEC    | Total Electron Content             |
| TECU   | Total Electron Content Units       |
| TV     | Television                         |
| UHF    | Ultra High Frequency               |
| UT     | Universal Time                     |
| UV     | Ultraviolet                        |
| VHF    | Very High Frequency                |
| VTEC   | Vertical Total Electron Content    |

## LIST OF SYMBOLS

|                |                                                                             |
|----------------|-----------------------------------------------------------------------------|
| H              | Hydrogen                                                                    |
| He             | Helium                                                                      |
| N              | Nitrogen                                                                    |
| $S_4$          | Amplitude Scintillation                                                     |
| I              | Signal Intensity                                                            |
| f              | Frequency of Transmission Signal                                            |
| C              | Speed of light in m/s                                                       |
| l              | Position                                                                    |
| D, E & F       | Layers of Ionosphere                                                        |
| F1 & F2        | Sub-layers of F layer of Ionosphere                                         |
| m              | Metre                                                                       |
| $n_e(l)$       | Variable electron density along the path from the satellite to the receiver |
| dl             | Change in the distance between the receiver and the satellite               |
| O <sub>2</sub> | Oxygen                                                                      |
| $\leq$         | Less than or equal to                                                       |
| $\geq$         | Greater than or equal to                                                    |
| %              | Percentage                                                                  |

## CHAPTER ONE

### INTRODUCTION

#### 1.0 Background information

The Sun produces highly energetic particles such as X-rays and Ultraviolet (UV) radiations (Milos, 2014), all of which are lethal to living things. These dangerous particles are shielded from penetrating to the Earth by the Ozone layer, atomic Nitrogen (N) and Oxygen (O<sub>2</sub>) through absorption by atoms and air molecules and the magnetosphere. The continuous streaming of highly energetic particles from the Sun when it erupts and explodes are blocked by being depleted as they collide with atoms and molecules in the air when they enter the Earth's atmosphere (Eddy, 2009). Increased solar activity can lead to large release of coronal mass ejections (CME) and solar flares that when they reach the Earth, can cause a change in Total Electron Content (TEC) in the ionosphere. TEC is the total number of electrons in a column of 1 m<sup>2</sup> cross-section extending from a GPS receiver to a GPS satellite (Murkherjee *et al.*, 2010; Adewale *et al.*, 2012; Radicella, 2012; Ndeda & Odera, 2014; Magdaleno *et al.*, 2017). TEC is measured in TEC units (TECU) where 1 TECU is equal to 10<sup>16</sup> electrons per m<sup>2</sup>. Changes in TEC causes heightened levels of hazards in the Earth-space environment, storms and disruption, generation of strong electric currents in the atmosphere and changes in the reflective properties of the ionosphere (Kamide & Chian, 1997). Figure 1.1 shows a sample of a TEC plot obtained from a Global positioning system (GPS) station at Abidjan–Côte d'Ivoire. It shows dominant diurnal TEC variation with time during near solstice period.

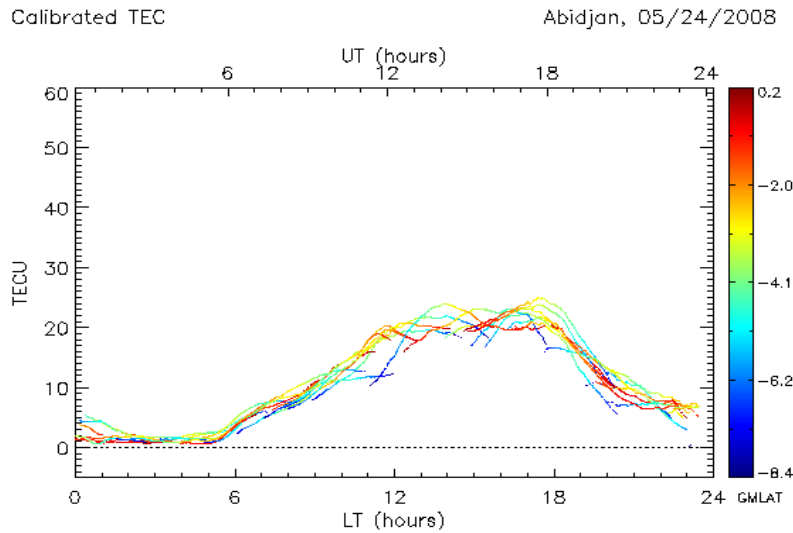


**Figure 1.1: A sample TEC plot from a GPS observing station located at Abidjan – Côte d’Ivoire (Groves *et al.*, 2009)**

The Sun is the ultimate source of space weather. Space weather refers to the short-term or long-term variability in the plasma environment of the Earth and other planets (Kamide & Chian, 2007). This variability usually affects performance and reliability of both space-based and ground-based technological systems. The Sun produces Electromagnetic (E.M) radiations, flares and eruptions of material including CME moving along with solar energetic particles (Eastwood *et al.*, 2017). The ionosphere plays a very important role in all these impacts (Wang *et al.*, 2018) since all signals coming from satellites have to pass through it on their way towards the Earth. The ionosphere can therefore change the shape, direction and speed of the signal (Milos, 2014). It shows marked variations in solar cycle and magnetic activity, longitude and latitude, season and the universal time which are all brought out in all ionospheric properties, electron density and ionospheric dynamics (Radicella, 2012). The effects of solar activity on Earth range from national, commercial and personal concerns: satellite telephone calls, space lift, national security, internet

banking, television (TV) reception, ground transport, petroleum pipeline transport and electrical power transmission (Schrijver *et al.*, 2015).

The ionosphere is the ionized portion of the atmosphere made up of positive ions and free electrons and it stretches from a height of about 50 km to 1000 km (Hunsucker & Hargreaves, 1995; Misra & Enge, 2001; Ndeda & Odera, 2014). It consists of three layers, which enable long distance radio wave propagation around the Earth (Rabiu *et al.*, 2007; Milos, 2014). These layers are designated as: D-layer which lies within 50-90 km, E-layer which lies within 90-150 km and F-layer which lies within 150-1000 km from lowest to the highest as shown in Figure 1.2.

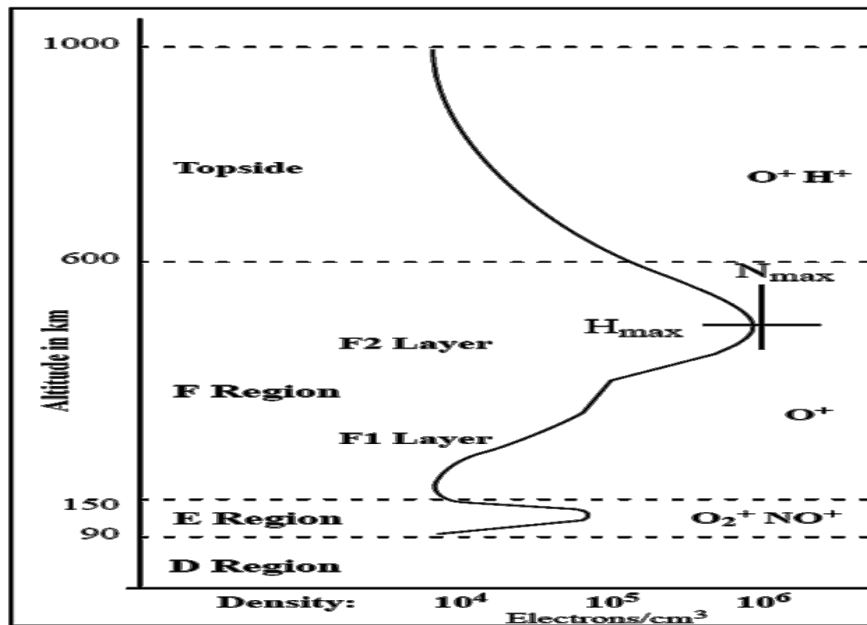


**Figure 1.2:** Depiction of the different layers of Earth's ionosphere (Anderson & Rowell, 1999)

The UV radiation from the sun causes ionization of the atmospheric gases resulting in a build-up of charges during the day. At night, recombination occurs between the positive ions and the electrons leading to thinning and subsequent disappearance of the sporadic E layer and the D layer shortly before midnight (Anderson & Rowell, 1999; Milos, 2014).

During the day, the F layer splits into two layers F1, about 170 km and F2, about 250 km altitude but at night, F1 layer diminishes and leaves F2 layer which persists throughout the night. The F-layer's lower regions rapidly recombine faster than its upper regions after sunset leading to a situation known as Rayleigh-Taylor Instability (RTI) (Haerendel, 1973; Kelley, 2009). RTI is an unstable condition where a heavy fluid is held on top of a lighter fluid (Adewale *et al.*, 2012) leading to bubbles of low density plasma being formed and pushed upwards to the upper denser regions. Smaller irregularities known as plasma bubbles starts forming as the bubbles grows. Equatorial plasma bubbles (EPBs) (Muella *et al.*, 2017; Barros *et al.*, 2018) are irregular plasma density depletions in the ambient electron density in the equatorial F-region ionosphere (Woodman & LaHoz, 1976) usually generated after sunset. They rise vertically and drift up for some hours with their dynamics following the generalized (non-linear) RTI in the bottomside of the F-layer (Otto, 1978). Once the instability has been set off, density irregularities begin to develop and field aligned depletions moves up through the F layer (Schunk & Nagy, 2009; Paznukhov *et al.*, 2012; D'ujanga & Taabu, 2014).

Scientists have carried out studies on the physical processes that take place in the ionosphere leading to the occurrences of EPBs using the Global Navigation satellites systems (GNSS). GPS has been used widely in these studies due its accurate consistent performance worldwide (Makela *et al.*, 2004; Paznukhov *et al.*, 2012; Adewale *et al.*, 2012; Magdaleno *et al.*, 2017; Eyalade *et al.*, 2017; Eastwood *et al.*, 2017; Barros *et al.*, 2018). In these studies, TEC is the key parameter (Fayose *et al.*, 2012; Wang *et al.*, 2018) that has been very useful in the mitigation of ionospheric effects on radio systems. Makela *et al.*, (2004) analyzed seasonal variation of EPB occurrence from Haleakala, Hawaii

between January 2002 and August 2003 (near solar maximum) period using both Airglow and GPS data. They found that the probability for EPB development was 45% in April and 83% in September. Adewale *et al.*, (2012) in a study carried out with a GPS station in Lagos, Nigeria, showed the presence of large scale depletions of TEC after sunset and the depletions of TEC corresponded well with increased fluctuation of rate of change of TEC. Paznukhov *et al.*, (2012) carried out a study on occurrence of EPBs in Africa during solar minimum and their results showed increased rate of EPB occurrence in June solstice. They observed that seasonal occurrence of EPBs tended to shift towards summer with fewer occurrences in equinox seasons. Magdaleno *et al.*, (2017) used GPS data to study climatology characterization of EPBs between 1998-2008 using 67 international GNSS stations around the geomagnetic Equator and the obtained results on spatial analysis of EPBs showed that the largest EPB occurrence rate was at the Dip Equator in South American sector of the ionosphere but decreased as the distance from magnetic equator increased. Barros *et al.*, (2018) studied the characteristics of EPBs using ground based network of more than 220 GNSS ground based receivers by mapping TEC over South-America between November 2012 and January 2016 for both quiet and disturbed days. Their results showed that EPBs occurred majorly between September to March.

Despite recent studies on characterization and occurrence of EPBs having been carried out in the equatorial regions, more research needs to be done within East Africa in order to bring out the ionospheric dynamics over the region, since the ionosphere is highly dynamic and changes from region to region. This study covered TEC depletion,  $S_4$  index, Rate of change of TEC (ROT) and Rate of change of TEC Index (ROTI) in inferring EPB

occurrence for the selected quiet and storm days between 1<sup>st</sup> January 2013 and 31<sup>st</sup> December 2014, which was a high solar activity period for solar cycle 24.

### **1.1 Statement of the Problem**

The ionosphere is a highly variable medium resulting from ionizing radiation from the Sun. It is the main source of range errors for satellite-based radars and GNSS operating near equatorial regions due to frequent occurrence of plasma density irregularities that leads to degradation of GPS signals. The problem in this study was to investigate the occurrence of EPBs over Kisumu, Kenya during selected quiet and disturbed (storm) days from 1<sup>st</sup> January 2013 to 31<sup>st</sup> December 2014, which was a high solar activity period for solar cycle 24 using TEC and amplitude scintillation ( $S_4$ ) data.

### **1.2 Objectives**

The main objective of this study was to investigate the occurrence of Equatorial plasma bubbles over Kisumu, Kenya between 1<sup>st</sup> January 2013 and 31<sup>st</sup> December 2014 using SCINDA-GPS receiver.

#### **1.2.1 Specific Objectives**

The Specific objectives of this study were:

- i) To establish the occurrence of TEC depletions and amplitude scintillations over Kisumu, Kenya between 1<sup>st</sup> January 2013 and 31<sup>st</sup> December 2014 for selected storm and quiet days.
- ii) To investigate the rate of change of TEC (ROT) and rate of change of TEC Index (ROTI) for selected storm and quiet days between 1<sup>st</sup> January 2013 and 31<sup>st</sup> December 2014.

- iii) To infer the occurrence of EPBs over Kisumu, Kenya between 1st January 2013 and 31<sup>st</sup> December 2014 period using TEC depletion, S<sub>4</sub> index, ROT and ROTI.

### **1.3 Justification of the Study**

The study of EPBs is needed so as to be able to relate the extent of ionospheric irregularities to the possible disruptions of High Frequency (HF) communication signals as implied by S<sub>4</sub>. This has important implications for the navigation and communications sectors. Kisumu is a transport and commercial hub hosting the Kisumu international airport and various telecommunication facilities. The details of ionospheric dynamics, particularly on the occurrence of EPBs and their impact on GPS systems which is the focus of this study is vital in ensuring safety in the aviation industry and reliability in the telecommunication systems in the region.

### **1.4 Scope and Limitations**

The study was confined to a period of only two years (1<sup>st</sup> Jan. 2013 to 31<sup>st</sup> Dec. 2014). This was a high solar activity period for solar cycle 24 which had a maximum Smoothed Sunspot number (SSN) of 81.9 (Schrodet *et al.*, 2017). There were some data gaps due to frequent power outages at the Kisumu SCINDA-GPS station. However these data gaps did not affect the results.

The main limitation of this study was that it relied on data from only one SCINDA-GPS receiver.

## CHAPTER TWO

### LITERATURE REVIEW

#### 2.0 Background Information

In this chapter an overview on the ionosphere, the use of GPS to study TEC, ionospheric scintillations, geomagnetic storms and occurrence of EPBs is discussed and a review of various studies in this area presented.

#### 2.1 The ionosphere

The ionosphere is the ionized portion of the atmosphere extending from about 50km to 1000km. Photoionization of neutral molecules through solar Extreme Ultra-Violet (SEUV) and soft X-ray radiations is the main source of ionospheric plasma (Anderson & Rowell, 1999; Schunk & Nagy, 2009). The produced ions undergo chemical reactions, recombine with electrons, are transported by neutral winds or diffuse to either lower or higher altitudes. The Earth's magnetic field which is dipolar at ionospheric latitudes strongly influences these transport and diffusion effects (Schunk & Naggy, 2009). At low latitudes, some unique transport effects are introduced nearly horizontal to geomagnetic field lines. One of the transport effects includes the meridional neutral winds which induces inter-hemispherical plasma flow along horizontal field lines. The other transport effect is the equatorial fountain which is associated with neutral winds induced currents which are eastward during the day and lifts plasma upwards, diffuses it down the magnetic field lines and moves it away from the equator due to action of gravity and pressure gradients forces (Schunk & Nagy, 2009). As much as different processes are seen to dominate in the different latitudinal domains, electron density variation is displayed by the electron density profile made up of the D, E, F1 and F2 layers. The F2 layer is the most important in

satellite communication since electron concentrations reach their highest (Anderson & Rowell, 1999).

The low latitude and high latitude F- region ionosphere at certain local times may become highly turbulent due to the presence of small scale irregularities known as ionospheric scintillations. In the high latitudes these irregularities occur at any time (day or night) but in the low latitude region, they are generated after sunset and last for several hours (Anderson & Rowell, 1999). These irregularities seriously affect radio waves as they propagate through the ionosphere (Milos, 2014).

## **2.2 Total Electron Content (TEC)**

TEC is the total number of electrons in a column of  $1\text{m}^2$  between a GPS satellite and a GPS receiver. TEC is a key parameter that has been used to depict the charge densities of various ionospheric layers (Ya'a cob *et al.*, 2010; Fayose *et al.*, 2012; Wang *et al.*, 2018). Electron concentration increases with solar intensity and hence there is an increased TEC during equinoxes (when the Earth is highly exposed to the Sun) (Dieter, 2001). TEC is the integral of electron density along the ray path between the receiver and the satellite expressed as,

$$TEC = \int_{l_1}^{l_2} n_e(l) dl \quad (2.1)$$

where  $l_1$  and  $l_2$  are the positions of the receiver and the satellite respectively,  $n_e(l)$  is the variable electron density along the path from the satellite to the receiver and  $dl$  is the change in the distance between the receiver and the satellite (Misra & Enge, 2001). TEC depletions are sudden decreases in the TEC value lasting for about 10 to 60 minutes and

are mostly followed by a TEC enhancement (a recovery of TEC) just after the depletion as indicated by the arrows in Figure 2.1. They are mostly produced by plasma bubbles between the GPS satellite and receiver (Dashora & Pandey, 2005; Seemala & Valladares, 2011).

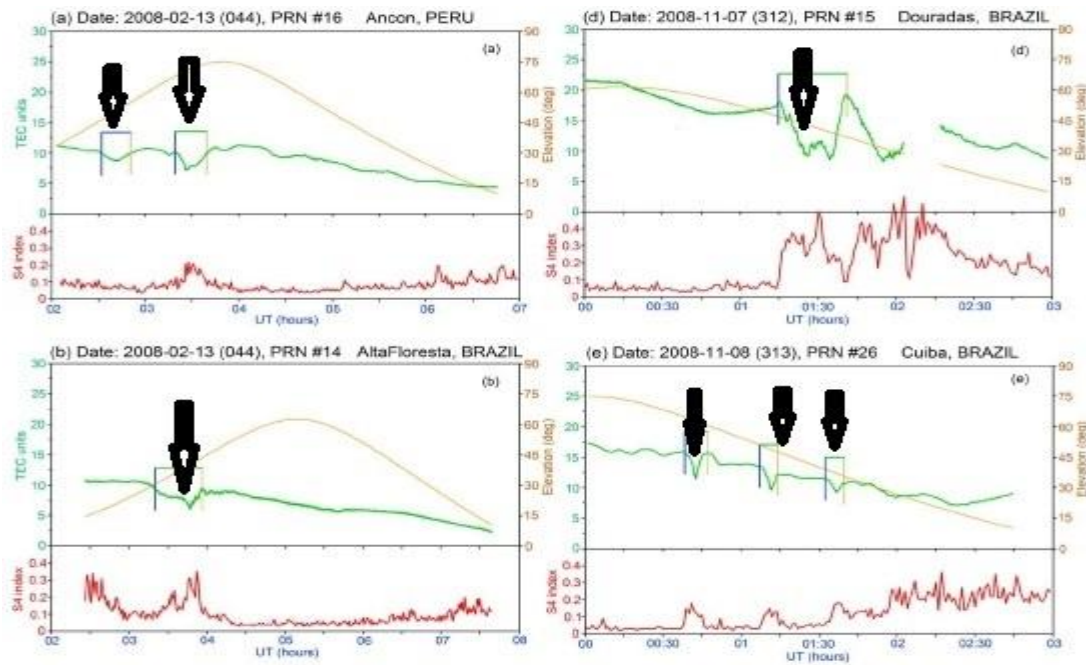


**Figure 2.1: Sample of TEC depletions and S<sub>4</sub> (Seemala & Valladares, 2011)**

Seemala and Valladares, (2011) studied TEC depletions over the continent of South America in 2008 using Low Latitude Ionospheric Network (LISN). TEC depletions having periods between 10 and 120 minutes were observed and were accompanied by stronger levels of scintillations. The characteristics of TEC depletion development were related with the onset of plasma bubbles in the equatorial F-layer ionosphere after sunset.

Olwendo *et al.*, (2012) studied TEC depletions and enhancement over Kenya using SCINDA-GPS located at University of Nairobi (UoN) for March 2011. Their results showed TEC depletions having a good correspondence with S<sub>4</sub> index patches. However the observed TEC enhancements did not correlate with increases in S<sub>4</sub> index. They interpreted

TEC depletions as plasma irregularities and TEC enhancement as appearances of plasma density enhancements which were connected with the equatorial ionization anomaly crest over the region.

ROT is the change of TEC per unit time. It is used to trace the ionospheric irregularities level (disturbance of the ionosphere) and is obtained by equation 2.2 (Pi *et al.*, 1997).

$$ROT = \frac{TEC_t - TEC_{t-1}}{\Delta t} \quad (2.2)$$

where,  $\Delta t$  = time range in minutes

t and t-1 = time difference between the epochs in minutes

ROTI is the standard deviation of ROT over time interval, obtained as in equation 2.3.

That is,

$$ROTI = \sqrt{\langle ROT^2 \rangle - \langle ROT \rangle^2} \quad (2.3)$$

ROTI provides spatial variation of electron density (Pi *et al.*, 1997; Bhattacharrya *et al.*, 2000; Jacobsen, 2014).

ROT and ROTI are parameters that are extensively used for the determination of occurrence and characterization of ionospheric plasma irregularities (plasma bubbles) (Pi *et al.*, 1997; Nishioka *et al.*, 2008; Adewale *et al.*, 2012; Jacobsen, 2014).

Studies done by Nishioka *et al.*, (2008) on the occurrence characteristics of plasma bubbles using 23 GPS ground based receivers from 2000 to 2006 indicated that plasma bubbles caused TEC depletions, increased ROT fluctuations and high ROTI values between sunset and midnight. The plasma bubbles detected in TEC data and the ROTI observed corresponded well for all satellites.

Azzouzi *et al.*, (2016) studied the variability of ROTI and VTEC with impact of a high-speed solar wind stream on 13<sup>th</sup> October 2012. They used ROTI as indicator of ionospheric scintillation for the impact of very high-speed solar wind stream in the low and middle latitude ionosphere. They observed that the arrival of CMEs led to an increase in VTEC depletion, hence high ROTI which then decreased after the impact. They attributed the increase in VTEC depletion to be due to the physical process of PPEF and a reduction in VTEC to DDEF.

### 2.3 Amplitude scintillation index ( $S_4$ )

Amplitude scintillation index is defined as the ratio of the standard deviation of signal intensity and the averaged signal intensity (Briggs & Parkin, 1963) and given as,

$$S_4 = \sqrt{\frac{\langle I^2 \rangle - \langle I \rangle^2}{\langle I \rangle^2}} \quad (2.4)$$

where,  $I$  represents the signal intensity (amplitude squared).

$S_4$  is interpreted as the fractional fluctuation of the signal resulting from ionospheric modulation. The  $S_4$  values approaching 0 shows non-existence of scintillation (hence does not affect the signal) while  $S_4$  less than 0.3 usually indicates weak scintillation.  $S_4$  values lying between 0.3 and 0.6 show presence of moderate scintillations while  $S_4$  values that are more than 0.6 indicates a strong scintillation (which affects GPS signals) (Humphreys *et al.*, 2010; Akala *et al.*, 2016). Most receivers are affected by loss-of-lock which may last up to about one hour when  $S_4$  index attains large values. This leads to severe disturbance on communication and navigation link.

D'ujanga & Taabu, (2014) studied characteristics of ionospheric scintillations over East Africa using SCINDA-GPS and VHF spaced receivers at UoN in 2011 and Makerere University in 2012. The percentage occurrence of scintillations at both frequencies exhibited a seasonal dependence:  $S_4$  index were higher in equinoctial months than in other months. Intense scintillations were observed in 2011 than in 2012 and this was due to the intense geomagnetic storms and higher solar activity in October 2011.

Akala *et al.*, (2016) investigated GPS scintillation over Kampala, Uganda between 2010 and 2011 using SCINDA-GPS receiver. The results indicated that amplitude scintillations occurred mostly after sunset and decayed around midnight. Highest occurrence was in equinoctial months while low occurrence was in June solstice. Scintillation occurrences increased with increase with geomagnetic and solar activity.

Muella *et al.*, (2017) studied ionospheric scintillations at the equatorial anomaly crest region using a GNSS station at Cachoera Paulista, Brazil between 1997 and 2014. The obtained results revealed maximum scintillation occurrence in the December solstice. This was attributed to a large magnetic declination angle over the region. The largest occurrence was 80% in 2001-2002 (solar maximum of solar cycle 23) and began subsiding after 2002 to 2009 with decrease in solar activity. The decrease in frequency was due to the suppression of the fountain effect and the anomalous reduction in the background electron density observed at the equatorial ionization anomaly region.

Alagbe *et al.*, (2017) in a study on the effect of geomagnetic activity on amplitude scintillation in 2012 at low latitude region in Ilorin, Kwara state, Nigeria observed that  $S_4$  occurrences were higher during quiet days than storm day. The  $S_4$  occurrences were seen

to be enhanced during pre-midnight hours but were hindered during post-midnight hours for both quiet and storm days.

## 2.4 Geomagnetic storms

A geomagnetic storm is a disturbance of the Earth’s magnetic field (Kamide & Chian, 2007). It develops when the Sun’s surface (Corona) erupts and sends large streams of its matter in form of CMEs away at very high speeds towards the Earth’s surface (Gonzalez *et al.*, 1994). Geomagnetic storms block radio communications and disrupt power systems on the Earth’s surface (Schwenn, 2006; Gonzales-Hernandez *et al.*, 2016).

### 2.4.1 Geomagnetic storm indices

Geomagnetic storm indices are used to measure the strength of geomagnetic storms. Some of the widely used scales include the planetary K (Kp) index and the Disturbance storm time (Dst) index.

#### 2.4.1.1 The Kp index

Kp index is a geomagnetic storm index based on 3 hour measurements of Kp indices for each of the past days and is obtained from magnetometer stations at mid-latitudes (Bartels *et al.*, 1939). It can be used to measure the strength of geomagnetic storm. It gives indicators of the severity of the disturbance of the ionosphere and is determined by averages ranging from 0 to 9 where 0 means very little geomagnetic activity while 9 means extreme geomagnetic activity (Bartels *et al.*, 1939) as indicated in Table 2.1.

**Table 2.1: Kp index ([www.swpc.noaa.gov/NOAAscales](http://www.swpc.noaa.gov/NOAAscales)), accessed on 27<sup>th</sup> January 2019**

| K <sub>p</sub> Scale | 0     | 1     | 2     | 3          | 4      | 5           | 6              | 7            | 8            | 9             |
|----------------------|-------|-------|-------|------------|--------|-------------|----------------|--------------|--------------|---------------|
| Activity             | Quiet | Quiet | Quiet | Un-settled | Active | Minor storm | Moderate storm | Strong storm | Severe storm | Intense Storm |

### 2.4.1.2 The Dst index

Dst index gives information on the strength of the ring current caused by solar protons and electrons around the Earth (Sugiura, 1964). It estimates the globally averaged change of the horizontal component of the magnetic field of the Earth at the magnetic equator from a few magnetometer stations near the equator. It is computed once per hour and reported in near real time. Storm days are identified by checking for days having Dst values below -50 nT. A sample of a Dst index plot for April 2014 is in Figure 2.2.



**Figure 2.2:** Dst Index plot for April 2014 ([wdc.kugi.kyoto.u.ac.jp/dst-final/index.html](http://wdc.kugi.kyoto.u.ac.jp/dst-final/index.html)), accessed on 27<sup>th</sup> January 2019

A study on the effects of geomagnetic storm on GPS derived TEC was reported by Kumar and Singh (2010) at Varanasi in India during two storms which occurred on 20<sup>th</sup> November 2007 and 9<sup>th</sup> March 2008. They observed an increase in TEC during the geomagnetic storm period.

Edemsky *et al.*, (2018) investigated ionospheric effects during a moderate geomagnetic storm of 15<sup>th</sup> August 2015 which was caused by the CMEs of 12<sup>th</sup> August 2015 and observed a localized TEC enhancement (LTE) centred to the southward of Africa.

Bhattacharrya *et al.*, (2019) in the study on how magnetic storms and thermospheric changes affect occurrence of EPBs, observed that despite the occurrence of EPBs having been largely controlled by the presence of disturbance dynamo electric fields (DDEF) and

prompt penetration electric field (PPEF) during storm days, the thermospheric changes in the concentration of atomic oxygen in the F region in the aftermath of a geomagnetic storm also affected the maximum height to which EPBs rose.

Bolaji *et al.*, (2019), characterized ionospheric irregularities at different longitudes during disturbed and quiet geomagnetic conditions in March 2015. They observed that geomagnetic storms did not inhibit the development of irregularities in all the stations under study in the American sector. However in the African sector, the storm appeared to hinder development of irregularities during storm days in all stations. This was attributed to differences in storm timing and the effects of PPEF and DDEF.

### **2.5 Equatorial Plasma Bubbles (EPBs)**

EPBs are irregular plasma density depletions in the ambient electron density in the equatorial F-region ionosphere often generated after sunset. The Rayleigh-Taylor instability (RTI) (Michael, 2009; Zhang *et al.*, 2015; Muella *et al.*, 2017) which develops shortly after sunset causes an unstable ionospheric condition where the lower F-region moves upward into the higher F-region, creating a bubble which forms and rises to the top part of the F region ionosphere and is ‘frozen’ into the moving ionosphere. These frozen structures in the moving ionosphere are known as the plasma bubbles (Olowendo *et al.*, 2012; Paznukhov *et al.*, 2012). Figure 2.3 shows EPB formation stages: (a), (b), (c) and (d).

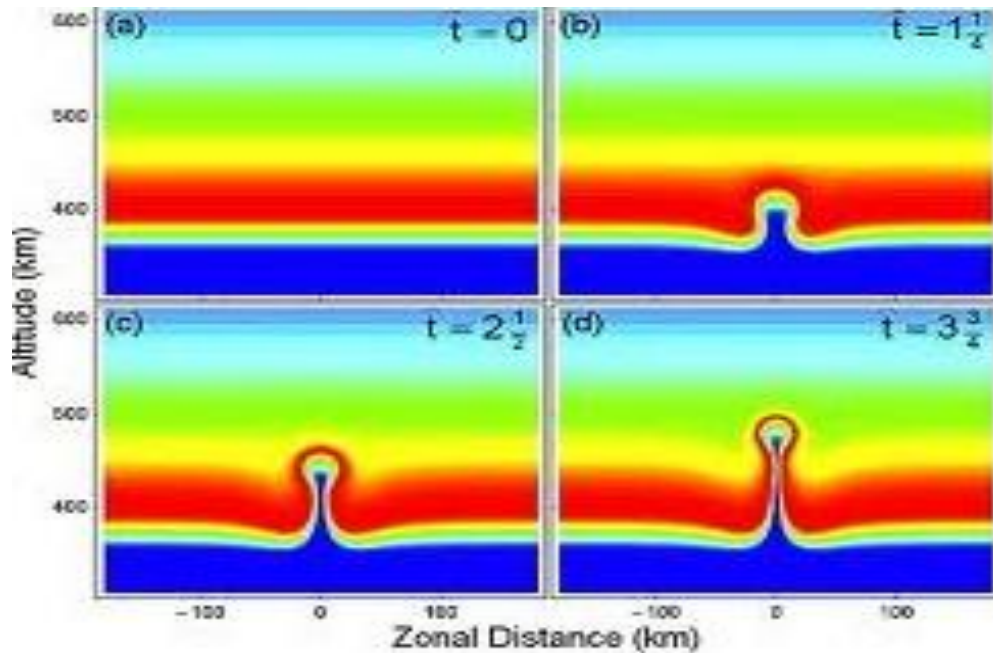


**Figure 2.3: The temporal development of the equatorial plasma bubbles within the Ionosphere (Bernhardt, 2007)**

EPBs bring disruptions to telecommunication and navigation systems (Paznukhov *et al.*, 2012) which hinders real-time and accurate transfer of information between distant regions (Datta-Barua *et al.*, 2003; Carrano & Groves, 2010) through serious signal damping leading to inaccurate or no position information in GPS receivers at all. The plasma interchange instabilities in the equatorial ionosphere after sunset usually generate large-scale depletions in the ambient electron density. During the day, the dynamo electric fields which are generated by thermospheric winds in the equatorial E region are propagated to the F-region altitudes along the magnetic field lines. These dynamo electric fields are usually eastward during the day and brings an increase in the upward  $\mathbf{E} \times \mathbf{B}$  plasma drift (Omondi *et al.*, 2014; D’ujanga & Taabu, 2014; Adetayo *et al.*, 2017; Caruana *et al.*, 2018) that diffuses down the magnetic field lines and moves away from the equator due to the action of gravity and pressure gradient force. This upward  $\mathbf{E} \times \mathbf{B}$  plasma drift results

into the formation of ionization peaks in the sub-tropics on both sides of magnetic equator called the equatorial ionization anomaly (EIA) (Hargreaves, 1992; Basu *et al.*, 1999; DasGupta *et al.*, 2004; Bagiya *et al.*, 2009; Mukherjee *et al.*, 2010; Olwendo *et al.*, 2012; Ndeda & Odera, 2014). Hargreaves, 1992; Basu *et al.*, 1999; Bagiya *et al.*, 2009; Mukherjee *et al.*, 2010; Chauhan *et al.*, 2015). EIA is the occurrence of concentrated ionization in the ionosphere within the regions approximately  $\pm 15^\circ$  of the dip equator (Luhr *et al.*, 2003; DasGupta *et al.*, 2004) and is an important phenomena in the study of scintillations as it is responsible for the formation of plasma density irregularities that give rise to stronger scintillations (DasGupta *et al.*, 2004; Ndeda & Odera, 2014) than at the magnetic equator. Figure 2.4 shows a cross-section of the F-region showing the EIA peaks for two different sunspots numbers.

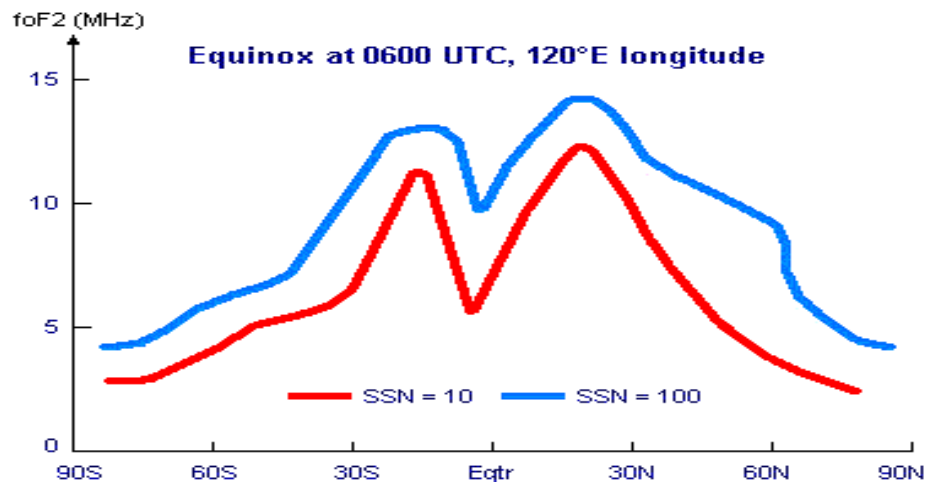


**Figure 2.4: N-S Cross-section of the F- region showing the equatorial anomaly peaks for two different sunspots numbers (Brown, 2012)**

The occurrences of EPBs have greatly been researched on using different techniques since its first observation by Booker & Wells, (1938). Some of the techniques used include:

Ionosondes (Abdu *et al.*, 1981, 2003, 2012), Optical imagers (Pimenta *et al.*, 2003; Arruda *et al.*, 2006; Wiens *et al.*, 2006; Paulino *et al.*, 2011), Global Navigation satellite system receivers (GNSS) (Makela, *et al.*, 2004; De Rezende *et al.*, 2007; Li *et al.*, 2010; Adewale *et al.*, 2012; Paznukhov *et al.*, 2012; Takahashi *et al.*, 2015, 2016; Akala *et al.*, 2016; Magdaleno *et al.*, 2017; Barros *et al.*, 2018), Very High Frequency radars (VHF) (Tsunoda, 1981; Abdu *et al.*, 2009), Satellites (Huang *et al.*, 2001; Mc Namara *et al.*, 2013; Park *et al.*, 2015) and rockets (Abdu *et al.*, 1991). Most of these mentioned techniques are not able to monitor EPBs continuously over a large two dimensional area (Barros *et al.*, 2018). For example, the VHF radar, all-sky-imager and Ionosonde cannot cover a wide range even though they can monitor EPBs at high spatial resolution, hence being able to analyze fine structures of EPBs (Abdu *et al.*, 2009). Observations done by Rockets and Satellites produces high spatial resolution ion density profiles but its measurements can only be made in situ (in its original position or place) (Muralikrishna *et al.*, 2007). The only technique that stands out in the monitoring of EPBs by mapping out the depletion of TEC is the ground-based network of GNSS receiver like the one used in this study. This is because observations made with GNSS receivers continuously covers all longitudinal sectors (covers a wide area) with very minimal lack of data (Nishioka *et al.*, 2008).

Makela *et al.*, (2004), carried out a study on seasonal variation of EPB occurrence using airglow and GPS scintillation data over 300 nights from Haleakala volcano in Hawaii between January 2002 and August 2003 which was a period near solar maximum of solar cycle 23. The seasonal trends of occurrence of EPBs in the pacific sector showed high bubble development of 45% in April and 83% in September. The maximum EPB occurrence of 62% was observed between June and October.

Li *et al.*, (2010) in their study on effects of magnetic activity on plasma bubbles over Equatorial and low latitude regions of East Asia, used ROTI based on the ROT within a period of 5 minutes to detect plasma bubbles using TEC data gathered from 3 equatorial ground based GPS stations and 3 low latitude ground based GPS stations between 2001 and 2004. Their results indicated that most plasma bubbles commenced at 20:00 LT and lasted for over 1 hour but in the presence of magnetic activity, the occurrence was suppressed by a time delay of about 3 hours.

Adewale *et al.*, (2012) studied scintillations and TEC depletions at a GPS station in Lagos, Nigeria using a Novatel GSV4004B SCINDA-GPS from February 2010 to August 2010. ROT indices were used to investigate the irregularities and the results showed the presence of some large scale TEC depletions which were taken to be plasma bubbles after sunset and it was established that enhanced  $S_4$  corresponded well with TEC depletions and increased fluctuation in ROT. They observed that despite present studies on scintillations and ionospheric tomography having been carried out in other regions, significant work had not been carried out in the African equatorial region due to scarcity of GPS scintillation data.

Paznukhov *et al.*, (2012) also carried out a study on EPBs and L-band scintillations in Africa in 2010 which was a solar minimum of solar cycle 23 using data from 10 SCINDA-GPS stations distributed around Africa. They employed the spectral analysis method developed by Seemala and Valladares in 2011 to identify EPBs from TEC data. They observed presence of EPBs and scintillations during equinoctial periods whose rate was seen to have increased during June solstice. The seasonal occurrence of EPBs showed higher occurrence in summer solstice and lower occurrences in equinoctial period. Their

results showed that the occurrence of EPBs over Africa had some correspondence with  $S_4$  index.

Barros *et al.*, (2018) studied the characterization of EPBs using a network of over 220 GNSS receivers over South America and observed EPBs by analyzing TEC map data bases for both quiet and disturbed days between November 2012 and January 2016 which was a high solar activity phase for solar cycle 24. The obtained results showed that EPB occurred majorly between September and March.

Bolaji *et al.*, (2019) also investigated the dynamics of ionospheric irregularities at different sectors of world in both quiet and storm periods of March 2015 and the results showed presence of severe irregularities prominent in African and American sectors but rarer in Asian and Oceania sectors. However the strength was seen to reduce eastward.

From the above studies, various techniques have been applied to study the occurrence of EPBs including using airglow and SCINDA data. In this research, we studied the occurrence of EPBs using SCINDA data from a single station. This was done by incorporating TEC depletion,  $S_4$  index, ROT fluctuations and ROTI, for the period between 1<sup>st</sup> January 2013 and 31<sup>st</sup> December 2014, which was a high solar activity period for solar cycle 24.

## CHAPTER THREE

### MATERIALS AND METHODS

#### 3.0 Introduction

In this chapter an overview on data collection from the Scintillation Network Decision Aid- Global Positioning System (SCINDA-GPS) receiver, identifying the quiet and storm days using Dst and Kp indices and analysis procedure using TEC depletion,  $S_4$  index, ROT fluctuation and ROTI is discussed.

#### 3.1 Data sources

Receiver independent exchange format (RINEX) TEC data from 1<sup>st</sup> January 2013 to 31<sup>st</sup> December 2014 was retrieved from the Kisumu high data-rate NovAtel GSV4004B SCINDA-GPS receiver situated at Maseno University (Geomagnetic coordinates: 9.64°S, 108.59°E; Geographic coordinates 0.02°S, 34.6°E).

The high data-rate Novatel GSV4004B GPS receiver is a ground GPS receiver that monitors scintillations caused by electron density irregularities in the ionosphere (Grooves *et al.*, 1997). It has the following 6 components as shown in Figure 3.1.



**Figure 3.1: GPS-SCINDA system component (Carrano, 2007)**

The selected quiet and storm days for 2013 and 2014 from Dst index values were obtained from the link: [www.wdc.kugi.kyoto-ua.ac.jp/dstdir](http://www.wdc.kugi.kyoto-ua.ac.jp/dstdir). The selected quiet days considered in this study were days having Dst values  $> -50\text{nT}$  and having Kp values between 0 and 2 as indicated in Tables 3.1 and 3.2 while the selected storm days were days having Dst values  $\leq -50\text{nT}$  and Kp values between 3 and 9 as indicated in Tables 3.3 and 3.4. The level of the geomagnetic activity was obtained using the Kp index values which were downloaded from the link: [www.kugi.kyoto-ua.ac.jp/kp](http://www.kugi.kyoto-ua.ac.jp/kp).

**Table 3.1: Selected quiet days from Dst and Kp index for 2013, accessed on 27<sup>th</sup> January 2019**

| Month          | Date       | Dst Index (nT) | Maximum Kp Index | Geomagnetic Specification |
|----------------|------------|----------------|------------------|---------------------------|
| March 2013     | 26-03-2013 | -10            | 1                | Quiet                     |
| April 2013     | 18-04-2013 | 0              | 0                | Quiet                     |
|                | 19-04-2013 | 0              | 0                | Quiet                     |
| May 2013       | 10-05-2013 | -5             | 1                | Quiet                     |
| June 2013      | 17-06-2013 | -5             | 1                | Quiet                     |
|                | 26-06-2013 | -6             | 1                | Quiet                     |
| July 2013      | 04-07-2013 | -5             | 1                | Quiet                     |
|                | 24-07-2013 | -5             | 1                | Quiet                     |
| August 2013    | 11-08-2013 | -3             | 0                | Quiet                     |
| September 2013 | 07-09-2013 | -5             | 1                | Quiet                     |
|                | 26-09-2013 | -3             | 0                | Quiet                     |
| November 2013  | 21-11-2013 | -1             | 0                | Quiet                     |

**Table 3.2: Selected quiet days from Dst and Kp index for 2014, accessed on 27<sup>th</sup> January 2019**

| Month          | Date       | Dst Index (nT) | Maximum Kp Index | Geomagnetic Specification |
|----------------|------------|----------------|------------------|---------------------------|
| January 2014   | 16-01-2014 | 0              | 0                | Quiet                     |
| February 2014  | 03-02-2014 | -3             | 0                | Quiet                     |
| March 2014     | 07-03-2014 | -2             | 0                | Quiet                     |
| April 2014     | 16-04-2014 | -1             | 0                | Quiet                     |
| May 2014       | 02-05-2014 | -5             | 1                | Quiet                     |
|                | 13-05-2014 | -2             | 0                | Quiet                     |
| August 2014    | 26-08-2014 | 0              | 0                | Quiet                     |
| September 2014 | 07-09-2014 | -2             | 0                | Quiet                     |
| October 2014   | 07-10-2014 | -10            | 1                | Quiet                     |
|                | 13-10-2014 | -5             | 1                | Quiet                     |
| November 2014  | 26-11-2014 | -20            | 2                | Quiet                     |
| December 2014  | 11-12-2014 | -10            | 1                | Quiet                     |

**Table 3.3: Selected storm days from Dst and Kp index for 2013, accessed on 27<sup>th</sup> January 2019**

| Month         | Date       | Dst Index (nT) | Maximum Kp Index | Geomagnetic Specification |
|---------------|------------|----------------|------------------|---------------------------|
| March 2013    | 01-03-2013 | -50            | 4                | Active                    |
| April 2013    | 24-04-2013 | -60            | 4                | Active                    |
| May 2013      | 01-05-2013 | -90            | 4                | Active                    |
|               | 18-05-2013 | -60            | 4                | Active                    |
| June 2013     | 01-06-2013 | -130           | 5                | Minor storm               |
| July 2013     | 06-07-2013 | -90            | 4                | Active                    |
|               | 10-07-2013 | -60            | 4                | Active                    |
|               | 14-07-2013 | -90            | 4                | Active                    |
| August 2013   | 05-08-2013 | -50            | 4                | Active                    |
| November 2013 | 09-11-2013 | -90            | 4                | Active                    |
|               | 11-11-2013 | -70            | 4                | Active                    |
| December 2013 | 08-12-2013 | -60            | 4                | Active                    |

**Table 3.4: Selected storm days from Dst and Kp index for 2014, accessed on 27<sup>th</sup> January 2019**

| Month          | Date       | DSt index (nT) | Maximum Kp Index | Geomagnetic Specification |
|----------------|------------|----------------|------------------|---------------------------|
| February 2014  | 19-02-2014 | -120           | 5                | Minor storm               |
|                | 20-02-2014 | -100           | 5                | Minor storm               |
| March 2014     | 01-03-2014 | -50            | 4                | Active                    |
| April 2014     | 12-04-2014 | -90            | 4                | Active                    |
| May 2014       | 04-05-2014 | -50            | 4                | Active                    |
| June 2014      | 07-06-2014 | -50            | 4                | Active                    |
| August 2014    | 28-08-2014 | -50            | 4                | Active                    |
| September 2014 | 12-09-2014 | -100           | 5                | Minor storm               |
| November 2014  | 10-11-2014 | -60            | 4                | Active                    |

### 3.2 Methods

The satellite and differential code biases file for the satellite were retrieved from the SCINDA-GPS receiver. The data from the GPS receiver which is stored in zipped files, scintillation (.Scn) and position of receiver (.Psn) files was then sorted and unzipped using the WinRAR program. The unzipped .Scn files which contain the time of data storage, elevation angle of satellite, azimuth angle, longitudes and latitudes of ionospheric pierce points (IPP) and the unzipped .Psn files in RINEX format were created in one folder. The folder containing .Scn and .Psn hourly files were dragged into an open Gopi Software which processed the raw GPS data and obtained a text (.Cmn output) file which was a more simplified ten column daily file of ionospheric observables separated by a tab: Jdatet,

time, PRN, Az, Ele, Lat, Lon, Stec, Vtec and  $S_4$  and a mean TEC output (**Std**) file in the directory of data files. The output files for selected quiet and disturbed days of 2013 and 2014 shown in Tables 3.1, 3.2, 3.3 and 3.4 were considered and were used for further analysis. To reduce multipath effects, the data selected was for elevation angles of  $40^\circ$  and above. The average daily data of VTEC,  $S_4$  and UT for all PRNs for the selected quiet and disturbed days were obtained using SQL Server2017 program. The SQL Server2017 program produced the average daily VTEC and  $S_4$  values by averaging the VTEC and  $S_4$  values for all identical pseudo-random numbers (PRNs) within a 24 hour period.

### **3.2.1 Establishing TEC depletions**

VTEC,  $S_4$  and UT columns for quiet days for 2013 indicated in Table 3.1 were fed into MATLAB software to produce VTEC and  $S_4$  plots for each selected quiet day of 2013 as indicated in Chapter Four by Figure 4.1.1. The process was repeated for all the selected quiet days of 2014 indicated in Table 3.2, storm days of 2013 indicated in Table 3.3 and storm days of the year 2014 indicated in Table 3.4. The corresponding VTEC and  $S_4$  plots for quiet days of the year 2014, storm days of the year 2013 and storm days for the year 2014 were also plotted as indicated in Chapter Four by Figures 4.1.2 and 4.1.3, 4.1.4 respectively. TEC depletions and  $S_4$  index from the plots were investigated and observations on their correspondence made. TEC depletion was identified by checking for abrupt decrease in TEC values lasting for at least 10 minutes followed by a TEC enhancement preceding the depletion (Dashora & Pandey, 2005).

### **3.2.2 Investigating ROT and ROTI**

ROT for each quiet and storm day indicated in Tables 3.1, 3.2, 3.3 and 3.4 were directly obtained from the average daily VTEC data within intervals of 120 seconds using equation

2.2 in Chapter Two. ROTI was calculated from ROT with 4 minutes window using equation 2.3 in Chapter Two. A sampling rate of 4 minutes was chosen so as to lower the ROTI values (Jacobsen, 2014). The obtained ROT and ROTI values for each quiet and storm days of 2013 and 2014 were also fed into MATLAB program to obtain ROT and ROTI against UT plots. ROT and the corresponding ROTI values were examined from the plots to check on their correspondence for the few selected quiet and storm days of 2013 and 2014 as indicated by Figures 4.2.1, 4.2.2, 4.2.3 and 4.2.4 in Chapter Four.

### **3.2.3 Inferring occurrence of EPBs using TEC depletion, $S_4$ , ROT and ROTI**

The VTEC,  $S_4$ , ROT and ROTI plots for the corresponding selected quiet and storm days of 2013 and 2014 period were examined to infer the occurrence of EPBs during the period. Plasma bubble is a post-sunset phenomenon which causes TEC fluctuation and high ROTI values (Nishioka *et al*, 2008). To infer presence of EPBs for each day, TEC depletions were set at depletion depth  $\geq 7$  TECU. The observed TEC depletions were to correspond with enhanced  $S_4$  (Adewale *et al*, 2012) and increased fluctuations of ROT and high ROTI values of at least 1.5 TECU/min (Azzouzi *et al*, 2016) after local sunset (16:00-22:00 UT). EPB occurrence for the selected quiet and storm days for the years 2013 and 2014 were analyzed by plotting bar graphs showing percentage EPB occurrence for each year as indicated by Figures 4.3.5 and seasonal variation of EPB occurrence for the years 2013 and 2014 as indicated by Figure 4.3.6 in Chapter Four. The results obtained from these VTEC and  $S_4$  plots, ROT and ROTI plots and the bar graphs formed basis for our discussions.

## CHAPTER FOUR

### RESULTS AND DISCUSSIONS

#### 4.0 Introduction

This chapter presents and discusses the results on TEC depletions,  $S_4$  index, ROT and ROTI against UT and their correspondence with an aim of inferring the occurrence of plasma bubbles for the selected quiet and storm days in the year 2013 and 2014. The results on percentage occurrence and seasonal variation of EPBs for the years 2013 and 2014 were also presented.

#### 4.1 Establishing TEC depletions

TEC depletions are identified using TEC depletion depths. TEC depletion depth is obtained by calculating the difference resulting from the TEC value at time of TEC depletion and TEC value after the TEC enhancement. TEC depletion is considered significant if it lasts for about 10 to 60 minutes and is immediately followed by a gradual TEC enhancement (Dashora & Pandey, 2005).

##### 4.1.1 TEC depletions for selected quiet days of the year 2013

Figures 4.1.1(a), 4.1.1(b), 4.1.1(c), 4.1.1(d), 4.1.1(e) 4.1.1(g), 4.1.1(j), 4.1.1(k) and 4.1.1(l) shows TEC depletions which corresponded with increased amplitude scintillation values of more than 0.2 after local sunset for 26<sup>th</sup> March 2013, 18<sup>th</sup> April 2013, 19<sup>th</sup> April 2013, 10<sup>th</sup> May 2013, 17<sup>th</sup> June 2013, 4<sup>th</sup> July 2013, 7<sup>th</sup> September 2013, 29<sup>th</sup> September 2013 and 21<sup>st</sup> November 2013 respectively. However, the TEC depletions on 26<sup>th</sup> June 2013 and 11<sup>th</sup> August 2013 didn't correspond with amplitude scintillation increase as indicated in Figures 4.1.1(f) and 4.1.1(i).

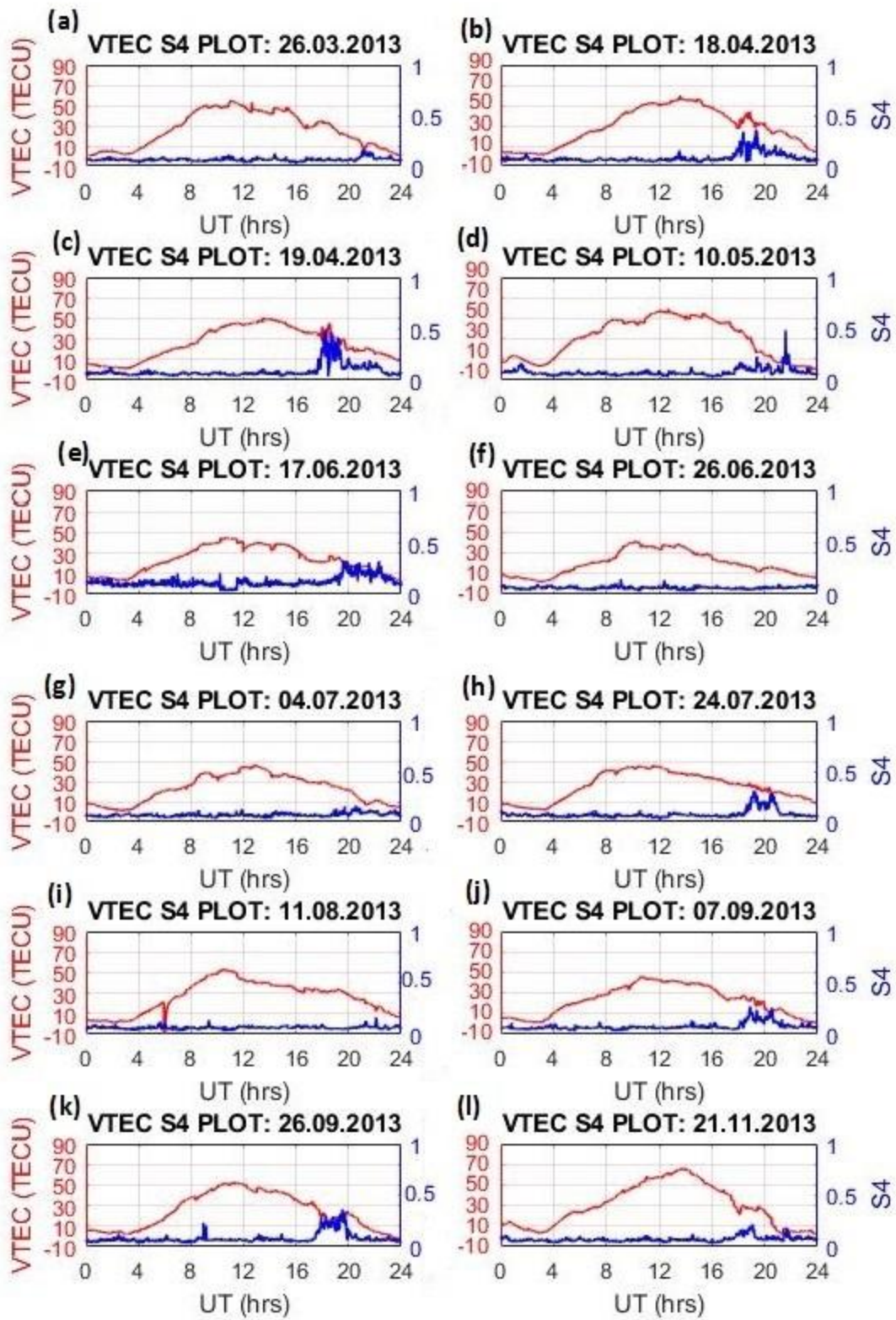


Figure 4.1.1: VTEC and S<sub>4</sub> plots for selected quiet days between March-Dec 2013

The selected quiet days of 2013 showed a minimum TEC during pre-sunrise hours (02:00–03:00 UT) with a magnitude of between 0-2 TECU. TEC was observed to rise steadily from 04:00 UT to around 12:00 UT where it attained maximum TEC value (45 -70 TECU) between 10:00-14:00 UT before reducing gradually up to 18:00 UT. From 18:00 UT, a TEC depletion depth of between 3 TECU and 25 TECU was attained before finally reducing to its minimum a few hours after local sunset. The highest maximum TEC value (70 TECU) was attained on 21<sup>st</sup> November 2013 as indicated in Figure 4.1.1(l). TEC depletions having large depletion depth (25 TECU) was on 19<sup>th</sup> April 2013 as shown in Figure 4.1.1(c) while TEC depletions having smaller depletion depths (5 TECU) were observed on 26<sup>th</sup> June 2013 as shown in Figure 4.1.1(f), 4<sup>th</sup> July 2013 as in Figure 4.1.1(g), and 7<sup>th</sup> September 2013 as shown in Figure 4.1.1(j).

TEC depletions for the selected quiet days of 2013 were summarized in Table 4.1 and TEC depletion depth and S<sub>4</sub> plotted as in Figure 4.1.1.1.

**Table 4.1: Summary of TEC depletions for selected quiet days of 2013**

| Month          | Date       | Dst Index (nT) | Maximum TEC (TECU) | TEC depletion depth | Maximum S <sub>4</sub> |
|----------------|------------|----------------|--------------------|---------------------|------------------------|
| March 2013     | 26-03-2013 | -10            | 50 at 11:00 UT     | 15 TECU             | 0.2                    |
| April 2013     | 18-04-2013 | 0              | 60 at 14:00 UT     | 15 TECU             | 0.35                   |
|                | 19-04-2013 | 0              | 50 at 14:00 UT     | 25 TECU             | 0.5                    |
| May 2013       | 10-05-2013 | -5             | 50 at 12:00 UT     | 16 TECU             | 0.35                   |
| June 2013      | 17-06-2013 | -5             | 45 at 12:00 UT     | 15 TECU             | 0.3                    |
|                | 26-06-2013 | -6             | 40 at 10:00 UT     | 5 TECU              | 0.1                    |
| July 2013      | 04-07-2013 | -5             | 50 at 13:00 UT     | 5 TECU              | 0.15                   |
|                | 24-07-2013 | -5             | 50 at 12:00UT      | 5 TECU              | 0.3                    |
| August 2013    | 11-08-2013 | -3             | 55 at 11:00 UT     | 7 TECU              | 0.15                   |
| September 2013 | 07-09-2013 | -5             | 50 at 12:00 UT     | 5 TECU              | 0.25                   |
|                | 26-09-2013 | -3             | 50 at 11:00 UT     | 16 TECU             | 0.35                   |
| November 2013  | 21-11-2013 | -1             | 70 at 13: 00UT     | 11 TECU             | 0.2                    |

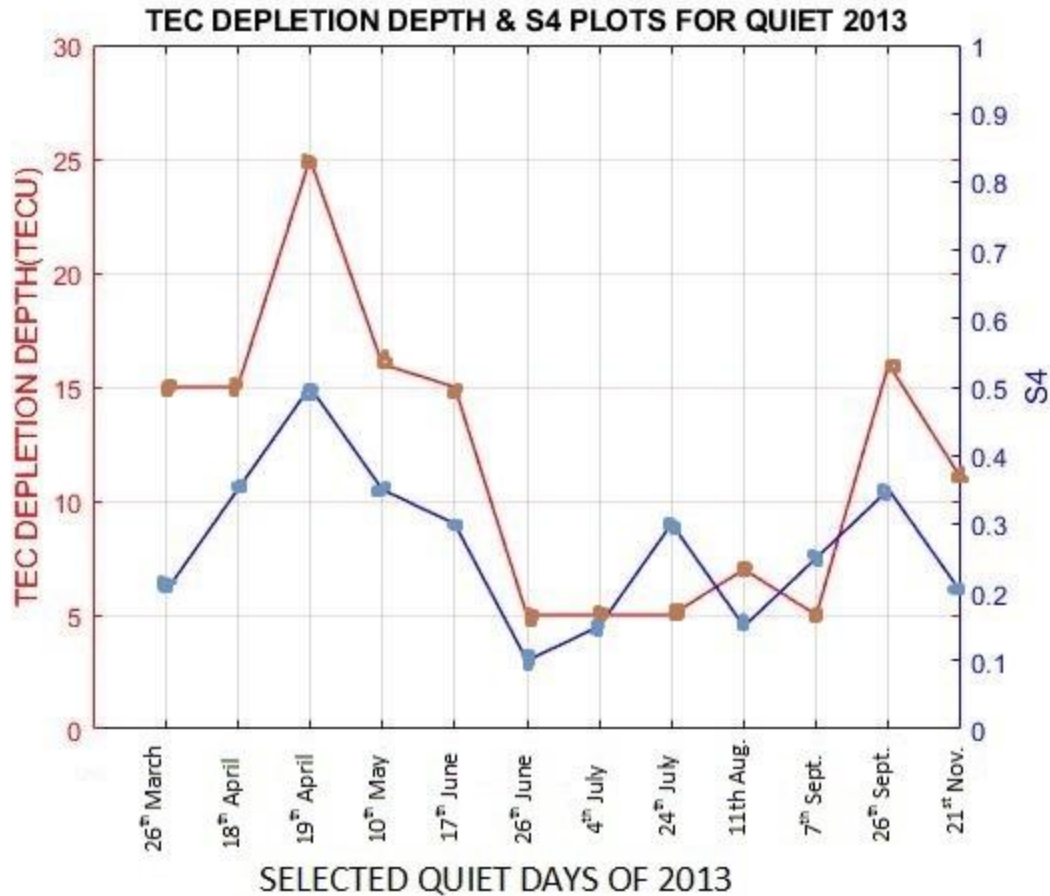


**Figure 4.1.1.1: TEC depletion depth & S<sub>4</sub> plot for selected Quiet days of 2013**

18<sup>th</sup> April 2013 had the largest TEC depletion depth (25 TECU) with a corresponding highest S<sub>4</sub> value of 0.5 for the selected quiet days of 2013 as indicated in Figure 4.1.1.1. This was followed by 26<sup>th</sup> September 2013 which had a TEC depletion depth of 16 TECU with a corresponding S<sub>4</sub> value of 0.35. The large TEC depletion depths observed during these two days is attributed to the increased solar intensity since the days are within the equinoctial period.

Smaller TEC depletion depths (5 TECU) were observed on 26<sup>th</sup> June, 4<sup>th</sup> July and 24<sup>th</sup> July as indicated in Figure 4.1.1.1. The days lie within the solstice period and hence, low solar intensity might have contributed to the smaller TEC depletion depths.

#### **4.1.2 TEC depletions for selected quiet days of the year 2014**

Figures 4.1.2(b), 4.1.2(c), 4.1.2(d), 4.1.2(e), 4.1.2(f), 4.1.2(g), 4.1.2(i), 4.1.2(k) and 4.1.2(l) shows TEC depletions which corresponded with increased amplitude scintillation values of more than 0.3 after local sunset for 3<sup>rd</sup> February 2014 as in Figure 4.1.2(b), 7<sup>th</sup> March 2014 as in Figure 4.1.2(c), 16<sup>th</sup> April 2014 as in Figure 4.1.2(d), 2<sup>nd</sup> May 2014 as in Figure 4.1.2(e), 13<sup>th</sup> May 2014 as in Figure 4.1.2(f), 26<sup>th</sup> August 2014 as in Figure 4.1.2(g), 7<sup>th</sup> October 2014 as in Figure 4.1.2(i), 26<sup>th</sup> November 2014 as in Figure 4.1.2(k) and 11<sup>th</sup> December 2014 as in Figure 4.1.2(l) respectively. However, the TEC depletions on 16<sup>th</sup> January 2014, 7<sup>th</sup> September 2014 and 13<sup>th</sup> October 2014 didn't correspond with amplitude scintillations increase as indicated in Figures 4.1.2(a), 4.1.2(h) and 4.1.2(j) respectively.

The selected quiet days of 2014 showed a minimum TEC during pre-sunrise hours (02:00–03:00 UT) with a magnitude of between 0-2 TECU. TEC was observed to rise steadily from 04:00 UT to around 12:00 UT where it attained maximum TEC value (50 - 70 TECU) between 11:00 - 14:00 UT before reducing gradually up to 18:00 UT. From 18:00 UT, a TEC depletion depth of between 3 TECU and 20 TECU was attained before finally reducing to its minimum a few hours after local sunset. The highest maximum TEC value (70 TECU) was attained on 7<sup>th</sup> March 2014 as in Figure 4.1.2(c), 16<sup>th</sup> April 2014 as shown in Figure 4.1.2(d) and 26<sup>th</sup> August 2014 as shown in Figure 4.1.2(g). The largest TEC depletion depths (20 TECU) were attained on 16<sup>th</sup> April 2014 and 26<sup>th</sup> August 2014 while the smallest depletion depth (3 TECU) was attained on 13<sup>th</sup> October 2014 as shown in Figure 4.1.2(j).

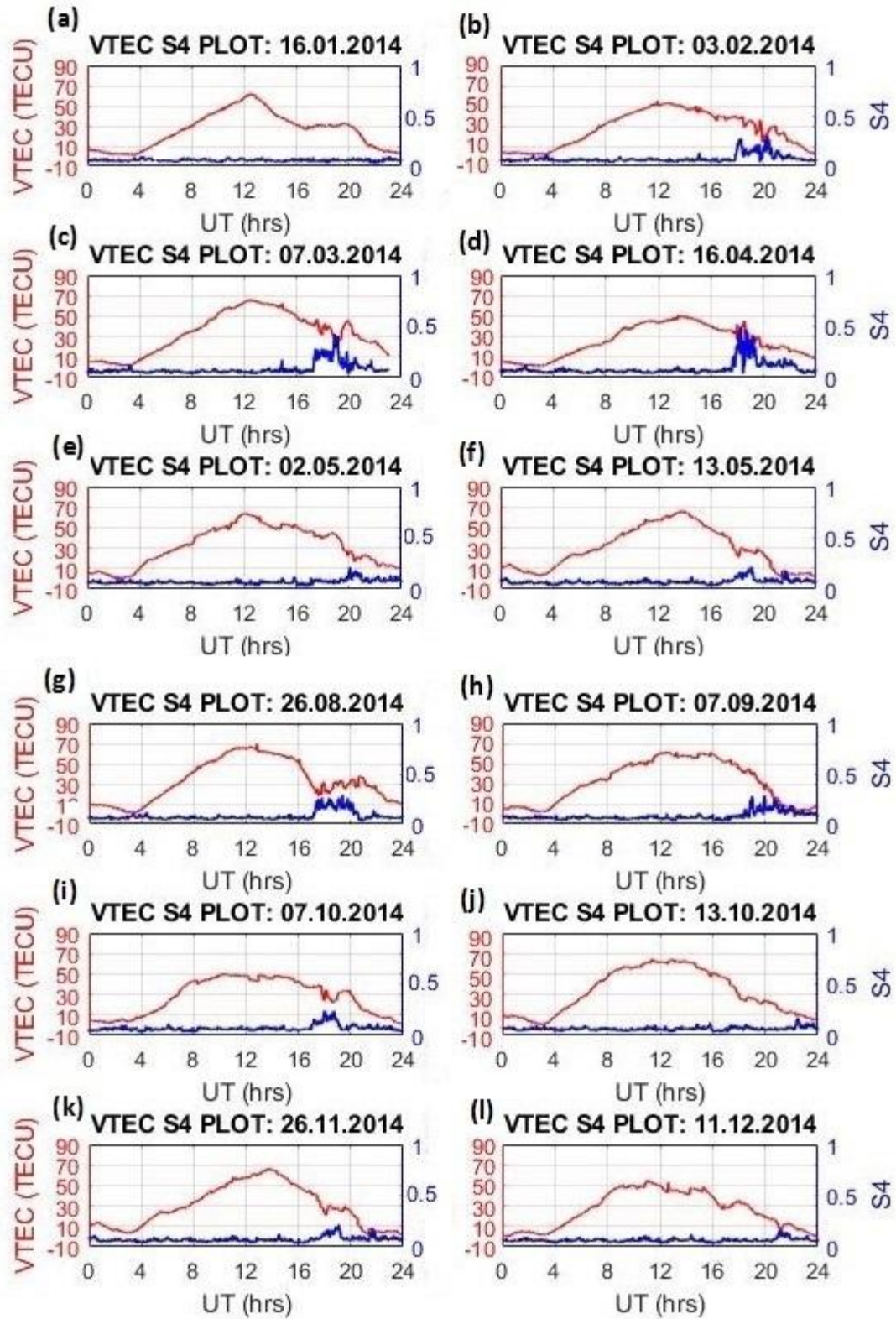


Figure 4.1.2: VTEC and S<sub>4</sub> plots for selected quiet days between Jan-Dec. 2014

TEC depletions for the selected quiet days of 2014 were summarized in Table 4.2 and TEC depletion depth and  $S_4$  plotted as in Figure 4.1.2.1.

**Table 4.2: Summary of TEC depletions for selected quiet days of 2014**

| Month          | Date       | DSt Index (nT) | Maximum TEC (TECU) | TEC depletion depth | Maximum $S_4$ |
|----------------|------------|----------------|--------------------|---------------------|---------------|
| January 2014   | 16-01-2014 | 0              | 60 at 13:00 UT     | 5 TECU              | 0.1           |
| February 2014  | 03-02-2014 | -5             | 50 at 13:00 UT     | 15 TECU             | 0.3           |
| March 2014     | 07-03-2014 | -2             | 70 at 12:00 UT     | 12 TECU             | 0.4           |
| April 2014     | 16-04-2014 | -1             | 70 at 12:00 UT     | 20 TECU             | 0.5           |
| May 2014       | 02-05-2014 | 0              | 60 at 12:00 UT     | 12 TECU             | 0.3           |
|                | 13-05-2014 | -2             | 70 at 14:00 UT     | 11 TECU             | 0.2           |
| August 2014    | 26-08-2014 | 0              | 70 at 12:00 UT     | 20 TECU             | 0.3           |
| September 2014 | 07-09-2014 | -10            | 60 at 13:00 UT     | 5 TECU              | 0.3           |
| October 2014   | 07-10-2014 | -10            | 50 at 12:00 UT     | 15 TECU             | 0.25          |
|                | 13-10-2014 | -5             | 65 at 12:00 UT     | 3 TECU              | 0.2           |
| November 2014  | 26-11-2014 | -20            | 65 at 14:00 UT     | 5 TECU              | 0.2           |
| December 2014  | 11-12-2014 | -10            | 55 at 11:00 UT     | 5 TECU              | 0.2           |

16<sup>th</sup> April and 26<sup>th</sup> August 2014 had the largest TEC depletion depths (20 TECU) with a corresponding highest  $S_4$  value of 0.5 on 16<sup>th</sup> April 2014. The smallest TEC depletion depth (3 TECU) was observed on 13<sup>th</sup> October 2014 with a corresponding  $S_4$  value of 0.2 as indicated in Figure 4.1.2.1.

Generally, the largest TEC depletion depths for the selected quiet days of the years 2013 and 2014 were on 19<sup>th</sup> April 2013 (25 TECU) as indicated in Figure 4.1.1.1, 16<sup>th</sup> April 2014 (20 TECU) and 26<sup>th</sup> August 2014 (20 TECU) as indicated in Figure 4.1.2.1. These large TEC depletion depths which corresponded with enhanced  $S_4$  values of more than 0.3 were attributed to the increased solar intensity: since the days fall in the equinoctial period. All the selected quiet days of 2013 and 2014 showed comparatively high maximum TEC values ranging within 40 and 70 TECU between 10:00 and 14:00UT as indicated by the VTEC and  $S_4$  plots in Figures 4.1.1 and 4.1.2. It was noted that the TEC depletions and TEC enhancements occurred consecutively and corresponded with increased  $S_4$  index for

most days after sunset as indicated in VTEC and  $S_4$  plots in Figures 4.1.1 and 4.1.2. Bhuyan *et al.*, (2007), associated these TEC enhancements with the secondary fountain effect resulting from occurrence of strong eastward electric field in the equatorial latitude after sunset. However, there was a gradual decrease in TEC with very small recovery segment on 13<sup>th</sup> October 2014, as shown in Figure 4.1.2(j). This might be attributed to the effect of the nighttime decay of the F-layer.

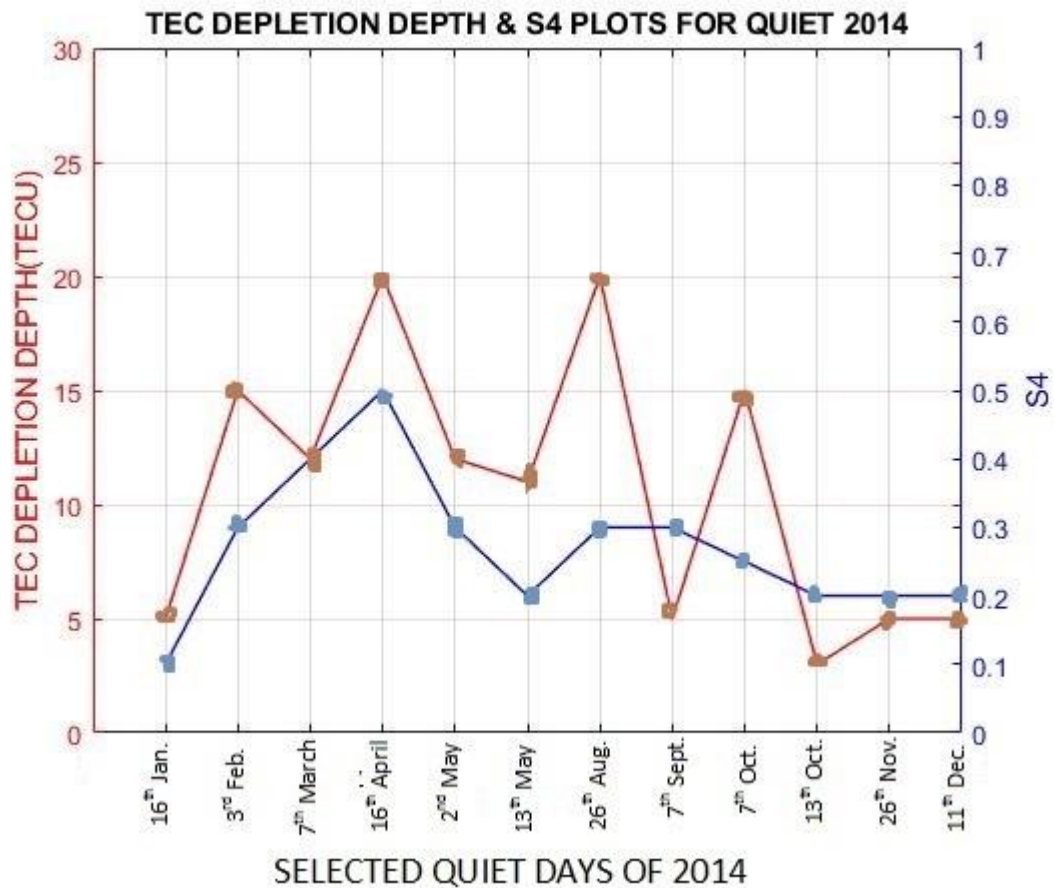


**Figure 4.1.2.1: TEC depletion depth &  $S_4$  plot for selected Quiet days of 2014**

The highest  $S_4$  index attained (0.5) for the selected quiet period of 2013 and 2014 was on 19<sup>th</sup> April 2013 and 16<sup>th</sup> April 2014. These days also happen to have the largest TEC depletion depths for the selected quiet days of the year 2013 and 2014 as indicated in Figures 4.1.1.1 and 4.1.2.1.

Looking at the TEC depletion depths and  $S_4$  plots in Figures 4.1.1.1 and 4.1.2.1 for the selected quiet days of 2013 and 2014, it is noted that the TEC depletion depths corresponded positively with a rise in  $S_4$  values for most days.

#### **4.1.3 TEC depletions for selected storm days of the year 2013.**

Figures 4.1.3(b), 4.1.3(c), 4.1.3(e), 4.1.3(i), 4.1.3(j) and 4.1.3(k) shows TEC depletions which corresponded with increased amplitude scintillation values of more than 0.2 after local sunset for 24<sup>th</sup> April 2013, 1<sup>st</sup> May 2013, 5<sup>th</sup> August 2013, 9<sup>th</sup> November 2013 and 11<sup>th</sup> November 2013 respectively. The TEC depletion on 1<sup>st</sup> June 2013 and 6<sup>th</sup> July 2013 didn't correspond with amplitude scintillation occurrence as indicated in Figures 4.1.3(e) and 4.1.3(f) respectively.

The selected storm days of 2013 showed a minimum TEC during pre-sunrise hours (02:00–03:00 UT) with TEC values between 0-2 TECU. TEC was observed to rise steadily from 04:00 UT to around 12:00 UT where it attained maximum TEC value (40-70 TECU) between 12:00 -14:00 UT before reducing gradually up to 18:00 UT. From 18:00 UT, a TEC depletion depth of between 2 TECU and 15 TECU was attained before finally reducing to its minimum a few hours after local sunset. The highest maximum TEC value (70 TECU) was attained on 1<sup>st</sup> May 2013 as shown in Figure 4.1.3(c), 9<sup>th</sup> November 2013 as shown in Figure 4.1.3(j) and 11<sup>th</sup> November 2013 as indicated in Figure 4.1.3(k).

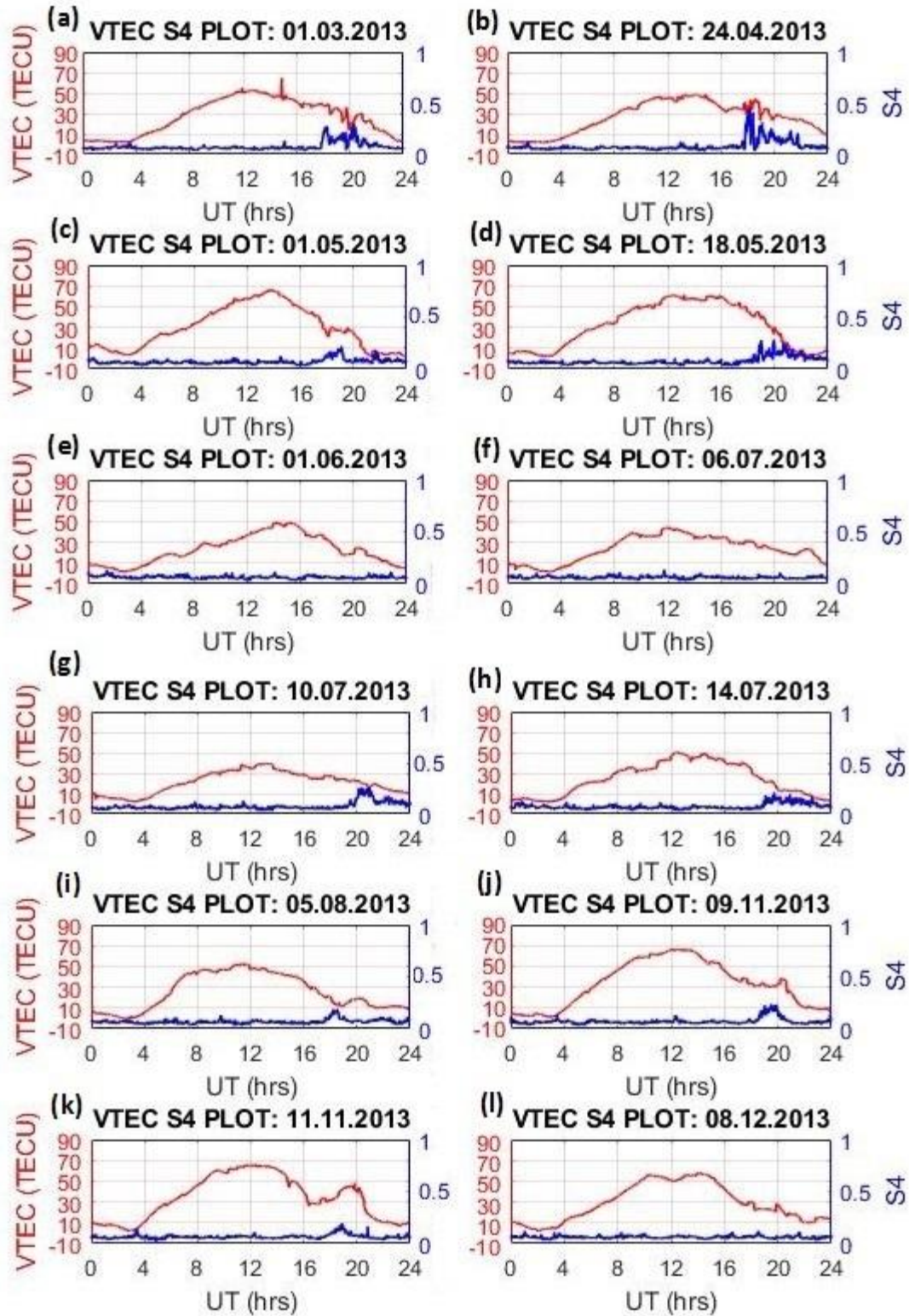


Figure 4.1.3: VTEC and S<sub>4</sub> plots for selected storm days between March-Dec. 2013

The largest TEC depletion depths (16 TECU) were attained on 11<sup>th</sup> November 2013 as indicated in Figures 4.1.3(k) and 4.1.3.1 while the smallest TEC depletion depth (2 TECU) was attained on 14<sup>th</sup> July 2013 as indicated in Figures 4.1.3(h) and 4.1.3.1 .

TEC depletions for the selected storm days of 2013 were summarized in Table 4.3 shown and TEC depletion depths and S<sub>4</sub> plotted as in Figure 4.1.3.1.

**Table 4.3: Summary of TEC depletions for selected storm days of 2013**

| Month         | Date       | DSt Index (nT) | Maximum TEC (TECU) | TEC depletion depth | Maximum S <sub>4</sub> |
|---------------|------------|----------------|--------------------|---------------------|------------------------|
| March 2013    | 01-03-2013 | -50            | 60 at 12:00 UT     | 5 TECU              | 0.1                    |
| April 2013    | 24-04-2013 | -60            | 50 at 14:00 UT     | 15 TECU             | 0.5                    |
| May 2013      | 01-05-2013 | -90            | 70 at 14:00 UT     | 12 TECU             | 0.2                    |
|               | 18-05-2013 | -60            | 60 at 13:00 UT     | 5 TECU              | 0.3                    |
| June 2013     | 01-06-2013 | -130           | 50 at 15:00 UT     | 4 TECU              | 0.1                    |
| July 2013     | 06-07-2013 | -90            | 45 at 12:00 UT     | 5 TECU              | 0.1                    |
|               | 10-07-2013 | -60            | 40 at 12:00UT      | 3 TECU              | 0.3                    |
|               | 14-07-2013 | -90            | 50 at 12:00 UT     | 2 TECU              | 0.2                    |
| August 2013   | 05-08-2013 | -50            | 50 at 12:00 UT     | 15 TECU             | 0.3                    |
| November 2013 | 09-11-2013 | -90            | 70 at 12:00 UT     | 10 TECU             | 0.2                    |
|               | 11-11-2013 | -70            | 70 at 12:00 UT     | 16 TECU             | 0.2                    |
| December 2013 | 08-12-2013 | -60            | 50 at 14:00 UT     | 10 TECU             | 0.1                    |

The day to day variation of TEC depletions for the selected storm days of 2013 was examined and the largest TEC depletion depth of 16 TECU with a corresponding S<sub>4</sub> value 0.2 was observed on 11<sup>th</sup> November 2013 as indicated in 4.1.3.1. The smallest TEC depletion depth value of 2 TECU was observed on 14<sup>th</sup> July 2013 with a corresponding S<sub>4</sub> value of 0.2. 24<sup>th</sup> April 2013 had a TEC depletion depth of 15 TECU with a corresponding S<sub>4</sub> value of 0.5.

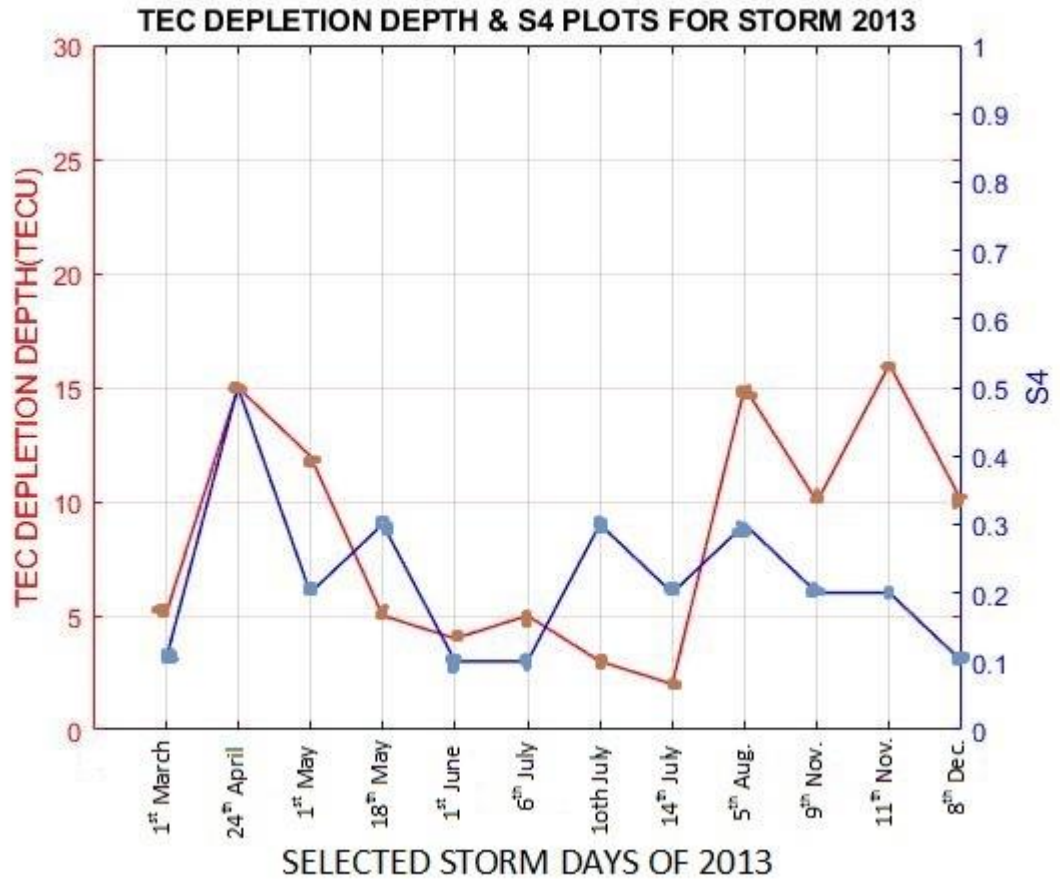


**Figure 4.1.3.1: TEC depletion depth & S<sub>4</sub> plot for selected Storm days of 2013**

#### 4.1.4 TEC depletions for selected storm days of the year 2014

Figures 4.1.4(a), 4.1.4(b), 4.1.4(c), 4.1.4(d), 4.1.4(g), 4.1.4(h) and 4.1.4(i) shows TEC depletions which corresponded with increased amplitude scintillation values of more than 0.2 after sunset for 19<sup>th</sup> February 2014, 20<sup>th</sup> February 2014, 1<sup>st</sup> March 2014, 12<sup>th</sup> April 2014, 28<sup>th</sup> August 2014, 12<sup>th</sup> September 2014 and 10<sup>th</sup> November 2014 respectively.

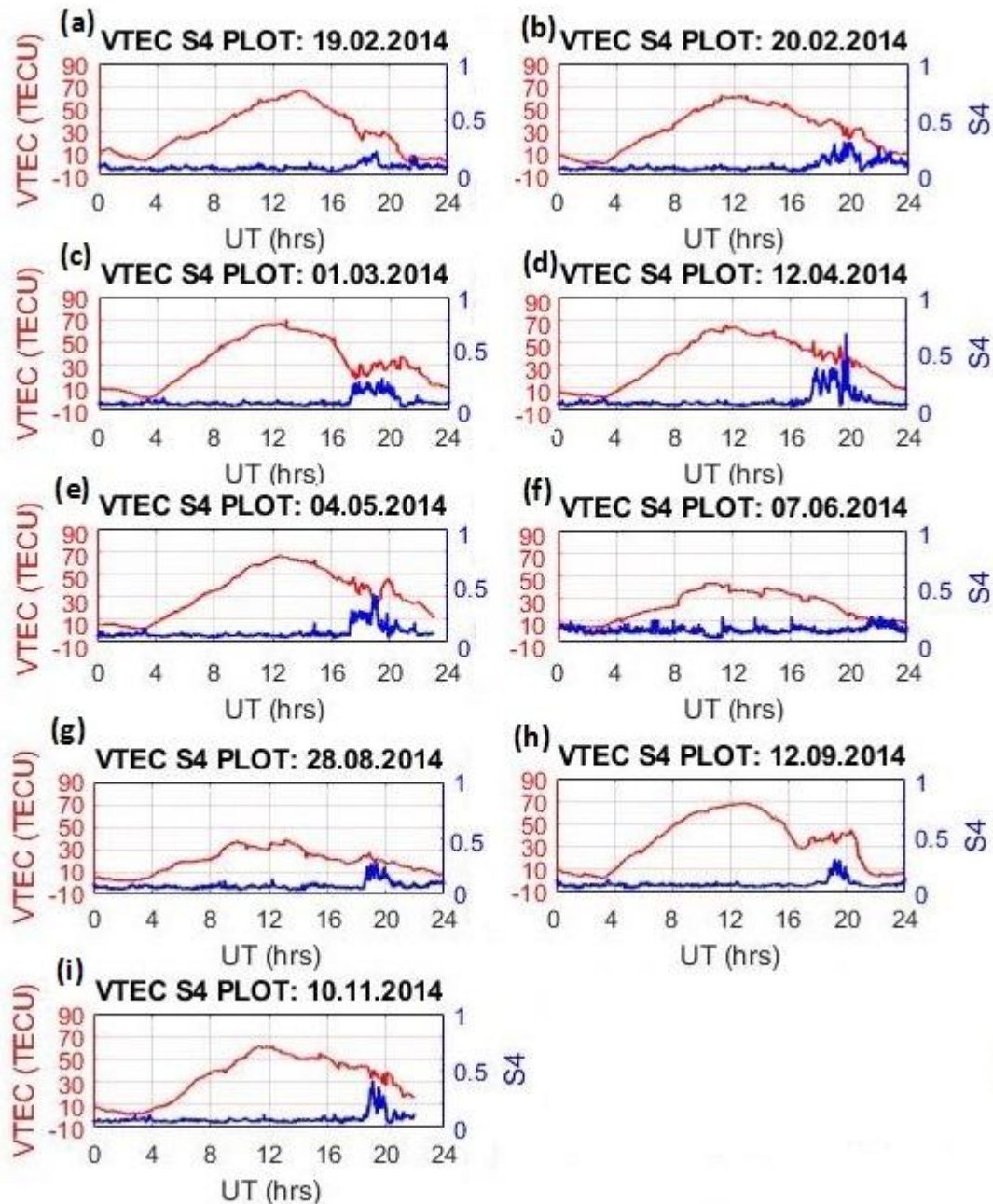


**Figure 4.1.4: VTEC and  $S_4$  plot for selected storm days between February-Nov 2014**

For most of the storm days of 2014, TEC was minimum during pre-sunrise hours (02:00 - 03:00 UT) with a magnitude of about 4 TECU. TEC rose steeply between 03:00 -09:00 UT. It increased steadily from 10:00 UT to 12:00 UT where a maximum TEC of between (40 -70 TECU) was attained before beginning to decrease gradually up to 18:00 UT. TEC then increased by about 10-18 TECU before finally falling to its minimum a few hours

after sunset. The largest maximum TEC value (70 TECU) was attained on 19<sup>th</sup> February 2014 and 12<sup>th</sup> September 2014 as indicated in Figures 4.1.4(a) and 4.1.4(h) respectively. The largest TEC depletion depths (18 TECU) were attained on 1<sup>st</sup> March 2014 and 4<sup>th</sup> May 2014 as shown in Figures 4.1.4(c) and 4.1.4(e) respectively while the smallest TEC depletion depth (3 TECU) was attained on 7<sup>th</sup> June 2014 as shown in Figure 4.1.4(f). TEC depletions for the selected storm days of 2014 were summarized in Table 4.4 and TEC depletion depths and  $S_4$  plotted as in Figure 4.1.4.1.

**Table 4.4: Summary of TEC depletions for selected storm days of 2014**

| Month          | Date       | DSt index (nT) | Maximum TEC (TECU) | TEC depletion depth | Maximum $S_4$ |
|----------------|------------|----------------|--------------------|---------------------|---------------|
| February 2014  | 19-02-2014 | -120           | 70 at 14:00 UT     | 12 TECU             | 0.2           |
|                | 20-02-2014 | -100           | 60 at 12:00 UT     | 10 TECU             | 0.3           |
| March 2014     | 01-03-2014 | -50            | 65 at 13:00UT      | 18 TECU             | 0.3           |
| April 2014     | 12-04-2014 | -90            | 65 at 12:00 UT     | 15 TECU             | 0.7           |
| May 2014       | 04-05-2014 | -50            | 65 at 13:00 UT     | 18 TECU             | 0.4           |
| June 2014      | 07-06-2014 | -50            | 42 at 11:00UT      | 3 TECU              | 0.2           |
| August 2014    | 28-08-2014 | -50            | 40 at 13:00UT      | 10 TECU             | 0.3           |
| September 2014 | 12-09-2014 | -100           | 70 at 13:00UT      | 8 TECU              | 0.3           |
| November 2014  | 10-11-2014 | -60            | 65 at 12:00 UT     | 10 TECU             | 0.4           |

The largest TEC depletion depths (18 TECU) were observed on 1<sup>st</sup> March 2014 and 4<sup>th</sup> May 2014 with corresponding enhanced  $S_4$  values of 0.3 and 0.4 respectively. The smallest TEC depletion depth for the selected storm days of 2014 was on 3 TECU and was attained on 6<sup>th</sup> June 2014 with a corresponding enhanced  $S_4$  of 0.2.

Generally, the selected storm days of the years 2013 and 2014 had the largest TEC depletion depths on 24<sup>th</sup> April 2013 (15 TECU) and 11<sup>th</sup> November 2013 (16 TECU) as indicated in Figure 4.1.3.1, 1<sup>st</sup> March 2014 (18 TECU) and 4<sup>th</sup> May 2014 (18 TECU) as indicated in Figure 4.1.4.1. This was attributed to increased solar intensity. The TEC depletion depths were seen to correspond with increase in  $S_4$  index values for most selected

quiet and storm days of the years 2013 and 2014 as indicated in Figures 4.1.3.1 and 4.1.4.1. However, there was a gradual decrease in TEC with very small recovery segments for some days like 14<sup>th</sup> July 2013 and 7<sup>th</sup> June 2014 as shown in Figures 4.1.3(h) and 4.1.4(f) respectively. This was attributed to the nighttime decay of the F-layer. Some of the selected storm days of 2013 and 2014 had their TEC enhancement appearing after more than 3 hours. Examples of these days included 6<sup>th</sup> July 2013, 11<sup>th</sup> November 2013, 1<sup>st</sup> March 2014 and 12<sup>th</sup> September 2014 as indicated in Figures 4.1.3(f), 4.1.3(k), 4.1.4.(c) and 4.1.4(h) respectively. This was attributed to background electron density persisting for several hours after sunset. Olwendo *et al*, (2012) reported that TEC depletions corresponding with increase in  $S_4$  index after sunset was a manifestation of presence of plasma density depletions. This argument was used later in this Chapter to infer the occurrence of plasma bubbles. The highest  $S_4$  index of 0.7 was attained on 12<sup>th</sup> April 2014 which was a storm day having a Dst index of -100nT as indicated in Figure 4.1.4.1 and a solar flux F10.7cm of about 150sfu. This might have been attributed to the effect of a geomagnetic storm that occurred on that day and on the effect of increased solar intensity. The enhanced  $S_4$  and large TEC depletion depths for selected quiet days of 2013 and 2014 after local sunset were attributed to the effect of RTI.

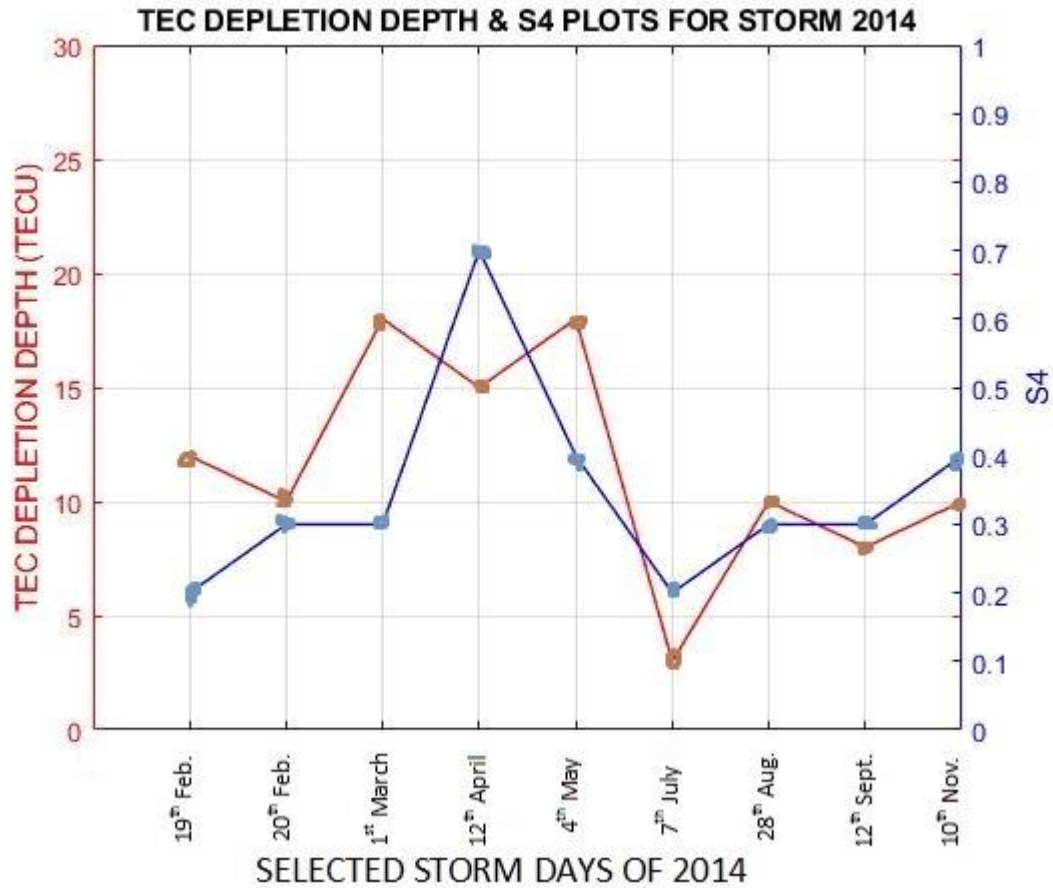


**Figure 4.1.4.1: TEC depletion depth & S<sub>4</sub> plot for selected Storm days of 2014**

The variability of TEC depletions for the selected storms days for the years 2013 and 2014 were very low as compared to the selected quiet days of the years 2013 and 2014. This was observed by the quiet days of the years 2013 and 2014 having larger TEC depletion depths of 25 TECU (on 19<sup>th</sup> April 2013) and 20 TECU (on 16<sup>th</sup> April 2014 & 26<sup>th</sup> August 2014) respectively while the selected storm days of the years 2013 and 2014 had smaller TEC depletion depths of 16 TECU (on 11<sup>th</sup> November 2013) and 18 TECU (on 1<sup>st</sup> March 2014 & 4<sup>th</sup> May 2014) respectively. This is because the ionospheric behaviour during geomagnetically disturbed periods is controlled by several competing dynamics including PPEF, DDEF and reduction in electron density due to increased recombination rates. A

similar scenario was reported by Azzouzi *et al.*, (2016) in their study on the daily variability of ROTI and VTEC in October 2012.

Considering both selected quiet and storm days of years 2013 and 2014, the VTEC and S<sub>4</sub> plots for the whole period showed a diurnal variation with minimum TEC at pre-sunrise, maximum TEC during daytime and at minimum TEC during nighttime. This diurnal variation of TEC was similar to that reported by Fayose *et al.*, (2012) in their study on TEC variation and their effect on GNSS over Akure in Nigeria in 2010. The maximum TEC during daytime was attributed to increased photoionization due to intense solar radiation while minimum TEC during pre-sunrise and nighttime was attributed to a reduced photoionization due to low solar radiation (Bolaji *et al.*, 2012). All the selected quiet and storm days of the years 2013 and 2014 also showed comparatively high maximum TEC values ranging within 40 and 70 TECU between 10:00 and 14:00UT as indicated by the VTEC and S<sub>4</sub> plots in Figures 4.1.1, 4.1.2, 4.1.3 and 4.1.4. The daily average TEC values were highest during equinoctial months (March, April, August and September) with 59 TECU while lower TEC values were observed during solstice months (June, July, November and December) with 55 TECU. These observations are also similar to results reported by Fayose *et al.*, (2012) in TEC variations over Akure, Nigeria in 2010; Oron *et al.*, (2013) in TEC variation over Kampala, Uganda between 2010 and 2011 and Omondi *et al.*, (2019) in TEC and scintillations over Maseno, Kenya in 2014 where high average TEC was observed in equinoctial months while lower average TEC was observed in solstice months. It was observed that the TEC depletions and TEC enhancements occurred consecutively and corresponded with increase in S<sub>4</sub> index for most days after sunset. Bhuyan *et al.*, (2007), associated this TEC enhancement with the secondary

fountain effect caused by post-sunset occurrence of strong eastward electric field in the equatorial latitude.

The percentage occurrence of scintillations for the selected quiet and storm days of the years 2013 and 2014 also exhibited a seasonal dependence. This was depicted by equinoctial months exhibiting a higher average  $S_4$  index (of about 0.4) index than the solstice months (about 0.26). This seasonal dependence of amplitude scintillations are similar to results reported by D'ujanga & Taabu (2014) in their study of ionospheric scintillations over East Africa and Omondi *et al.*, (2019) in their study of TEC and scintillations over Maseno, Kenya. The higher average  $S_4$  index during equinoctial months was attributed to increased solar intensity resulting from the close alignment of the solar terminator and the geomagnetic meridian (Tsunoda, 1985). Comparing the selected quiet and storm days of 2013 and 2014, it was noted that the quiet days had a lower average  $S_4$  index (about 0.3) while the storm days had a higher average  $S_4$  index (about 0.35). The higher average  $S_4$  index during storm days was attributed to the effect of the geomagnetic storms which increased background ionization density of the ionosphere. However, the average  $S_4$  index for the selected quiet and storm days of the years 2013 and 2014 were very low. This might have been due to the smaller number of sunspots in solar cycle 24, as observed by Muella *et al.*, (2017).

The scintillation events observed in this study for the selected quiet and storm days of the years 2013 and 2014 occurred majorly after 16:00UT (post-sunset). This post-sunset occurrence of scintillations in the low latitude region was believed to have been caused by the rapid rise of the F-layer and the increase in the vertical  $\mathbf{E} \times \mathbf{B}$  plasma drift due to the

pre-reversal enhancement (PRE) of the eastward electric field as reported by D'ujanga and Taabu, (2014).

## **4.2 Investigating ROT and ROTI**

ROT and ROTI are useful in identifying small scale ionospheric fluctuations.

### **4.2.1 ROT and ROTI plots for selected quiet days of 2013**

Figures 4.2.1(a), 4.2.1(b) and 4.2.1(c) shows presence of increased fluctuation of ROT between 18:00 UT and 20:00 UT for 26<sup>th</sup> March 2013, 18<sup>th</sup> April 2013 and 19<sup>th</sup> April 2013 respectively. The ROT fluctuations corresponded with high ROTI values of about 1.9 TECU/min, 1.6 TECU/min and 1.9 TECU/min respectively after sunset. ROT and ROTI exhibited a similar trend for the 24 hour period for the three days.

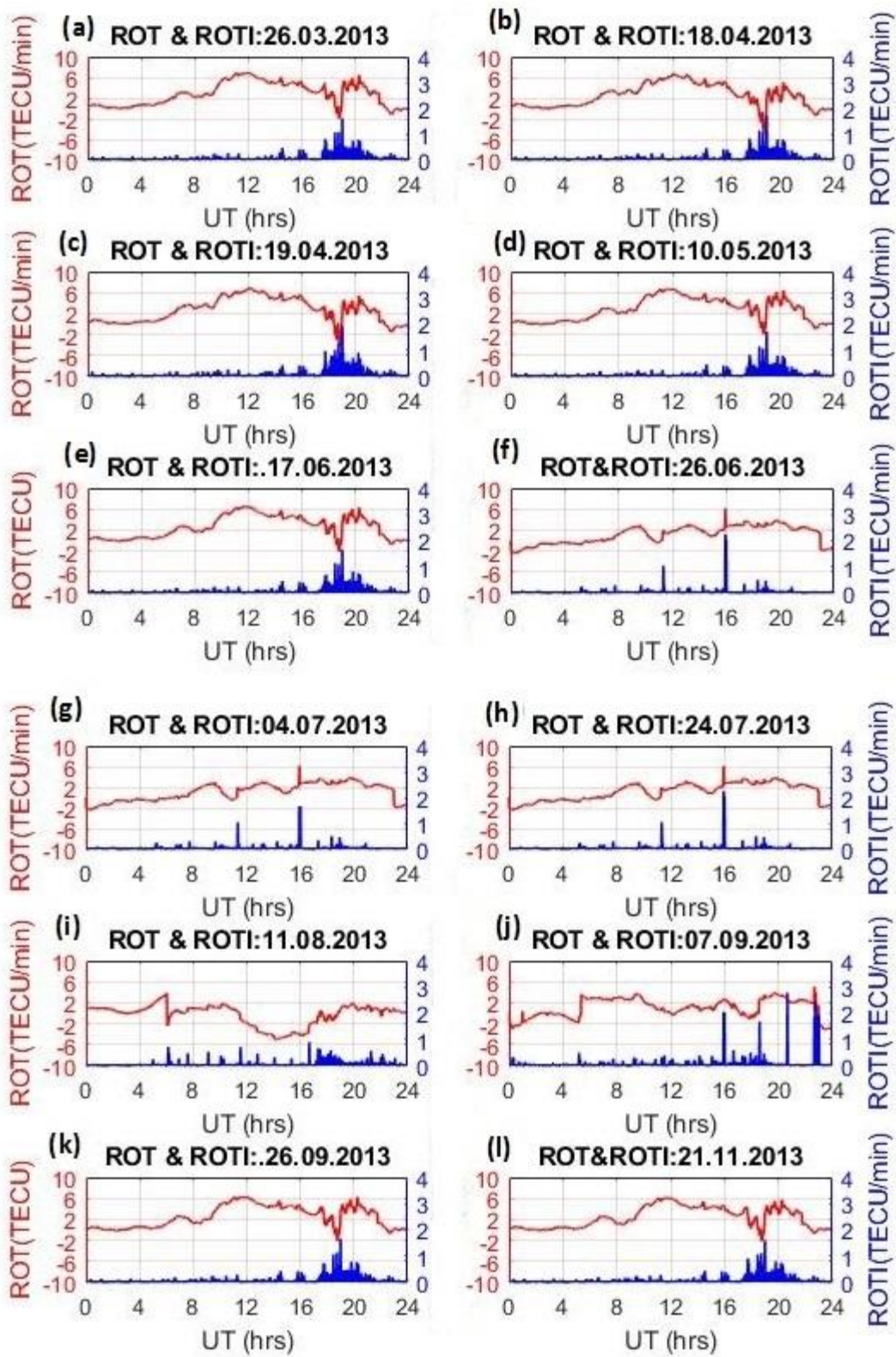


Figure 4.2.1: ROT and ROTI plots for selected quiet days between March-Nov. 2013

Figures 4.2.1(d) and 4.2.1(e) showed presence of increased ROT fluctuation between 18:00 UT and 20:00 UT on 10<sup>th</sup> May 2013 and 17<sup>th</sup> June 2013 respectively and they corresponded with high ROTI values of about 1.8 TECU/min after sunset for the two days. Figure 4.2.1(f) showed no ROT fluctuation on 26<sup>th</sup> June 2013 between 18:00 UT and 20:00UT with low ROTI values throughout the whole day.

Figures 4.2.1(g), 4.2.1(h) and 4.2.1(i) shows ROT and ROTI plots for 4<sup>th</sup> July 2013, 24<sup>th</sup> July 2013 and 11<sup>th</sup> August 2013 respectively. Both 4<sup>th</sup> July and 24<sup>th</sup> July 2013 showed a similar trend for ROT and ROTI for the 24 hour period by having minimum ROT fluctuation between 18:00 UT and 20:00 UT. On 11<sup>th</sup> August 2013, a notable ROT fluctuation was observed between 12:00 UT and 20:00 UT with a corresponding high ROTI value of about 1.5 TECU/min within the same period. Figures 4.2.1(j), 4.2.1(k) and 4.2.1(l) shows ROT and ROTI plots for 7<sup>th</sup> September 2013, 26<sup>th</sup> September 2013 and 21<sup>st</sup> November 2013. There was a ROT fluctuation between 17:00 UT and 18:00 UT on 7<sup>th</sup> September 2013. There was an increased ROT fluctuation and high ROTI values of about 1.8 TECU/min between 16:00 UT and 21:00 UT for 26<sup>th</sup> September 2013 and 21<sup>st</sup> November 2013 as indicated in Figures 4.2.1(k) and 4.2.1(l) respectively. The results obtained from the graphs of the selected quiet days of the year 2013 indicated that the highest levels of irregularities were on 26<sup>th</sup> March 2013 and 19<sup>th</sup> April 2013 as estimated by the highest ROTI values of 1.9 TECU/min. The highest ROTI values attained on these two days might have been brought by impact of the large TEC depletions. That is: 15 TECU for 26<sup>th</sup> March 2013 and 25 TECU for 19<sup>th</sup> April 2013.

#### **4.2.2 ROT and ROTI plot for selected quiet days of 2014**

Figures 4.2.2(a), 4.2.2(b) and 4.2.2(c) shows ROT and ROTI plots for 16<sup>th</sup> January 2014, 3<sup>rd</sup> February 2014 and 7<sup>th</sup> March 2014 respectively. The ROT and ROTI plots for 16<sup>th</sup> January and 7<sup>th</sup> March 2014 showed fluctuation of ROT and a rise in ROTI between 18:00 to 19:00UT. There was a notable ROT fluctuation and high ROTI values of about 1.8 TECU/min between 16:00 UT and 20:00 UT on 3<sup>rd</sup> February 2014 as indicated in Figure 4.2.2.1(b). Figures 4.2.2(d), 4.2.2(e) and 4.2.2(f) showed ROT and ROTI plots for 16<sup>th</sup> April 2014, 2<sup>nd</sup> May 2014 and 13<sup>th</sup> May 2014 respectively. From the plots, the three days exhibited increased ROT fluctuation and corresponding high ROTI values of about 1.8 TECU/min between 16:00 UT and 21:00 UT

Figures 4.2.2(g), 4.2.2(h) and 4.2.2(i) shows ROT and ROTI plots for 26<sup>th</sup> August 2014, 7<sup>th</sup> September 2014 and 7<sup>th</sup> October 2014 respectively. The ROT and ROTI values exhibited a similar behaviour of increased ROT fluctuation and high ROTI values of about 1.8 TECU/min between 16:00UT and 21:00 UT on 26<sup>th</sup> August and 7<sup>th</sup> October 2014. There was a ROT fluctuation and a rise in ROTI values between 17:00 UT and 18:00 UT on 7<sup>th</sup> September 2014 as shown in Figure 4.2.2(h). Figures 4.2.2(j), 4.2.2(k) and 4.2.2(l) show ROT and ROTI plots for 13<sup>th</sup> October 2014, 26<sup>th</sup> November 2014 and 11<sup>th</sup> December 2014 respectively. All the three days exhibited similar behaviour for ROT and ROTI. That is, a ROT fluctuation and a rise in ROTI between 17:00 UT and 18:00 UT.

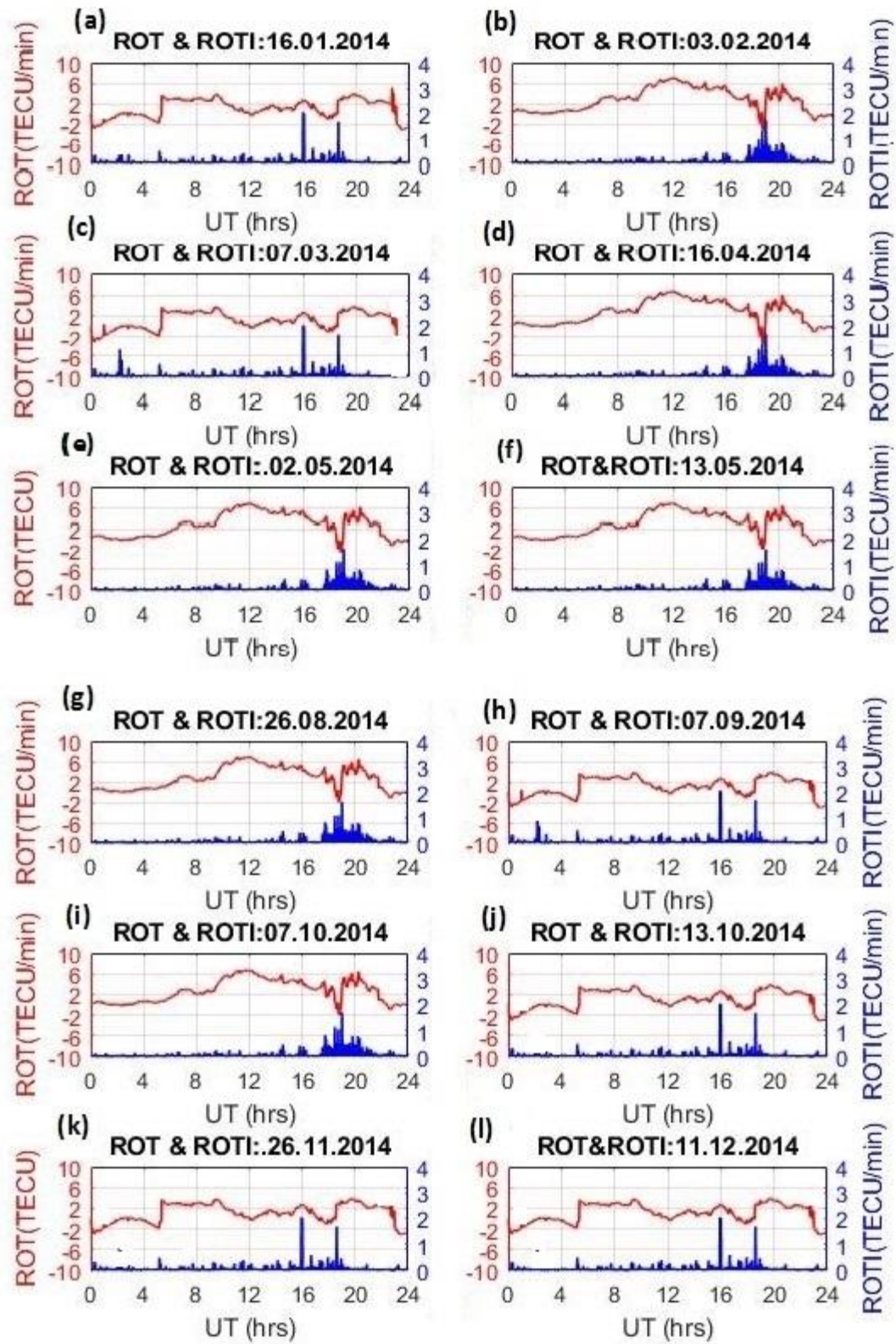


Figure 4.2.2: ROT and ROTI plots for selected quiet days between Jan.-Dec. 2014

The results obtained from the graphs of the selected quiet days of 2014 indicated that the highest level of irregularities were on 3<sup>rd</sup> February 2014, 16<sup>th</sup> April 2014, 2<sup>nd</sup> May 2014, 13<sup>th</sup> May 2014, 26<sup>th</sup> August 2014, and 7<sup>th</sup> October 2014, estimated by the highest ROTI values of 1.8 TECU/min. The high ROTI values attained on these days were attributed to the large TEC depletion depths as indicated in Table 4.2 in Chapter Four and the impact of the increased solar wind speeds.

The selected quiet days of the years 2013 and 2014, displayed a relatively consistent variation pattern of the highest ROTI values of 1.9 TECU/min and 1.8 TECU/min for the year 2013 and in the year 2014 respectively. This consistent variation pattern might have risen from ionospheric currents driven by heat energy coming from the sun.

#### **4.2.3: ROT and ROTI plots for selected storm days of 2013**

Figures 4.2.3 (a), 4.2.3(b) and 4.2.3(c) shows ROT and ROTI plots for 1<sup>st</sup> March 2013, 24<sup>th</sup> April 2013 and 1<sup>st</sup> May 2013 respectively. 24<sup>th</sup> March and 1<sup>st</sup> May 2013 showed an increased ROT fluctuation and high ROTI values of about 1.8 TECU/min between 16:00 UT and 21:00 UT. On 1<sup>st</sup> March 2013, there was no ROT fluctuation between 16:00 UT and 21:00 UT and the corresponding ROTI values were almost constant for the whole 24 hour period. Figures 4.2.3(d), 4.2.3(e) and 4.2.3(f) shows ROT and ROTI plots for 18<sup>th</sup> May 2013, 1<sup>st</sup> June 2013 and 6<sup>th</sup> July 2013 respectively. 1<sup>st</sup> June and 6<sup>th</sup> July showed a similar trend for ROT and ROTI values for the whole 24 hour period.

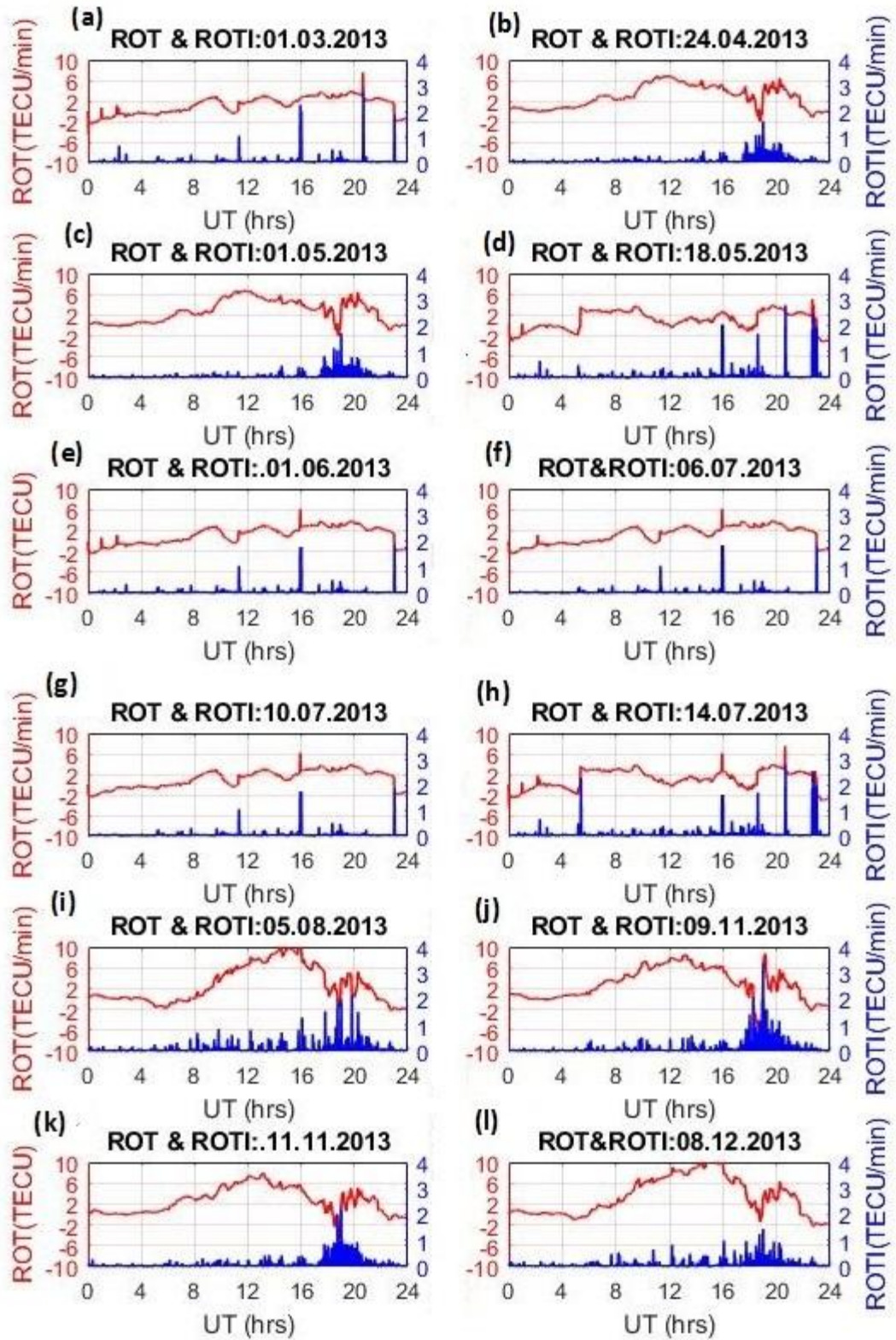


Figure 4.2.3: ROT and ROTI plot for selected storm days between Jan.- Dec. 2013

No notable ROT fluctuation was observed between 16:00 and 21:00 UT for these two days and the ROTI values were constant. 18<sup>th</sup> May 2013 showed a ROT fluctuation and a rise in ROTI values between 16:00 and 21:00 UT as indicated in Figure 4.2.3(d).

Figures 4.2.3(g), 4.2.3(h) and 4.2.3(i) shows ROT and ROTI plots for 10<sup>th</sup> July 2013, 14<sup>th</sup> July 2013 and 5<sup>th</sup> August 2013 respectively. There was no notable ROT fluctuation between 16:00 and 21:00 UT for 10<sup>th</sup> July 2013 as indicated in Figure 4.2.3(g). 14<sup>th</sup> July 2013 showed a ROT fluctuation and a rise in ROTI between 17:00UT and 18:00 UT as shown in Figure 4.2.3(h). There was a notable increased fluctuation of ROT and high ROTI values of about 2 TECU/min between 16:00UT and 21:00 UT for 5<sup>th</sup> August 2013 as indicated in Figure 4.2.3(i). Figures 4.2.3(j), 4.2.3(k) and 4.2.3(l) showed ROT and ROTI plots for 9<sup>th</sup> November 2013, 11<sup>th</sup> November 2013 and 8<sup>th</sup> December 2013 respectively. The three days exhibited increased ROT fluctuation and high ROTI values of about 3.5 TECU/min, 2.1 TECU/min and 1.5 TECU/min respectively between 16:00 UT and 21:00 UT. The results obtained from the graphs of the selected storm days of 2013 indicated that the highest level of irregularity was on 9<sup>th</sup> November 2013 as estimated by the highest ROTI value of 3.5 TECU/min. 9<sup>th</sup> November had the largest TEC depletion (18 TECU) for the selected storm days of 2013 with a solar wind speed of 500km/s and a solar flux F10.7cm of 145sfu. The high ROTI value might therefore be attributed to the impact of the high speed solar wind which led to an increase in TEC depletion, hence a higher ROTI value.

#### **4.2.4: ROT and ROTI plot for selected storm days of 2014**

Figure 4.2.4 shows selected storm days of 2014. Figures 4.2.4(a), 4.2.4(b) and 4.2.4(c) showed ROT and ROTI plots for 19<sup>th</sup> February 2014, 20<sup>th</sup> February 2014 and 1<sup>st</sup> March

2014 respectively. The plots show increased fluctuation of ROT and high ROTI values of about 2 TECU/min between 16:00 and 21:00 UT for the three days. Figures 4.2.4(d), 4.2.4(e) and 4.2.4(f) show ROT and ROTI plots for 12<sup>th</sup> April 2014, 4<sup>th</sup> May 2014 and 7<sup>th</sup> June 2014 respectively. The three days showed a notable increased ROT fluctuation and high ROTI values of about 3.4 TECU/min, 2.2 TECU/min and 2 TECU/min between 16:00UT and 21:00 UT respectively. There was no notable ROT fluctuation between 16:00UT and 21:00 UT on 7<sup>th</sup> June 2014 as indicated in Figure 4.2.4(f).

Figures 4.2.4(g), 4.2.4(h) and 4.2.4(i) shows ROT and ROTI plots for 28<sup>th</sup> August 2014, 12<sup>th</sup> September 2014 and 10<sup>th</sup> November 2014 respectively. 28<sup>th</sup> August 2014 showed an increased fluctuation of ROT and high ROTI value between 16:00 UT and 21:00 UT as shown in Figure 4.2.4(g). The ROT and ROTI plot for 10<sup>th</sup> November 2014 showed a notable increased ROT fluctuation and high ROTI value of about 1.8 TECU/min between 16:00 UT and 21:00 UT as shown in Figure 4.2.4(i). The results obtained from the graphs of the selected storm days of 2014 indicated that the highest level of irregularity was on 1<sup>st</sup> March 2014, estimated by the highest ROTI value of 3.5 TECU/min. 1<sup>st</sup> March 2014 had the highest TEC depletion depth (18 TECU) for the selected storm days of the year 2014. The day exhibited a solar wind speed of 400km/s and a solar flux F10.7cm of 160sfu.

The selected storm days of the years 2013 and 2014 displayed highest ROTI values of 3.5 TECU/min and 3.4 TECU/min respectively. Besides these highest ROTI values being connected to the large TEC depletion depths, they also might have been driven by increased solar winds speeds ranging between 250km/s and 750 km/s and solar flux F10.7cm between 110sfu and 160sfu. Generally, the storm days of the years 2013 and 2014 had higher ROTI values than the quiet days after local sunset as indicated in Figures

4.2.1, 4.2.2, 4.2.3, and 4.2.4 and these higher ROTI values during selected storm days reflects the ionospheric TEC response to geomagnetic disturbance.

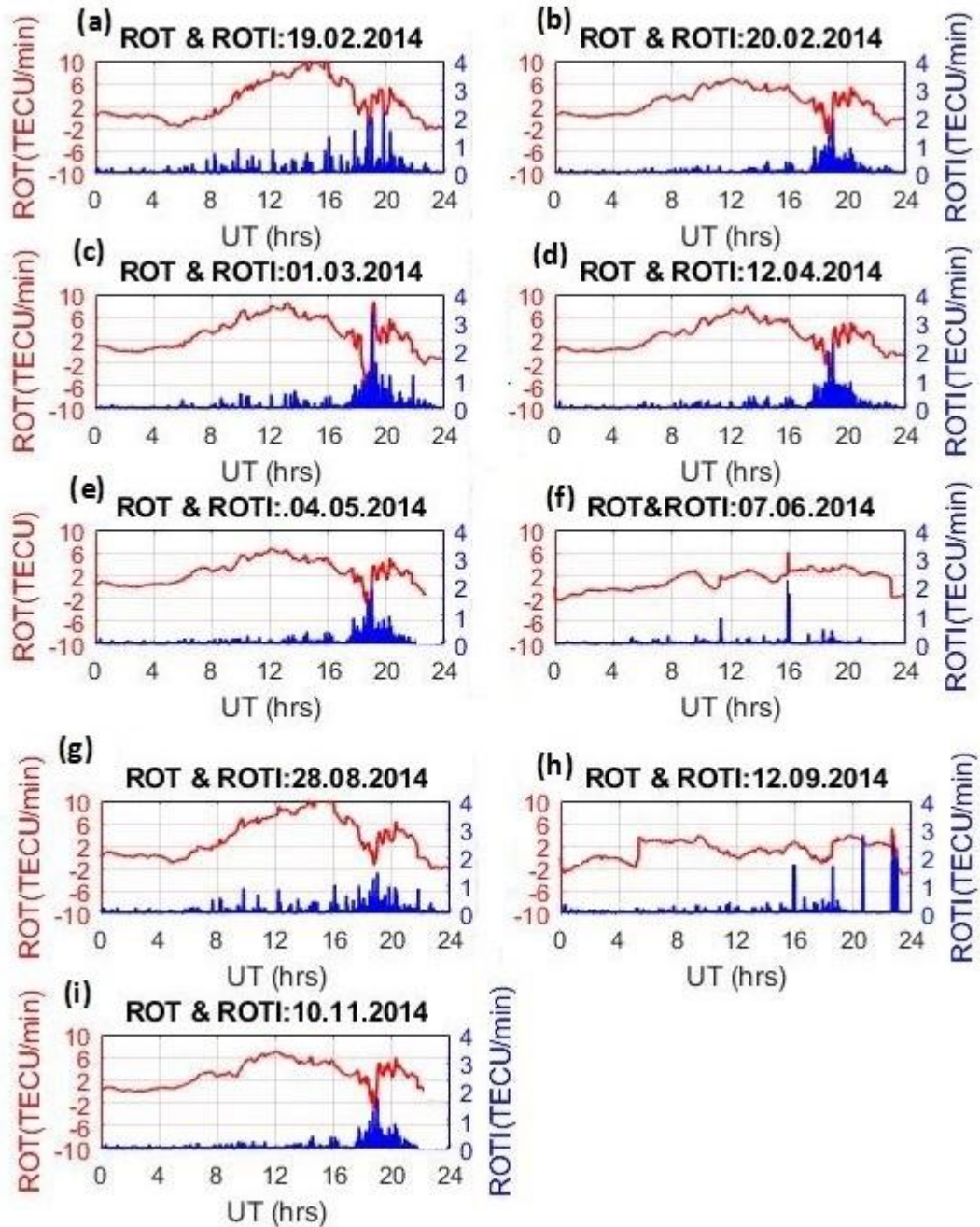


**Figure 4.2.4: ROT and ROTI plots for selected storm days between Feb. – Oct. 2014**

From these results, it can be noted that for most days the increase in solar flux and solar wind speeds led to large TEC depletion depth which led to higher ROTI values after local

sunset. These results conform to those reported from a study by Azzouzi *et al.*, (2016) on the impact of high speed solar wind stream on the variability of TEC and ROTI.

Generally, the ROT and ROTI plots in Figures 4.2.1, 4.2.2, 4.2.3 and 4.2.4 highlighted both day and night time trends. The period showing presence of ionospheric post-sunset plasma irregularities was manifested through increased ROT fluctuation and higher ROTI values of more than 1.5 TECU/min after local sunset while a period showing absence was manifested through minimal or no fluctuation of ROT and lower ROTI values of below 1.5 TECU/min after local sunset. A similar diurnal trend was also observed by Nishioka *et al.*, (2008) in their study on the occurrence of plasma bubble using global ground-based GPS receiver networks between 2000 and 2006 where ROTI was low and constant during the day and night on some days and low and constant during the day and larger after sunset. ROT and ROTI showed a positive correspondence after local sunset where increased ROT fluctuations corresponded well with large ROTI values while small ROT fluctuations corresponded with very low ROTI values for some selected quiet and storm days as indicated by the ROT and ROTI plots in Figures 4.2.1, 4.2.2, 4.2.3 and 4.2.4.

### **4.3 Inferring presence of EPBs using TEC depletion, S<sub>4</sub> index, ROT and ROTI**

When inferring occurrence of EPBs in this study, TEC depletions of TEC depletion depths of at least 7 TECU were to correspond with a rise in S<sub>4</sub> index, increased ROT fluctuations with ROTI reaching their largest values of more than 1.5 TECU/min just after local sunset. This was used a proxy for identification of plasma bubbles.

### 4.3.1. Inferring EPBs for selected quiet days of 2013

The variation of TEC depletions,  $S_4$  index, ROT and ROTI indicated in Figures 4.1.1 and 4.2.1 were summarized in Table 4.5 and TEC depletion depths and ROTI plotted as in Figure 4.3.1.

**Table 4.5: Summary of TEC depletion,  $S_4$ , ROT and ROTI for selected quiet days of 2013**

| Month          | Date       | TEC depletion depth | Maximum $S_4$ | ROT fluctuation (16:00-22:00 UT) | ROTI (16:00-22:00 UT)(TECU/min) |
|----------------|------------|---------------------|---------------|----------------------------------|---------------------------------|
| March 2013     | 26-03-2013 | 15 TECU             | 0.2           | Increased                        | High ROTI (1.9)                 |
| April 2013     | 18-04-2013 | 15 TECU             | 0.35          | Increased                        | High ROTI (1.6)                 |
|                | 19-04-2013 | 25 TECU             | 0.5           | Increased                        | High ROTI (1.9)                 |
| May 2013       | 10-05-2013 | 16 TECU             | 0.35          | Increased                        | High ROTI (1.8)                 |
| June 2013      | 17-06-2013 | 15 TECU             | 0.3           | Increased                        | High ROTI (1.8)                 |
|                | 26-06-2013 | 5 TECU              | 0.1           | None                             | None                            |
| July 2013      | 04-07-2013 | 5 TECU              | 0.15          | None                             | None                            |
|                | 24-07-2013 | 5 TECU              | 0.3           | None                             | None                            |
| August 2013    | 11-08-2013 | 7 TECU              | 0.15          | Increased                        | High ROTI (1.5)                 |
| September 2013 | 07-09-2013 | 5 TECU              | 0.25          | Slight                           | Low ROTI (0.2)                  |
|                | 26-09-2013 | 16 TECU             | 0.35          | Increased                        | High ROTI (1.8)                 |
| November 2013  | 21-11-2013 | 11 TECU             | 0.2           | Increased                        | High ROTI (1.8)                 |

In Figure 4.3.1, the highest value of ROTI (1.9 TECU/min) was on 19<sup>th</sup> April 2013 with a corresponding TEC depletion depth of 25 TECU while the lowest value of ROTI (0.2 TECU/min) was on 7<sup>th</sup> September 2013 between 16:00 and 22:00 UT. Large values of ROTI ( $\geq 1.5$  TECU/min) were seen to correspond with increased TEC depletion of depletion depths  $\geq 7$  TECU and increased ROT fluctuations after local sunset (16:00-22:00UT) on 26<sup>th</sup> March 2013, 18<sup>th</sup> April 2013, 19<sup>th</sup> April 2013, 10<sup>th</sup> May 2013, 17<sup>th</sup> June 2013, 11<sup>th</sup> August 2013, 26<sup>th</sup> September 2013 and 21<sup>st</sup> November 2013. This correspondence led us infer presence of EPBs on 26<sup>th</sup> March 2013, 18<sup>th</sup> April 2013, 19<sup>th</sup> April 2013, 10<sup>th</sup> May 2013, 17<sup>th</sup> June 2013, 11<sup>th</sup> August 2013, 26<sup>th</sup> September 2013 and 21<sup>st</sup> November 2013.

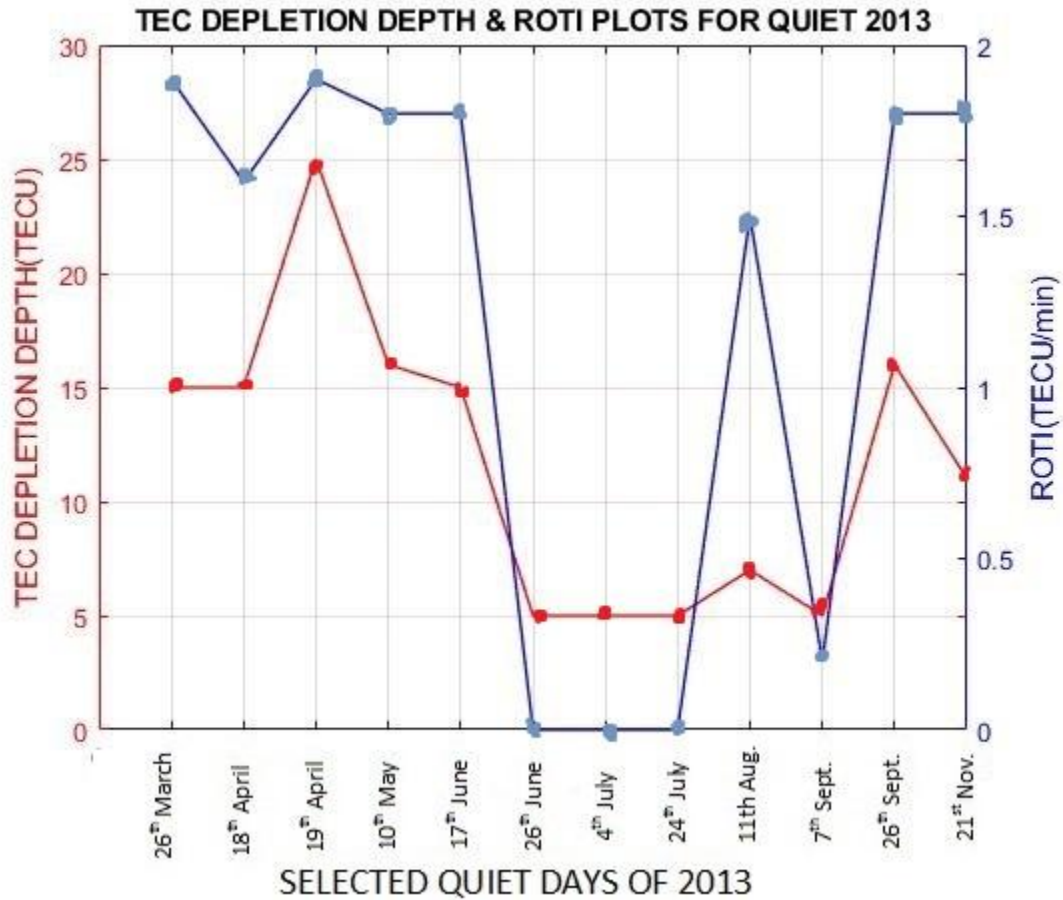


**Figure 4.3.1: TEC depletion depth & ROTI plot for selected Quiet days of 2013**

Most quiet days of the year 2013 in which the presence of EPBs were inferred had larger TEC depletion depths corresponding with higher ROTI values after local sunset as indicated by the TEC depletion depths and ROTI plot in Figure 4.3.1.

### 4.3.2. Inferring EPBs for selected quiet days of 2014

The variation of TEC depletions,  $S_4$  index, ROT and ROTI in Figures 4.1.2 and 4.2.2 were summarized in Table 4.6 and TEC depletion depths and ROTI plotted as in Figure 4.3.2.

**Table 4.6: Summary of TEC depletion,  $S_4$ , ROT and ROTI for selected quiet days of 2014**

| Month          | Date       | TEC depletion depth | Maximum $S_4$ | ROT fluctuation (16:00-22:00UT) | ROTI (16:00-22:00 UT)(TECU/min) |
|----------------|------------|---------------------|---------------|---------------------------------|---------------------------------|
| January 2014   | 16-01-2014 | 5 TECU              | 0.1           | Slight increase                 | Low ROTI (0.2)                  |
| February 2014  | 03-02-2014 | 15 TECU             | 0.3           | Increased                       | High ROTI (1.8)                 |
| March 2014     | 07-03-2014 | 12 TECU             | 0.4           | Slight increase                 | Low ROTI(0.2)                   |
| April 2014     | 16-04-2014 | 20 TECU             | 0.5           | Increased                       | High ROTI (1.8)                 |
| May 2014       | 02-05-2014 | 12 TECU             | 0.3           | Increased                       | High ROTI (1.8)                 |
|                | 13-05-2014 | 11 TECU             | 0.2           | Increased                       | High ROTI (1.8)                 |
| August 2014    | 26-08-2014 | 20 TECU             | 0.3           | Increased                       | High ROTI (1.8)                 |
| September 2014 | 07-09-2014 | 5 TECU              | 0.3           | Slight increase                 | Low ROTI(0.2)                   |
| October 2014   | 07-10-2014 | 15 TECU             | 0.25          | Increased                       | High ROTI(1.8)                  |
|                | 13-10-2014 | 3 TECU              | 0.2           | Slight increase                 | Low ROTI (0.2)                  |
| November 2014  | 26-11-2014 | 5 TECU              | 0.2           | Slight increase                 | Low ROTI (0.2)                  |
| December 2014  | 11-12-2014 | 5 TECU              | 0.2           | Slight increase                 | Low ROTI (0.2)                  |

The highest value of ROTI after local sunset was 1.8 TECU/min on 3<sup>rd</sup> February 2014, 16<sup>th</sup> April 2014, 2<sup>nd</sup> May 2014, 13<sup>th</sup> May 2014, 26<sup>th</sup> August 2014 and 7<sup>th</sup> October 2014 while the lowest ROTI value was 0.2 TECU/min on 16<sup>th</sup> January 2014, 7<sup>th</sup> March 2014, 7<sup>th</sup> September 2014, 26<sup>th</sup> November 2014 and 11<sup>th</sup> December 2014. The large ROTI values ( $\geq 1.5$  TECU/min) were seen to correspond well with increased fluctuation of ROT and sharp depletion of TEC of depletion depths  $\geq 7$  TECU after local sunset on 3<sup>rd</sup> February 2014, 16<sup>th</sup> April 2014, 2<sup>nd</sup> May 2014, 13<sup>th</sup> May 2014, 26<sup>th</sup> August 2014 and 7<sup>th</sup> October 2014. This correspondence led us infer presence of EPBs on 3<sup>rd</sup> February 2014, 16<sup>th</sup> April 2014, 2<sup>nd</sup> May 2014, 13<sup>th</sup> May 2014, 26<sup>th</sup> August 2014 and 7<sup>th</sup> October 2014.

Largest TEC depletion depth of 20 TECU was observed on 16<sup>th</sup> April 2014 with a corresponding highest ROTI value of 1.8 TECU/min as indicated by the TEC depletion depths and ROTI plot in Figure 4.3.2.

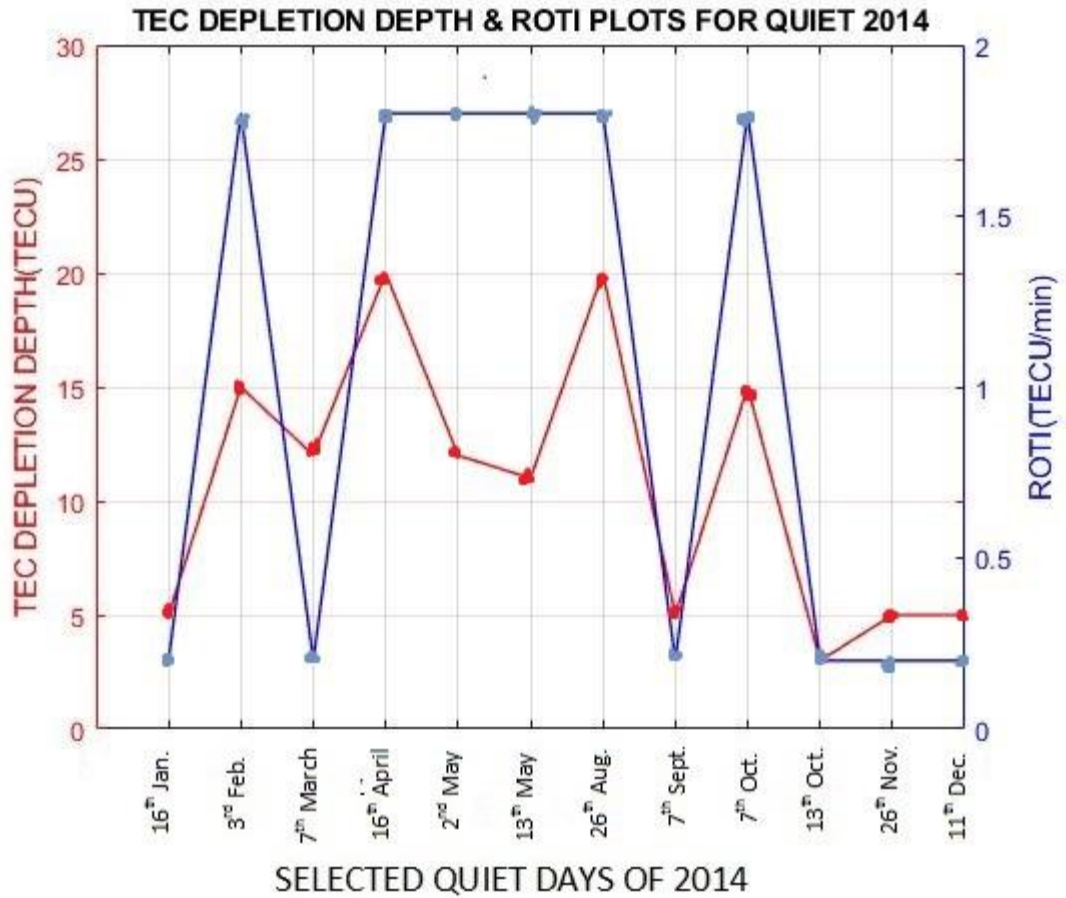


**Figure 4.3.2: TEC depletion depth & ROTI plot for selected Quiet days of 2014**

Most selected quiet days of the year 2014 also showed a positive correspondence between TEC depletion depths and ROTI where larger TEC depletion depths corresponded with higher ROTI values after local sunset for most days in which presence of EPBs were inferred.

### 4.3.3. Inferring EPBs for selected storm days of 2013

The variation of TEC depletions,  $S_4$  index, ROT and ROTI in Figures 4.1.3 and 4.2.3 were summarized in Table 4.7 and TEC depletion depths and ROTI plotted as in Figure 4.3.3.

**Table 4.7: Summary of TEC depletion,  $S_4$ , ROT and ROTI for selected storm days of 2013**

| Month         | Date       | TEC depletion depth | Maximum $S_4$ | ROT fluctuation (16:00-22:00UT) | ROTI (16:00-22:00 UT)(TECU/min) |
|---------------|------------|---------------------|---------------|---------------------------------|---------------------------------|
| March 2013    | 01-03-2013 | 5 TECU              | 0.1           | None                            | None                            |
| April 2013    | 24-04-2013 | 15 TECU             | 0.5           | Increased                       | High ROTI(1.7)                  |
| May 2013      | 01-05-2013 | 12 TECU             | 0.2           | Increased                       | High ROTI(1.8)                  |
|               | 18-05-2013 | 5 TECU              | 0.3           | Slight increase                 | Low ROTI (0.2)                  |
| June 2013     | 01-06-2013 | 4 TECU              | 0.1           | None                            | None                            |
| July 2013     | 06-07-2013 | 5 TECU              | 0.1           | None                            | None                            |
|               | 10-07-2013 | 3 TECU              | 0.3           | None                            | None                            |
|               | 14-07-2013 | 2 TECU              | 0.2           | Slight increase                 | Low ROTI (0.2)                  |
| August 2013   | 05-08-2013 | 13 TECU             | 0.3           | Increased                       | High ROTI (2)                   |
| November 2013 | 09-11-2013 | 11 TECU             | 0.2           | Increased                       | High ROTI (3.5)                 |
|               | 11-11-2013 | 16 TECU             | 0.2           | Increased                       | High ROTI (2.1)                 |
| December 2013 | 08-12-2013 | 10 TECU             | 0.1           | Increased                       | High ROTI (1.5)                 |

The highest ROTI value attained was 3.5 TECU/min on 9<sup>th</sup> November 2013 while the lowest ROTI value was 0.2 TECU/min on 18<sup>th</sup> May 2013 and 14<sup>th</sup> July 2013 as indicated in Figure 4.3.3. Some days including 1<sup>st</sup> March 2013, 1<sup>st</sup> June 2013, 6<sup>th</sup> July 2013 and 10<sup>th</sup> October 2013 showed no ROT fluctuation hence had very low ROTI values. The large ROTI values ( $\geq 1.5$  TECU/min) attained were seen to correspond well with increased ROT fluctuations and sharp depletions of TEC of depletion depths  $\geq 7$  TECU between 16:00 and 22:00 UT on 24<sup>th</sup> April 2013, 1<sup>st</sup> May 2013, 5<sup>th</sup> August 2013, 9<sup>th</sup> November 2013, 11<sup>th</sup> November 2013 and 8<sup>th</sup> December 2013. This led us infer presence of EPBs on 24<sup>th</sup> April 2013, 1<sup>st</sup> May 2013, 5<sup>th</sup> August 2013, 9<sup>th</sup> November 2013, 11<sup>th</sup> November 2013 and 8<sup>th</sup> December 2013.

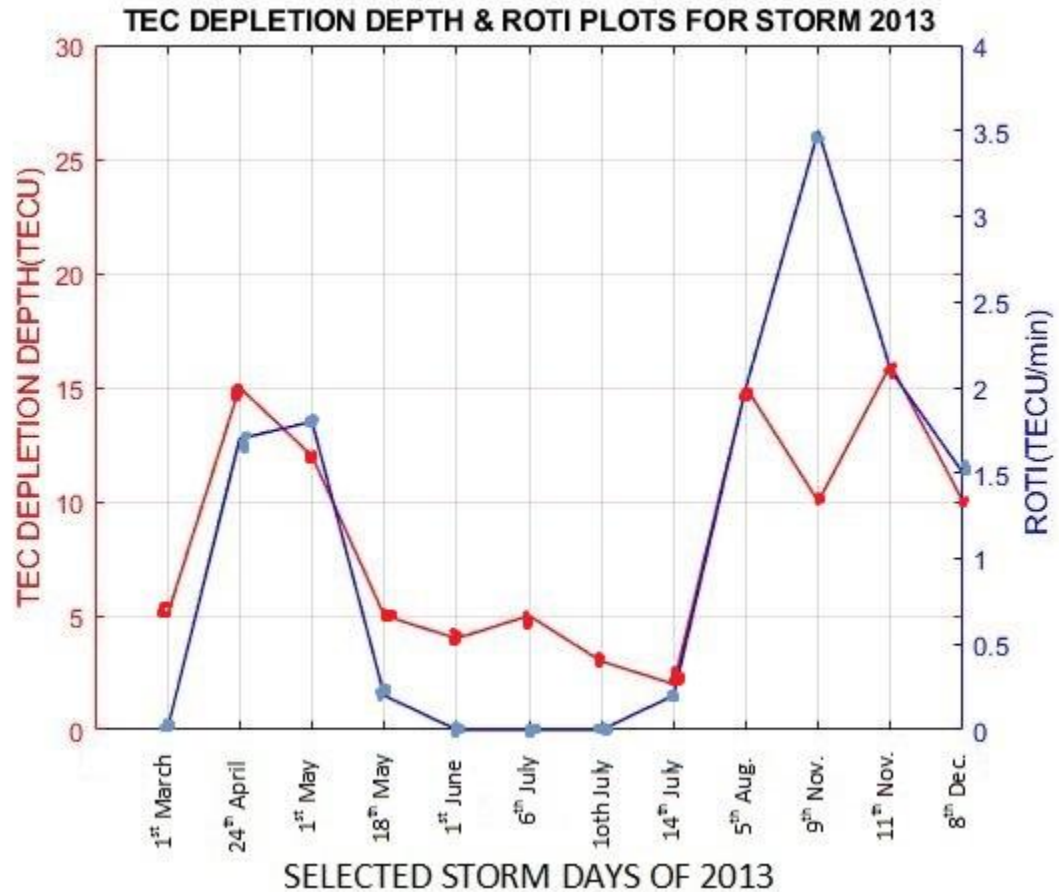


Figure 4.3.3: TEC depletion depth & ROTI plot for selected Storm days of 2013

#### 4.3.4. Inferring EPBs for selected storm days of 2014

The variation of TEC depletions,  $S_4$  index, ROT and ROTI in Figures 4.1.4 and 4.2.4 were summarized in Table 4.8 and TEC depletion depths and ROTI plotted in Figure 4.3.4.

Table 4.8: Summary of TEC depletion,  $S_4$ , ROT and ROTI for selected storm days of 2014

| Month          | Date       | TEC depletion depth | Maximum $S_4$ | ROT fluctuation (16:00-22:00UT) | ROTI (16:00-22:00 UT)(TECU/min) |
|----------------|------------|---------------------|---------------|---------------------------------|---------------------------------|
| February 2014  | 19-02-2014 | 12 TECU             | 0.2           | Increased                       | High ROTI (2)                   |
|                | 20-02-2014 | 10 TECU             | 0.3           | Increased                       | High ROTI (2)                   |
| March 2014     | 01-03-2014 | 18 TECU             | 0.3           | Increased                       | High ROTI (3.4)                 |
| April 2014     | 12-04-2014 | 15 TECU             | 0.7           | Increased                       | High ROTI(2.2)                  |
| May 2014       | 04-05-2014 | 18 TECU             | 0.4           | Increased                       | High ROTI(2)                    |
| June 2014      | 07-06-2014 | 3 TECU              | 0.2           | None                            | None                            |
| August 2014    | 28-08-2014 | 10 TECU             | 0.3           | Increased                       | High ROTI (1.5)                 |
| September 2014 | 12-09-2014 | 8 TECU              | 0.3           | Slight increase                 | Low ROTI (0.2)                  |
| November 2014  | 10-11-2014 | 10 TECU             | 0.4           | Increased                       | High ROTI (1.8)                 |

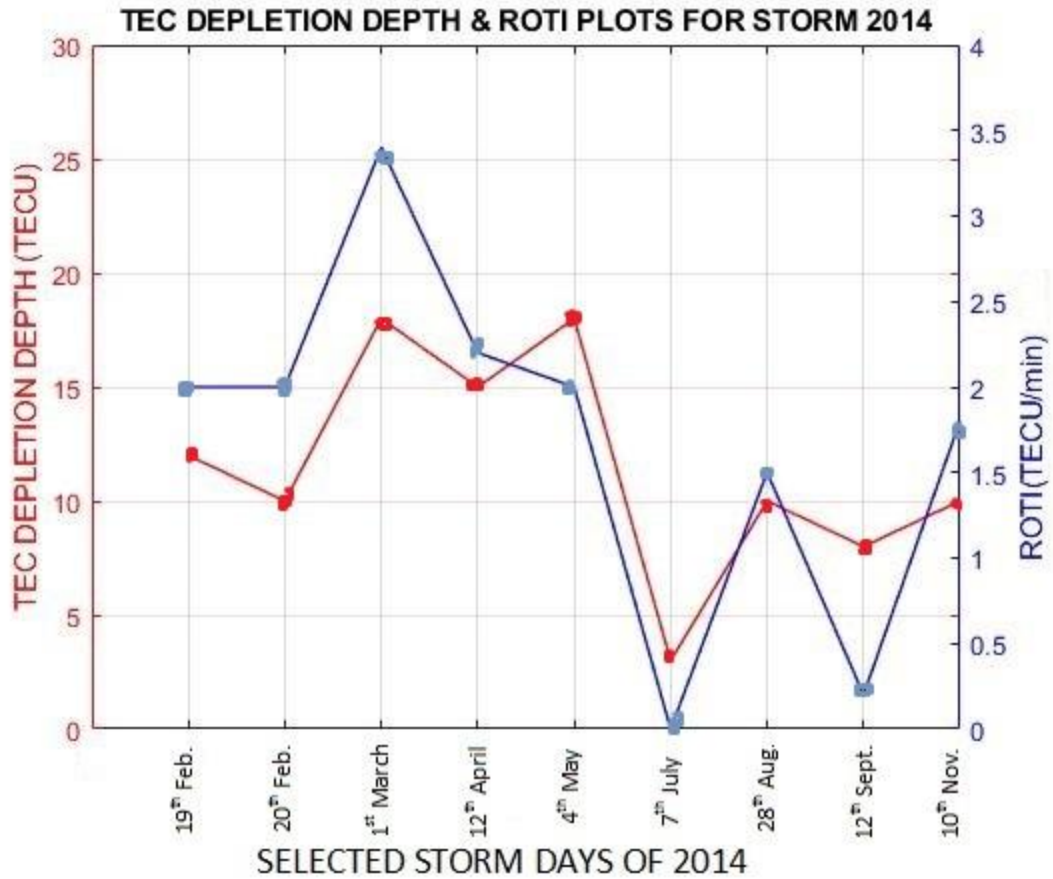


**Figure 4.3.4: TEC depletion depth & ROTI plot for selected Storm days of 2014**

The highest ROTI value of 3.4 TECU/min was attained on 1<sup>st</sup> March 2014 while the lowest ROTI value was 0.2 TECU/min on 12<sup>th</sup> September 2014 after local sunset as indicated in Figure 4.3.4. No ROT fluctuation was observed on 7<sup>th</sup> June 2014, hence low ROTI value was observed. High ROTI values ( $\geq 1.5$  TECU/min) attained corresponded well with increased ROT fluctuations and large depletions of TEC of depletion depths  $\geq 7$  TECU after local sunset on 19<sup>th</sup> April 2014, 20<sup>th</sup> February 2014, 1<sup>st</sup> March 2014, 12<sup>th</sup> April 2014, 4<sup>th</sup> May 2014, 28<sup>th</sup> August 2014 and 10<sup>th</sup> November 2014. This led us infer presence of EPBs on 19<sup>th</sup> April 2014, 20<sup>th</sup> February 2014, 1<sup>st</sup> March 2014, 12<sup>th</sup> April 2014, 4<sup>th</sup> May 2014, 28<sup>th</sup> August 2014 and 10<sup>th</sup> November 2014.

Large TEC depletion depths values were observed to correspond with higher ROTI values after local sunset for most days in which presence of EPBs were inferred.

It was observed from the TEC depletion depths and ROTI plots in Figures 4.3.1, 4.3.2, 4.3.3 and 4.3.4 that large TEC depletion depths resulted in high ROTI values in both quiet and disturbed conditions as indicated by the graphs. The large TEC depletion depths resulting in high ROTI values were also observed by DasGupta *et al.*, (2007). In this study, the enhancement of S<sub>4</sub> index corresponded well with TEC depletions of depletion depths  $\geq 7$  TECU, increased ROT fluctuations and high ROTI values of more than 1.5 TECU/min between 16:00- 22:00UT for all the days we inferred presence of EPBs. Generally, the correspondence of high ROTI values, increased ROT fluctuation, sharp depletion of TEC and increased S<sub>4</sub> enhancement between 16:00-22:00 UT which enable inferring presence of EPBs conform with results reported by Nishioka *et al.*, (2008); Zou and Wang, (2009); Zernov *et al.*, (2009) and Adewale *et al.*, (2012) in the studies on occurrence of EPBs using VTEC depletions, ROT and ROTI.

#### 4.3.5: Percentage occurrence of EPBs in the year 2013 and 2014

The percentage EPB occurrence for the selected quiet and storm days for years 2013 and 2014 was summarized as indicated in Table 4.9 and plotted as in Figure 4.3.5

**Table 4.9: Summary of percentage EPB occurrence for the years 2013 and 2014**

| Year | Available data days | Total EPBs for the year | % EPBs occurrence | Selected Storm days in the year | Observed EPB storm days | % EPBs for storm days | Selected Quiet days in the year | Observed EPB quiet days | % EPBs for quiet days |
|------|---------------------|-------------------------|-------------------|---------------------------------|-------------------------|-----------------------|---------------------------------|-------------------------|-----------------------|
| 2013 | 231                 | 15                      | 6.49%             | 28                              | 6                       | 21.42%                | 48                              | 9                       | 18.75%                |
| 2014 | 301                 | 13                      | 4.32%             | 32                              | 7                       | 21.88%                | 76                              | 6                       | 7.89%                 |

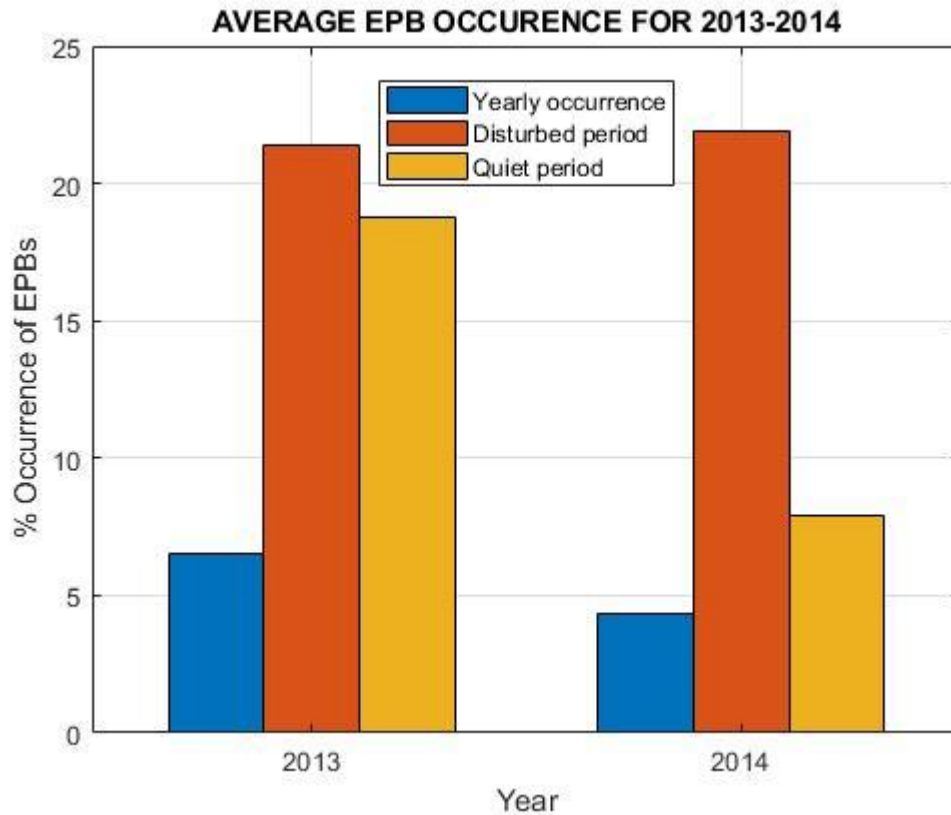


**Figure 4.3.5: Bar graph of percentage EPB occurrence for 2013 and 2014 as in Table 4.9**

Figure 4.3.5 shows percentage EPB occurrence of 6.49% in the year 2013 and of 4.32% in the year 2014. The percentage EPB occurrence in storm period of the year 2013 was 21.42% while in the year 2014 was 21.88%. The percentage EPB occurrence in the quiet period was 18.75% in the year 2013 and 7.89% in the year 2014. It was observed from these results that the percentage of EPB occurrence was higher during storm days than in quiet days of the years 2013 and 2014. These results conform with results from earlier studies done by Abdu *et al.*, (2003); Kil and Paxton, (2006); Li *et al.*, (2006) and Basu *et al.*, (2007) where the occurrence of EPBs were found to be enhanced by geomagnetic activity. Nakata *et al.*, (2018) showed that most EPBs occur during high geomagnetic activity period since the PPEF which is enhanced during storms favors the occurrence of

EPBs during such periods. When geomagnetic storms occur, the ionospheric electric fields at the polar (high latitude) region penetrate towards the low latitude (Nakara *et al.*, 2018). This penetrating electric field called PPEF (Basu *et al.*, 2007; Kikuchi *et al.*, 2008) which is short duration perturbations (taking a few hours) is eastward in the dusk ionosphere hence enhancing growth of RTI and it causes development of plasma bubbles (Abdu *et al.*, 2009; Cherniak *et al.*, 2019) due to increased  $\mathbf{E} \times \mathbf{B}$  upward drift. In the recovery phase (Huang *et al.*, 2001; Abdu *et al.*, 2009; Bolaji *et al.*, 2019), the direction changes in opposite direction due to the development of a shielding current (Kelley *et al.*, 1979; Kikuchi *et al.*, 2008) which increases the opposite polarity of the electric field hence inhibiting the occurrence of EPBs. This electric field is called DDEF (Blanc & Richmond, 1980; Bhattacharrya *et al.*, 2019). Besides the effect of PPEF and DDEF, the occurrence of EPBs is also affected by the storm winds which extend from the high latitude regions to low latitude regions. Storm winds lift the ionized regions and modify the atmospheric composition of equatorial ionosphere, hence affecting EIA, PRE, VTEC and ROTI. The occurrence of EPBs during disturbed days is therefore determined by the competing effects of PPEF, DDEF and the storm winds since the DDEF effect is usually delayed and lasts longer than PPEF (Richmond *et al.*, 2003). During quiet days, the interplanetary magnetic field (IMF Bz) is northward, hence the enhancement of the eastward electric field brings the occurrence of EPBs (Cherniak *et al.*, 2019).

#### **4.3.6: Seasonal occurrence of EPBs in the year 2013 and 2014**

Seasonal variation of equatorial plasma bubbles was also determined by classifying percentage EPB occurrence into four seasons for each year, as shown in Table 4.10 and Figure 4.3.6.

**Table 4.10: Summary of seasonal variation of EPBs for the year 2013 and 2014**

| YEAR | TOTAL EPB DAYS | SEASON            | MONTHS            | EPB DAYS | %EPB OCCURRENCE |
|------|----------------|-------------------|-------------------|----------|-----------------|
| 2013 | 15             | March Equinox     | March/April       | 5        | 33.33%          |
|      |                | June Solstice     | June/July         | 1        | 6.67%           |
|      |                | September Equinox | August/September  | 3        | 20%             |
|      |                | November Solstice | November/December | 3        | 20%             |
| 2014 | 13             | March Equinox     | March/April       | 4        | 30.76%          |
|      |                | June Solstice     | June/July         | 1        | 7.69%           |
|      |                | September Equinox | August/September  | 2        | 15.38%          |
|      |                | November Solstice | November/December | 1        | 7.69%           |

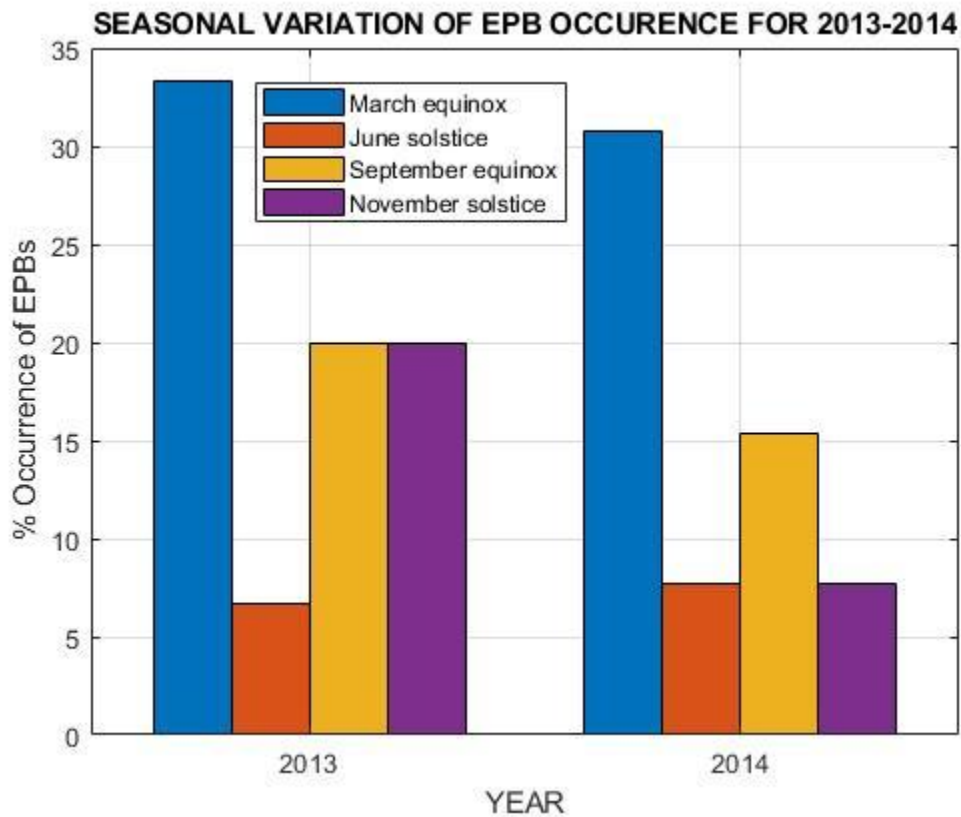


**Figure 4.3.6: Bar graph showing seasonal variation of EPBs for 2013/2014 period as in Table 4.10**

Figure 4.3.6 shows the results for seasonal variation of EPB occurrence for the years 2013 and 2014. The March equinox had 33.33% EPB occurrence for the year 2013 and 30.76% EPB occurrence for the year 2014. The September equinox showed percentage EPB

occurrence of 20.38% for the year 2013 and 17.26% for the year 2014. During the June solstice, the percentage EPB occurrence was 6.67% for the year 2013 and 7.69% for the year 2014 while for the November solstice, the percentage EPB occurrence was 30.76% in the year 2013 and 7.69% in the year 2014. The results clearly indicated that the percentage occurrence of EPBs was higher during equinoctial period than in the solstice period. This is because during equinoctial periods, the equatorial region is highly exposed to the Sun's intensity leading to the increase in rate of EPB occurrence. This increases background ionization, leading to formation of irregularities. Studies by Sahai *et al.*, (2000) and Huang *et al.*, (2001) have shown that the percentage of EPB occurrence increases during periods of high solar activity. This result conforms well with results obtained from earlier studies done by Paznukhov *et al.*, (2012) and Magdaleno *et al.*, (2017) where highest occurrence of EPBs were observed during equinoctial months. The increase in EPBs corresponding with increase in solar intensity could be attributed to the increase in background ionization in the ionosphere. The seasonal variation of EPB occurrence is attributed to the effect of PRE of the eastward electric field which induces increase in vertical  $\mathbf{E} \times \mathbf{B}$  drift (Abdu *et al.*, 1981; Batista *et al.*, 1996; Sobral *et al.*, 2002; Murkherjee *et al.*, 2010). The daytime  $\mathbf{E} \times \mathbf{B}$  drift velocities are larger in the equinoctial months (March, April, August and September) and November solstitial months (November and December) than in June solstitial months (June and July). June solstice had the lowest percentage EPB occurrence as also reported in studies by Cherniak *et al.*, (2019). This might be due to a lower  $\mathbf{E} \times \mathbf{B}$  vertical drift in the June solstice due to a reduced eastward electric field.

## CHAPTER FIVE

## CONCLUSIONS AND RECOMMENDATIONS

### 5.0 Conclusions

This chapter gives a summary of conclusions for each of the studied objectives and the recommendations for further research.

#### 5.0.1 Establishing TEC depletions over Kisumu, Kenya between 1<sup>st</sup> January 2013 and December 2014 for selected storm and quiet days

The results of this work showed that TEC underwent diurnal variation exhibited by a steady increase from pre-sunrise (02:00-04:00UT) and reached maximum in the afternoon (10:00-14:00 UT) before falling to attain a minimum value just after local sunset. The diurnal TEC variation was attributed to change in ionization resulting from solar radiation. The presence of TEC depletions with depletion depths of 10-20 TECU was noted after local sunset (16:00 -22:00 UT) for most days and these TEC depletions corresponded well with enhanced  $S_4$  values. The months of March, April, August and September (equinoctial months) exhibited higher average TEC values than the solstice months (June, July, November and December) due to increased solar intensity in the equatorial region during the equinoctial months. The TEC depletions were seen to correspond with increase in  $S_4$  index after sunset. However, the percentage occurrence of  $S_4$  index exhibited a seasonal dependence with higher average  $S_4$  index values (0.4) observed in equinoctial months and lower average  $S_4$  index values (0.26) observed in the solstice months. This was attributed to the increased solar intensity resulting from the close alignment of the solar terminator and the geomagnetic meridian.

#### 5.0.2 Investigating ROT and ROTI for selected storm and quiet days

ROTI was observed to undergo a diurnal trend where by ROTI was low and constant during the day and night for some days and low and constant during the day and larger after sunset. During storm days, ROTI values were averagely higher than during quiet days after sunset. The higher ROTI values observed during the storm days was attributed to the TEC response to the geomagnetic storms. Generally, there was a high correspondence between ROT and ROTI where the increased fluctuation of ROT corresponded well with higher ROTI values after sunset for most days. Increased solar wind speed was observed to have an impact of higher ROTI values arising from larger TEC depletion depth for both selected quiet and storm days of the years 2013 and 2014.

### **5.0.3 Inferring presence of EPBs over Kisumu, Kenya between 1<sup>st</sup> January 2013 and 31<sup>st</sup> December 2014 using TEC depletion, S<sub>4</sub> index, ROT and ROTI**

The enhancement of S<sub>4</sub> index corresponded well with TEC depletions of depletion depth of  $\geq 7$  TECU, increased ROT fluctuations and high ROTI values  $\geq 1.5$  TECU/min after local sunset. This relationship was a good proxy in inferring presence of EPBs from the TEC data. The percentage rate of EPB occurrence during equinoctial period (March/April) was higher than in the solstice periods (June/July and November/December). This implied that the occurrence of plasma bubbles positively corresponded with solar activity. The percentage occurrence of EPBs in the year 2013 was 6.49% while in the year 2014 was 4.32%. The storm days had a higher percentage occurrence of EPBs than quiet days. The higher percentage occurrence of EPBs during the storm days was attributed to the effect of increased PPEF and storm winds.

In conclusion, this study confirms the presence of EPBs over Kisumu, Kenya for the selected quiet and storm days of 2013 and 2014.

## **5.2 Recommendation for future Work**

This study was limited to data from a single SCINDA-GPS station in Kenya and out of the total targeted 730 days of 2013 and 2014, only data for 532 days was available for use. Future work should involve more SCINDA-GPS stations in East-Africa and an extension of this study should involve the correlation between ROTI and daily variability of **E x B** vertical plasma drift and F2 layer changes. The uplift to the F2 layer depends on the vertical plasma drift and hence the study would help in understanding the spatial distribution of EPBs over East-Africa for the solar cycle 24.

## **REFERENCES**

Abdu, M., Muralikrishna, P., Batista, I. and Sobral, J.(1991). Rocket observation of Equatorial Plasma bubbles over Natal, Brazil, using a high-frequency capacitance probe, J. Geophys. Res, -Space, 96, 7689-1991.

- Abdu, M. A., Batista, I. S., Takahashi, H, MacDougall , J., Sobral, J. H., Medeiros, A. F. and Trivedi B.(2003). Magnetospheric disturbance induced equatorial plasma bubble development and dynamics. *A case study in Brazilian sector*. Journal of Geophysical Research, 108(A12), 1449. <https://doi.org/10.1029/2002JA009721>.
- Abdu, M., Bittencourt, J. and Batista, I. (1981).Magnetic declination control of the equatorial F Region dynamo electric field development and spread F, J. Geophys. Res.-Space, 86, 11443-11446, 1981.
- Abdu, M., Batista, I., Reinisch, B., MacDougall, J., Kherani, E. and Sobral, J. (2012). Equatorial range spread F echoes from coherent backscatter and irregularity growth processes from conjugate point digital ionograms, Radio Sci., 47, <https://doi.org/10.1029/2012.RS005002>, 2012
- Abdu, M. A., Kherani, E. A., Batista, I. S. and Sobral, J. H. A.(2009). Equatorial evening pre-reversal vertical drift and spread F suppression by disturbance penetration electric field Geophys Res Lett 36:119103. <https://doi.org/10.1029/2009/GLO39919>.
- Adetayo, V. E., Adewale, A. O., Akala, A. O., Bolaji, O. S. and Rabiou A. B. (2017). Studying the variability of in the diurnal variations of GPS TEC over Nigeria. Ann. Geophys, 35,701-710, <https://doi.org/10.5194/angeo-35-701-2017>.
- Adewale, A. O.,Oyeyemi, E. O.,Adeloye, A. B.,Mitchell, C. N., Rose, J. A. R. and Cilliers, P. J. (2012). A study of L-band scintillations and total electron content at an Equatorial Station. Lagos, Nigeria. Radio science, vol. 47, RS2011, doi: 10.1029/2011RS004846, 2012.
- Akala, O. A., Idolor, R., D'ujanga, M., and Doherty, P. H. (2016). GPS-Amplitude Scintillation over Kampala during 2010-2011. Acta Geophysica, Vol. 64, no. 5, Oct. 2016,1903-1915, doi:10.1515/angeo-2016-0052.
- Alagbe, G. A., Ofalabi, O. O., Adagunodo, T. A., Rabiou, S. B., Akinwumi, S. A. and Omotosho, T. V.(2017).Study of Ionospheric Amplitude scintillation during Geomagnetic activities of 2012 at low latitude region. Vol. 9, No.2, pp251-256, 2017. ISSN 0975-5748.
- Anderson D. and Fuller-Rowell, T. (1999).Space environment. [Htps://sec.noaa.gov](https://sec.noaa.gov).
- Arruda, D. C., Sobral, J., Abdu, M., Castilho, V. M., Takahashi, H. Medeiros, A. and Buriti, R.(2006).Theoretical and experimental zonal drifts velocities of the ionospheric plasma Bubbles over the Brazilian region, Adv. Space Res., 38, 2610-2614, 2006.

- Azzouzi, I., Migoya-Orue, Y., Coisson, P., Amory Mazaudier, C., Fleury, R. and Radicella, S. M.(2016).Day to day variability of VTEC and ROTI in October 2012 with impact of high-speed solar wind stream on 13<sup>th</sup>October 2012.[www.researchgate.net/publication/299470637](http://www.researchgate.net/publication/299470637).
- Bagiya, M. S., Joshi, H. P., Iyer, K. N., Aggarwal, M., Ravindran, S., and Pathan, B. M. (2009).TEC variations during low solar activity period (2005-2007) near the Equatorial Ionospheric Anomaly Crest Region in India. *Annales Geophysicae*,27, pp.1047-1057. <https://dx.doi.org/10.5194/angeo-27-1047-2009>.
- Barros, D., Takahashi, H., Wrasse, C. M. and Figueiredo, C. A. O.B.(2018).Characteristics of Equatorial Plasma Bubbles observed by TEC map based on ground-based GNSS Receivers over South America.*Ann.Geophys.*,36,91-100,2018.<https://doi.org/10.5194/angeo-36-91-2018>.
- Bartels, J., Heck, N. H. and Johnson, H. F. (1939).The three-hour-range index measuring geomagnetic activity, *Terr. Magn. Atmos. Electr.*, 44, 411-454.
- Basu, S., Basu, S., Rich, F. J., Grooves, K. M., Mackenzie, E., Coller, C., Sahai, Y., Fagundes, P. R. and Becker-Guedes, F. (2007). Response to the equatorial ionosphere dusk to penetration electric fields during intense magnetic storms. *J Geophys Res* 112:A08308.<https://doi.org/10.1029/2006JA017966>.
- Basu, S., Grooves, K. M., Quinn, J. M. and Doherty, P. H.(1999).A comparison of TEC fluctuations and Scintillation at Ascension Island.*J. Atmos. Terr. Phys.* 61, 1219–1226, doi:10.1016/S1364-6826(99)00052-8.
- Batista, I., Medeiros, R. D., Abdu, M., Souza, J. D., Bailey, G. and Paula, E. D.(1996).Equatorial ionosphere vertical plasma drift model over Brazilian region, *J. Geophys. Res.-Space*, 101, 10887-10892,1996.
- Bhattacharrya, A., Beach,T. L., Basu, S. and Kinter, P. M.(2000).Night-time equatorial ionosphere: GPS scintillations and differential carrier phase fluctuations, *Radio Sci.*, 35(1), 209-234.
- Bhattacharrya, A., Fedrizzi, M., Fuller-Rowell, T. J., Gurram, P., Kakad, B. Sripathi, S. and Sunda, S.(2019). Effects of magnetic storm related thermospheric changes on evolution of Equatorial plasma bubbles.*Journal of Geophysical research, space physics*, 124, 2256-2770.<https://doi.org/10.1029/2018JA025995>.
- Bhuyan, P. K. and Borah, R. R. (2007). TEC derived from GPS network in India and comparison with the IRI. *Adv. Space Res.* 39, 830-840.
- Blanc, M. and Richmomd, A. D. (1980). The ionospheric disturbance dynamo. *J Geophys Res* 85:1669-1686.
- Briggs, B. H. and Parkin, I. A. (1963). On the variation of Radio star and satellite

scintillations With Zenith angle. Journal of Atmos. and Ter. phys., vol. 25, pg. 339-336, doi:10.1016/0021-9169(63)90150-8.

Brown, B. (2012).Down-Sizing of the Ionosphere (V): U.C.Berkeley. Retrieved September 19, 2012 from <http://www.astrosurf.com/luxorion/qs1-hf-tutorial-nm7m5.htm>.

Booker, H. G. and Wells, H. W. (1938). Scattering radio waves by the F-region of the ionosphere, J. Geophys. Res., 43, 249-256.

Bolaji, O. S., Adeniyi, J. O., Radicella, S. M. and Doherty, P. H.(2012).Variability of total electron content over an equatorial West African station during low solar activity, Radio Sci., 47, RS1001, <https://doi.org/10.1029/2011RS004812>.

Bolaji, O. S., Adebisi, S. J. and Fashae, J. B.(2019).Characterization of ionospheric irregularities at different longitudes during quiet and disturbed magnetic conditions. Journal of atmospheric and solar terrestrial physics. <https://doi.org/10.1016/j.jastp.2018.11.007>.

Carrano, C. S.(2007).GPS-SCINDA: A real-time GPS Data Acquisition and Ionospheric Analysis System for SCINDA. Atmospheric and Environmental Research, Inc., GPS-SCINDA.

Carrano, C. S. and Groves, K. M. (2010).Temporal decorrelation of GPS satellite signals due to multiple scattering from ionospheric irregularities: *Proceedings of the 2010 Institute of Navigation ION GNSS meeting*. Portland, OR, 21–24 September 2010.

Caruana, P., Du, J., Wilkinson, P., Thomas, R. and Cervera, M. (2018).Determination of equatorial ionospheric scintillations S<sub>4</sub> dual frequency GPS: *Proceedings WAR'00: Workshop on applications of Radio Science, 27-29 April 2000, La Trobe University*, pg. 85-90, <http://www.ips.gov.au/IPS/Hosted/NCRS/wars/wars2000/index.htm>.

Cherniak, I., Zakharenkova, I. and Sokolovsky, S. (2019).Multi-instrumental observation of storm induced ionospheric plasma bubbles at equatorial and middle latitudes..Journal of Geophysical Research.Spacephysics,124, 1497-1508<https://doi.org/10.29/2018JS026309>.

De Rezende, L., De Paula, E., Kantor, I. and Kintner, P.(2007). Mapping and Survey of plasma bubbles over Brazilian territory, J. Navigation, 60, 69-81, 2007.

DasGupta, A. and Basu, A. (1973).Investigation of ionospheric electron content in the equatorial region as obtained by orbiting beacon satellites, *Ann. Geophys.*,29, 409-419.

- DasGupta, A., Paul, A. and Das, A.(2007).Ionospheric Total Electron Content (TEC) studies with GPS in the Equatorial region. PACs No.94.20.Y<sub>X</sub>;94.20.V<sub>V</sub>.94.20.W<sub>W</sub>, 2007.
- DasGupta, A., Ray, S., Paul, A., Banerjee, P.and Bose, A.(2004). Errors in position-fixing by GPS in an environment of strong equatorial scintillations in the Indian zone, Radio Sci., 39, RS1S30, <https://doi.org/10.1029/2002RS002822>, 2004.
- Dashora, N. and Pandey, R. (2005). Observations in the equatorial anomaly region of total electron content enhancements and depletions. Ann. Geophys.23,2449-2456.
- Datta-Barua, P. H., Doherty, S. H., Dehel, T. and Klobuchar, J. A.(2003).Ionospheric Scintillation Effects on Single and Dual Frequency GPS Positioning: *Proceedings of the 16th International Technical Meeting of the Satellite Division of The Institute of Navigation* (ION GPS/GNSS 2003), Portland, OR, September 2003, 336–346.
- Dieter, B. (2001).International reference Ionosphere 2000, Radio science 36, no. 2, 261-275.
- D’ujanga, F. M. and Taabu, S. D.(2014) Study on the occurrence characteristics of VHF and L-band ionospheric Scintillations over East Africa.Indian Journal of Radio and space physics. PACs No.94.20wg; 94.20. V<sub>V</sub>, Vol. 43,263-273, 2014.
- Eastwood, J. P., Biffis, E., Hapgood, M. A., Green, L., Bisi, M. M., Bentley, R.D., Wicks, R., Mckinell, L.A., Gibbs, M. and Burnett, C.(2017).The Economic impact of space weather: *Where do we stand? Risk Analysis*, vol 37, No.2, 2017 Doi:10.1111/risa.12765.
- Edemsky, I., Lastovicka, J., Buresova, J., Habarulema, J. B. and Nepomnyashchikh, I.(2018). Un-expected Southern Hemisphere response to geomagnetic storm of 15 August 2015. Ann. Geophys.,36, 71-79 2018. <https://doi.org/10.5794/angeo-36-71-2018>.
- Eddy, J. A.(2009).The Sun, The Earth and near Earth Space- *A Guide to the Sun-Earth system*. ISBN. 978-0-16-01 308-8, NP[2009-1-066-GSFC. Tucson, Arizona.
- Eyalade, V. A., Adawale, A.O. , Akala, A. O., Olawale ,S. B. and Babatunde, R.A.(2017). Studying the variability in the diurnal and seasonal variations in GPS in total electron Content over Nigeria. Ann. Geophys. 35, 701-710, 2017. doi.org/10.5194/angeo-35-707-2017.
- Fayose, R.S., Oladosu, O.R., Rabiou, A.B. and Grooves, K.(2012).Variation of Total Electron Content [TEC] and their Effect on GNSS over Akure,Nigeria. doi:10.5539/apr.v4n2p105. <http://dx.doi.org/10.5539/apr.v4n2p105>.

- Grooves, K., Basu, S., Weber, E., Smithan, M., Kuenzler, H., Valladares, C., Sheehan, R., MacKenzie, E., Secan, J., Ning, P., McNell, W., Moonan, D., and Kendra, M.(1997).Equatorial scintillation and systems support. *Radio Sci.*, 32, 2047.
- Grooves, K. and Carrano, C. (2009).Scintillation Impacts on GPS Workshop for Sustainable Development in Navigation Studies and Technology in Africa, lecture delivered at Abdus Salam.*International Centre for Theoretical Physics (ICTP)*. Trieste, Italy, March 23-April 9.
- Gonzalez, W., Joselyn, J., Kamide, Y., Kroehl, H., Rostoker, G., Tsurutani, B. and Vasyliunas, V.(1994). What is a geomagnetic storm?, *J. Geophys. Res.*, 99, 5771-5792.
- Haerendel, G. (1973). Theory of equatorial spread-F, Report Max-planck Institute. *Fur phys. und Astrophysics. Res.*, Garching, Germany.
- Hargreaves, J. K. (1992).*The Solar-terrestrial Environment: An Introduction to Geospace – The Science of the Terrestrial Upper Atmosphere, Ionosphere and magnetosphere*. Cambridge University Press.
- Huang, C. Y., Burke, W. J., Machuzak, J. S., Gentile, L. C. and Sultan, P. J.(2001) DMSP observations of equatorial plasma bubbles in the topside ionosphere near solar maximum. *JGeophys Res* 106: 8131-8142. <https://doi.org/10.1029>.
- Humphreys, T. E., Psiaki, M. L., and Kintner, P. M. (2010).Modelling the effects of ionospheric scintillation on GPS carrier phase tracking, *IEEE transactions on Aerospace & Electronic systems*, 46, no. 4, 1624-1637.
- Hunsucker, R. D., and Hargreaves, J. K.(1995).*The high latitude Ionosphere and its effect on Radio propagation*.Cambridge University Press.
- Jacobsen, K. S.(2014). The impact of different sampling rates and calculation time intervals on ROTI values. *Jspace weather space Clim.*, 4, A33(2014). Doi:10.1051/swsc/2014031.
- Jordi Vila-Valls, Paus Glosas, Charles Fernandez-Prades, Jose A. Lopez-Salcedo and Gonzalo Seco-Granados.(2015).Adaptive GNSS carrier Tracking and ionospheric Scintillation: *Estimation and mitigation*.doi:10.1109/LCOMM.2015.2415789,IEEE, Communications Letters. Barcelona, Spain, 2015.
- Kamide, Y. and Chian, A.(2007).HandBook of the Solar-Terrestrial environment. Springer Berlin Heidelberg, New York.ISBN978-3-540-46314-6,Doi:10.007/6104478.

- Kelley, M. C.(2009). The Earth's ionosphere: Plasma physics and electrodynamics, Int, Geophys. Ser.96.
- Kelley, M. C., Fejer, B. G. and Gonzales, C. A.(1979).An explanation from anomalous equatorial ionospheric fields associated with a northward turning of the interplanetary magnetic field. Geophys Res Lett 6:301-304. <https://doi.org/10.1029/GL006i004P00301>.
- Kikuchi, T., Hashimoto, K. K. and Nozaki, K.(2008).Penetration of magnetospheric electric fields to the equator during a geomagnetic storm. J Geophys. Res 113.a06214. <https://doi.org/10.1029/2007JA012628>.
- Kil, H. and Paxton, L. J.(2006). Ionospheric disturbances during the magnetic storm of 15<sup>th</sup> July 2000: Role of the fountain effect and plasma bubbles for the formation of large equatorial plasma density depletions. JGeophysRes111.A1231, <https://doi.org/10.1029.2006JA011742>.
- Kumar, S. and Singh, A. K.(2010).The effect of geomagnetic storm on GPS derived total electron content (TEC) at Varanasi, India. J. Phys: Conf. Ser. 208 012062.
- Li, G., Ning, L., Hu, L., Liu, X., Yue, W., Wan, B.(2010).Longitudinal development of low-latitude ionospheric irregularities during the geomagnetic storms of July 2004. Journal of Geophysical Research, 115, A04304. <https://10/1029/2009JA014830>.
- Magdaleno, S., Herraiz M., Altadill, D. and De la Morena.(2017).Climatology characterization of equatorial plasma bubbles using GPS data.J. Space Weather Space Clim,7 A3 (2017). Doi: 10.1051/swsc/2016039.
- Makela, J. J., Ledvina, B. M., Kelley, M. C. and Kintner, P. M.(2004).Analysis of seasonal variation of Equatorial plasma bubbles occurrence observed from Haleakala, Hawaii. Annales Geophysicae (2004) 22:3109-3121.SRef-ID: 1432-0576/ag/2004-3109.
- McNamara, L., Caton, R., Parris, R., Pedersen, T., Thompson, D., Wiens, K. and Grooves, K.(2013). Signatures of equatorial plasma bubbles in VHF satellite scintillations and equatorial ionograms, Radio Si., 48, 89-101, 2013.
- Michael, K. C.(2009).The earth's ionosphere: plasma physics and electrodynamics, Int. Geophys. Ser. 96.
- Milos, M.(2014).Determination of TEC in the ionosphere using GPS Technology. Vol. 2, No. 2, Doi: 10.144 38/gn.2014.22.
- Misra, P. and Enge, P.(2001).Global positioning system signals, measurements and performance. Ganga-Jamuna press, Lincoln,Massachusetts, USA.

- Muella, M. T. A. H., Duarte-Silva, M. H., Moraes, A. O., de Paula E. R., de Rezende, L. F. C., Alfonzi, L. and Affonso, B. J. (2017). Climatology and modeling of ionospheric scintillations and irregularity zonal drifts at the equatorial anomaly crest region. *Ann. Geophys.*, 35, 1201-1218, 2017. <https://doi.org/10.5194/angeo-35-1201-2017>.
- Mukherjee, S., Sarkar, S., Purohit, P. K., and Gwal, A. K. (2010). Seasonal variation of Total Electron Content at crest of equatorial anomaly station during low solar activity conditions, *Adv. Spac Res.*, 46, 291-295, 2010.
- Muralikrishna, P., Vieira, L. P. and Abdu, M. A. (2007). Spectral features of E-and F-region irregularities as observed by rocket-borne electron density probes from Brazil, *Revista Brasileira de Geofísica*, 25, 115-128, 2007.
- Nakata, H., Takahashi, A., Takano, T., Jaito, A. and Sakanoi, T. (2018). Observation of equatorial plasma bubbles by airglow imager on ISS-IMAP. *Earth and planetary science*. <https://doi.org/10.1186/s40645-018-0227-0>.
- Ndeda, O. H., and Odera, P. O. (2014). Analysis of Longitudinal Advancement of the peak Total Electron Content in the African equatorial anomaly region using data from GPS receivers and GIS stations in Kenya, *Canadian centre of Sc. & Educ. Applied Phys. Research*: vol. 6, No. 1; 2014. Doi: 10.5539/apr.V6n.1p.19.
- Nishioka, M., Saito, A. and Tsugawa, T. (2008). Occurrence characteristics of plasma bubble derived from global ground-based GPS receiver networks. *Journal of Geophys. Research*, vol. 113, A05301, doi: 10.1029/2007JA012605.
- Olwendo, J. O., Cilliers, P. J., Baki, P. and Mito, C. (2012). Using GPS-SCINDA observations to study the correlation between scintillation, total electron content enhancement and depletions over the Kenyan region: *Advances in Space Research* 49 (2012) 1363–1372.
- Omondi, G., Ndinya, B. and Baki, P. (2014). Study of the Equatorial ionosphere over Nairobi during selected magnetically disturbed and quiet times for the year 2009 using co-located instruments. *IJARPS*, Vol 1, 18-26, 2014.
- Omondi, G. E., Baki, P. and Ndinya, B. O. (2019). Total Electron Content and Scintillations over Maseno, Kenya, during high solar activity year. *Acta Geophysica*. ISBN 1895-6572. Doi:10.1007/s11600-019-00354-7.
- Oron, S., Dujanga, F. M. and Sssengonga J. J. (2013). Ionospheric TEC variations during the ascending solar activity phase at an equatorial station in Uganda. *Ind. J. Radio space phys.* 42, 1, 7-17.
- Otto, E. (1978). Theory of Raleigh-Taylor bubbles in equatorial ionosphere. *J. Geophys. Res* 83, 2066.

- Park, J., Luhr, H. and Noja, M.(2015). Three-dimensional morphology of equatorial plasma bubbles from measurements onboard CHAMP, *Ann. Geophys.*, 33, 129-135, <https://doi.org/10.5194/angeo-33-12902015,2015>.
- Paznukhov, V. V., Carrano C. S., Doherty P. H., Grooves K. M., Caton R. G., Valladares C.E. , Seemala G.K., Bridgwood C.T., Adenyi J., Ameshi L.L.LN., Damtie B., Dujanga F. D., Ndeda J.O.H., Baki P.,Obrou O.K., Okere B. and Tsidu G. M (2012).Equatorial plasma bubbles and L-band scintillations in Africa during solar minimum: *Annales Geophysicae*, 30, 675–682, 2012.
- Pi, X, Mannucci, A. J., Lindquister, U. J. and HO, C. M.(1997).Monitoring of Global Ionospheric irregularities using the worldwide GPS network. *Geophys. Res. Lett*, 24 (18), 2283-2286, 1997. Doi: 10.1029/97GLO2273.
- Pimenta, A, Bittencourt, J, Fagundes, P., Sahai, Y., Buriti, R., Takahashi, H. and Taylor, M. J.(2003)Atmospheric plasma bubble zonal drifts over the tropical region: A study using OI 630nm emission all sky images, *J Atmos. sol-terr phys*, 65,1117,2003.
- Radiciella, S.(2012).Workshop on science applications of GNSS in developing countries (11-27 April) followed by the Seminar on Development and use of ionospheric Ne Quick model 30<sup>th</sup> April -1<sup>st</sup> May 2012.
- Richmond, A. D., Peymirat, C. and Roble, R. G.(2003).Long-lasting disturbances in the equatorial ionospheric electric field simulated with a coupled magnetosphere ionospherethermospheremodel. *JGeophysRes*108.1118. <https://doi.org/10.1029/2002JA009758>.
- Sahai, Y., Fagundes, P. and Bittencourt, J.(2000).Transequatorial F-region ionospheric plasma bubbles:Solar cycle effects, *J. Atmos. Sol.OTerr. Phys.*, 62, 1377-1383,2000.
- Schunk, R.W. and Nagy, A.F. (2009). *Ionospheres Physics, Plasma Physics and Chemistry*.Cambridge University Press.
- Schrijver, C.J., Bageral, F. and Sojka, J. J.(2015). *HelioPhysics V, Space Weather and society*.<http://www.lmsal.com/schrijver/HSS5/HSS5-2015105.pdf>.
- Schrodet, K. P., Mittag, M., Jack D., Schimit, J. H., Hempelmann, A. and Gonzalez-Perez, J. N.(2017).Carrington cycle 24: The solar chromospheric emission in a historical and stellar Perspective. Advance Access publication. *MINRAS* 470, 276-282(2017) Doi:10.1093/mnras/stx147.
- Schwenn, R. (2006). *Space weather: The solar perspective*. *Living Rev. Sol. Phys.* 3, 2 (2006). <https://doi.org/10.1294/Irsp-2006-2>.

- Seemala, G.K. and Valladares, C.E.(2011).Statistics of total electron content depletions observed over the South American continent for the year 2008. *Radio Sci.* 46, RS5019, doi:10.1029/2011RS004722.
- Sobral, J., Abdu, M., Takahashi, H., Taylor, M. J., De Paula, E., Zamlutti, C., De Aquino, M. and Borba, G.(2002). Ionospheric plasma bubble climatology over Brazil based on 22 years (1997-1998) of 630nm airglow observations, *J. Atmos. Sol.-Terr. Phys.*, 64, 1517-1524, 2002.
- Sugiura, M.(1964). Hourly values of equatorial Dst for IGY. *Ann. International Geophysical year 35(9)*, Pergamon press, Oxford.
- Takahashi, H., Wrasse, C., Denardini, C., Otsuka, Y., Ivo, A, Paulino, L., Medeiros, A. F., Denardini, C. M.,Gomes, V. C. F., Sant'Anna, N. and Shiokawa, K.(2015). Plasma bubble monitoring by TEC map and 630nm airglow image, *J. Atmos. Sol-Terr. phys.*,130, 151-158,2015.
- Takahashi, H., Wrasse, C., Denardini, C., Padua, M., Paula, E., Costa, S., Otsuka, Y. ,Shiokawa, K., Monico, J., Ivo, A. and Sant'Anna, N.(2016). Ionospheric TEC weather map over South America, *Adv. space Res.*, 4,937-949, 2016.
- Tsunoda, R. T(1981).Time evolution and dynamics of equatorial backscatter plumes:1. Growth phase,*J Geophys Res (USA)*,86(1981) 139.
- Tsunoda, R. T.(1985).Control of seasonal and longitudinal occurrence of equatorial scintillation by longitudinal gradient in integrated E region pederson conductivity, *J. Geophys, Res.* 90, A1., 447-456, DOI: 10.1029/JA090Ia0p00447.
- Wang, C., Shi, C., Fan, L. and Zhang, H. (2018).Improved modeling of Global Ionospheric Total Electron content using prior information.*Remote sens*2018,10,63 doi:10.3390/r10010063.
- Woodman, R. F. and LaHoz, C.(1976).Radar observations of F region equatorial irregularities. *J, Geophys. Res.*,81, 5447.
- Ya'acob, N., Abdullah, M., and Ismael, M.(2010).GPS Total Electron Content (TEC) prediction of ionosphere layer over the equatorial region, *Trends in Telecommunications Technologies*. <http://dx.org/10.577218474>.
- Zhang, Y., Wan, W., Li, G., Liu, L., Hu, L. and Ning, B.(2015).A comparative study of GPS ionospheric Scintillations and ionogram spread F over Sanya, *Ann.Geophys*,33,1421-1430, 2015.
- Zernov, N. N., Gherm, V. E. and Strangeways H. J.(2009). On the effects of scintillation of low-latitude bubbles on trans-ionospheric paths of propagation, *Radio Sci.*,44, doi:10.029/2008Rs004074.

Zou, Y. and Wang, D.(2009). A study of GPS ionospheric scintillations observed at Guilin, J. Amis. Sol. Terr.Phys.,71,1948-1958, doi:10.1016/j.jastp.2009.08.005.

## **APPENDICES**

## APPENDIX I: Sample of VTEC and S<sub>4</sub> filtering script for all PRNs using SQL Server

### 2017 program

```
OPEN SQL SERVER
EXPAND THE OPTION NAMED Nyongesa\documents ON THE LEFT
EXPAND DATABASES
SELECT THE DATABASE Research
```

CLICK 'New Query' to open a query page

ON THE QUERY PAGE, PASTE THIS LINE AND PRESS F5  
truncate table researchdata

```
OPEN EXCEL
SELECT CELL D2
PASTE THERE THE LINE BELOW
=CONCATENATE("insert into researchdata (dataUT,dataVTEC,dataS4) select ",A2,",",B2,",",C2)
```

```
insert into researchdata(dataUT,dataVTEC,dataS4) select 0.025278,6.0967,0.07
insert into researchdata(dataUT,dataVTEC,dataS4) select 0.041944,6.0867,0.0567
insert into researchdata(dataUT,dataVTEC,dataS4) select 0.058611,6.08,0.06
insert into researchdata(dataUT,dataVTEC,dataS4) select 0.075278,6.05,0.06
insert into researchdata(dataUT,dataVTEC,dataS4) select 0.091944,6.02,0.06
insert into researchdata(dataUT,dataVTEC,dataS4) select 0.108611,6.0133,0.0567
insert into researchdata(dataUT,dataVTEC,dataS4) select 0.125278,5.95,0.0633
insert into researchdata(dataUT,dataVTEC,dataS4) select 0.141944,5.8867,0.0767
insert into researchdata(dataUT,dataVTEC,dataS4) select 0.158611,5.8,0.0567
insert into researchdata(dataUT,dataVTEC,dataS4) select 0.175278,5.6867,0.0633
insert into researchdata(dataUT,dataVTEC,dataS4) select 0.191944,5.6667,0.06
insert into researchdata(dataUT,dataVTEC,dataS4) select 0.208611,4.6225,0.08
insert into researchdata(dataUT,dataVTEC,dataS4) select 0.225278,4.6025,0.0775
insert into researchdata(dataUT,dataVTEC,dataS4) select 0.241944,4.57,0.0625
insert into researchdata(dataUT,dataVTEC,dataS4) select 0.258611,4.495,0.08
insert into researchdata(dataUT,dataVTEC,dataS4) select 0.275278,4.48,0.085
```

PUT MOUSE ON BOTTOM RIGHT OF CELL D2 UNTIL MOUSE POINTER BECOMES +  
DOUBLE CLICK THE MOUSE TO APPLY THE FORMULA ON ALL ROWS

COPY ALL THE DATA IN COLUMN D, JUST DO CTRL + C

```
GO BACK TO SQL SERVER QUERY PAGE
DELETE ANY QUERIES ON THE QUERY PAGE
PASTE THE DATA COPIED FROM EXCEL AND PRESS F5
```

DONE!!

```
USE [Research]
GO
DECLARE @return_value int
EXEC @return_value = [dbo].[proc_LoadData]
SELECT 'Return Value' = @return_value
```

GO

## APPENDIX II: Sample of VTEC and S<sub>4</sub> MATLAB plotting code

```

clear all
close all
% .....
%
% % % % % SHEET1 BELOW: 26.03.2013.xlsx
% %
Scriptpath='C:\Users\Nyongesa\documents\MATLAB\26.03.2013.xlsx';
addpath(Scriptpath);
Datapath='C:\Users\Nyongesa\documents\MATLAB\';
datestr1='26.03.2013.xlsx';
sheet='sheet1';
filename=datestr1;
% % % % import Excel spreadsheet Datapath);
if exist(filename,'file')
    sheet1= xlsread(filename,sheet);

else
    fprintf('%s not found in %s \n',filename,Datapath);
end

UT=sheet1(:,1);VTEC=sheet1(:,2);S4=sheet1(:,3);

[AX,H1,H2] = plotyy(UT,VTEC,UT,S4,' plot');
set(get(AX(1),'Ylabel'),'String','VTEC (TECU)', 'Color','r');
set(AX(1),'YColor','r');
set(AX(2),'YColor','b');
set(get(AX(2),'Ylabel'),'String','S4','Color','b');
set(AX,'XLim',[0 24]);
set(AX,'XTick',0:4:24);
set(AX(1),'YTick',-10:10:90);
set(AX(1),'YLim',[-10 90]);
set(AX(2),'YTick',0:0.1:1);
set(AX(2),'YLim',[0 1]);
xlabel('UT (hrs)'); grid on
title('MASENO VTEC S4 PLOTS FOR 26.03.2013') ;
set(H1,'LineStyle','-');
set(H2,'LineStyle','-');
set(H1,'LineWidth',1);
set(H1,'Color','r');
set(H2,'LineWidth',1);
set(H2,'Color','b');

```

### **APPENDIX III: Sample of ROT calculating script using SQL Server 2017 program**

```

Create procedure rpt_CalculateROT
as
Set no count on

Create table #rot (timefrom float, timeto float, vtect float,vtect1 float, rot float)

Declare @minutecount float,@hourcount float, @hourvaluefrom float, @hourvalueto float,
        @vtect float,@vtect1 float,
        @mintime float,@maxtime float, @datetime float
Select @minutecount=0.00,@hourcount=0.00
        while @hourcount<24.00
Begin
Select @minutecount=0.00
        while @minutecount<60.00
Begin
Select @hourvaluefrom=(@hourcount * 3600.000000) + (@minutecount * 60.000000)
,@hourvalueto=(@hourcount * 3600.000000) + (@minutecount * 60.000000) + 120.000000

Select @hourvaluefrom=round(@hourvaluefrom,6), @hourvalueto=round(@hourvalueto,6)

Select @mintime= min(DateTime),@maxtime=max(DateTime) from researchdata
        where DateTime is not null and (DateTime * 3600.000000)>=@hourvaluefrom and
        (DateTime * 3600.000000)<@hourvalueto
Select @vtect=avg(DataVtec) from ResearchData where DateTime=@maxtime
Select @vtect1=avg(DataVtec) from ResearchData where DateTime=@mintime

Insert into #rot(timefrom,timeto,vtect,vtect1) select @hourvaluefrom,@hourvalueto,
        @vtect,@vtect1

UPDATE #rot set rot=(vtect-vtect1)/

        ((timeto-timefrom)/60)/** power(10.0000,16)*/ * 40.3 * 0.0004)

Select @hourvaluefrom=(@hourcount * 3600.000000) + (@minutecount * 60.000000) + 60.000000
,@hourvalueto=(@hourcount * 3600.000000) + (@minutecount * 60.000000) + 60.000000

Select @hourvaluefrom=round(@hourvaluefrom,6), @hourvalueto=round(@hourvalueto,6)

Select @mintime= min(DateTime),@maxtime=max(DateTime) from researchdata
        where DateTime is not null and (DateTime * 3600.000000)>=@hourvaluefrom and (DateTime *
        3600.000000)<@hourvalueto
Select @vtect=avg(DataVtec) from ResearchData where DateTime=@maxtime
Select @vtect1=avg(DataVtec) from ResearchData where DateTime=@mintime

Insert into #rot(timefrom,timeto,vtect,vtect1) select @hourvaluefrom,@hourvalueto,
        @vtect,@vtect1
        */
        select @minutecount = @minutecount + 2.00
        end
        select @hourcount = @hourcount + 1.00

End

Select * from #rot;          drop table #rot

```

#### **APPENDIX IV: sample of ROT and ROTI MATLAB plotting code**

```

clear all
close all
% .....
%
% % % % % SHEET1 BELOW: 26.03.2013.xlsx
% %
Scriptpath='C:\Users\Nyongesa\documents\MATLAB\26.03.2013.xlsx';
addpath(Scriptpath);
Datapath='C:\Users\Nyongesa\documents\MATLAB\';
datestr1='26.03.2013.xlsx';
sheet='sheet1';
filename=datestr1;
% % % % import Excel spreadsheet Datapath);
if exist(filename,'file')
    sheet1= xlsread(filename,sheet);

else
    fprintf('%s not found in %s \n',filename,Datapath);
end

UT=sheet1(:,1);ROT=sheet1(:,2);ROTI=sheet1(:,3);

[AX,H1,H2] = plotyy(UT,ROT,UT,ROTI,' plot');
set(get(AX(1),'Ylabel'),'String','ROT(TECU/min)', 'Color','r');
set(AX(1),'YColor','r');
set(AX(2),'YColor','b');
set(get(AX(2),'Ylabel'),'String','ROTI (TECU/min)', 'Color','b');
set(AX,'XLim',[0 24]);
set(AX,'XTick',0:4:24);
set(AX(1),'YTick',-10:4:10);
set(AX(1),'YLim',[-10 10]);
set(AX(2),'YTick',0:0.1:4);
set(AX(2),'YLim',[0 4]);
xlabel('UT (hrs)'); grid on
title(ROT AND ROTI: 26.03.2013') ;
set(H1,'LineStyle','-');
set(H2,'LineStyle','-');
set(H1,'LineWidth',1);
set(H1,'Color','r');
set(H2,'LineWidth',1);
set(H2,'Color','b');

```

## **APPENDIX V: Sample of year to year EPB variation MATLAB plotting code**

```
close all; clear all;clc
```

```

figure
set(gcf,'Menubar','none','Name','Mychart','Numbertitle','off','color',[0.8314 0.8157 0.7483]);
Year=[6.49 4.32];
Disturbed=[21.42 21.88];
Quiet=[18.75 7.89];
bar(1:2,['Year' 'Disturbed' 'Quiet'],1)
set(gca,'xtick',1:2,'xTicklabel',['2013';'2014']);
legend('Yearly occurrence' , 'Disturbed period','Quiet period');
xlabel('Year');ylabel('% Occurrence of EPBs');
title('AVERAGE EPB OCCURENCE FOR 2013-2014');
grid on;
save

```

## **APPENDIX VI: Sample of seasonal EPB variation MATLAB plotting code**

```

close all; clear all;clc
A=[33.33 30.76];
B=[6.67 7.69];
C=[20 15.38];
D=[20 7.69];
bar(1:2,['A' 'B' 'C' 'D'],1)
set(gca,'xtick',1:2,'xTicklabel',['2013';'2014']);
legend('March equinox','June solstice','September equinox','November solstice');
xlabel('YEAR');ylabel('% Occurrence of EPBs');
title('SEASONAL VARIATION OF EPB OCCURENCE FOR 2013-2014');
grid on

```